METAL VAPOR VACUUM ARC SWITCHING

by

David Banks Cope

S. B., Massachusetts Institute of Technology
(1979)

and

S. M., Massachusetts Institute of Technology
(1979)

SUBMITTED TO THE DEPARTMENT OF
PHYSICS
IN PARTIAL FULFILLMENT OF THE
REQUIREMENTS OF THE
DEGREE OF

DOCTOR OF PHILOSOPHY
IN PHYSICS

at the

MASSACHUSETTS INSTITUTE OF TECHNOLOGY

October 1983

Signature of Author David B. Cope
Department of Physics
October 14, 1983

Certified by Peter P. Mongeau
Peter P. Mongeau
Thesis Supervisor

Accepted by J. F. Koster
George F. Koster
Chairman, Department Committee

METAL VAPOR VACUUM ARC SWITCHING

by

David Banks Cope

Submitted to the Department of Physics
on 14 October 1983 in partial fulfillment of the
requirements for the Degree of Doctor of Philosophy
in Physics

ABSTRACT

A theoretical and experimental investigation of metal vapor vacuum arc switching was performed. Establishing a more complete physical model of vacuum arcs was the goal. The basic principles of operation of vacuum arcs is discussed. The extension of present theoretical ideas is discussed in detail in several areas. Theoretical considerations indicate magnetic field-augmented vacuum arcs have enhanced performance levels. Design, construction, data, and interpretation of an experimental vacuum arc device is presented.

Acknowledgments

This thesis is the culmination of two years of research. I would like to thank the many people who have been ever so helpful in this project. Most especially, I would like to thank those so intimately involved in the Electromagnetic Acceleration Group, (Dr. Henry Kolm, Whitney Hamnett, Lisa Davidson, Kenelm McKinney, and Scott Clifton) while at M.I.T. and, currently, at EML Research, Inc. in Cambridge. Their curiosity, ability, and natural intellect have aided me in every aspect of the word "Help!".

Every thesis student owes a tremendous amount to his advisor and I am no exception. Peter Mongeau took me out of the cold, that January, and prodded and kneaded me until I was ready to rise into the ranks of the professional physicists. Peter has done, for me, everything the way it should be done: directing not by fiat and helping not by pampering.

Table of Contents

Table of Contents (cont.)

List of Figures

List of Figures (cont.)

List of Figures (cont.)

List of Figures (cont.)

I. INTRODUCTION

Metal vapor vacuum arc switches have long been used to switch kiloampere level currents in a high voltage environment often higher than 100 kilovolts. These reasonably compact devices feature the ability to interrupt significant peak current levels at a zero crossing point which is commonly known as commutation. It is this unique aspect which makes them the subject of an intense research effort currently being performed at several labs throughout the world.

A metal vapor vacuum arc device is a multi-electrode device housed in a insulated vacuum vessel. Figure I.1 shows a schematic form of a metal vapor vacuum arc switch. The conduction medium is an ionized metal vapor generated from the surfaces of the cathode and/or anode. Conduction is initiated typically by either separating metal contacts or surface breakdown when a third electrode or trigger electrode applies a high voltage across a dielectric surface. This thesis is concerned exclusively with the latter, three electrode, device.

When triggered, surface breakdown injects a small amount of plasma into the interelectrode region. This plasma blowoff provides the nucleus for an avalanche of conducting particles. The conduction medium is then maintained by power deposition at the electrode surfaces.

Conduction continues until some competing particle-loss mechanism overwhelms the particle-creation mechanism. Recovery is said to occur if conduction ceases for an indefinitely long period of time. Figure I.2 shows in block diagram the phases of metal vapor vacuum arc switch.

Figure I.1

METAL VAPOR VACUUM ARC SWITCH (MVVAS)

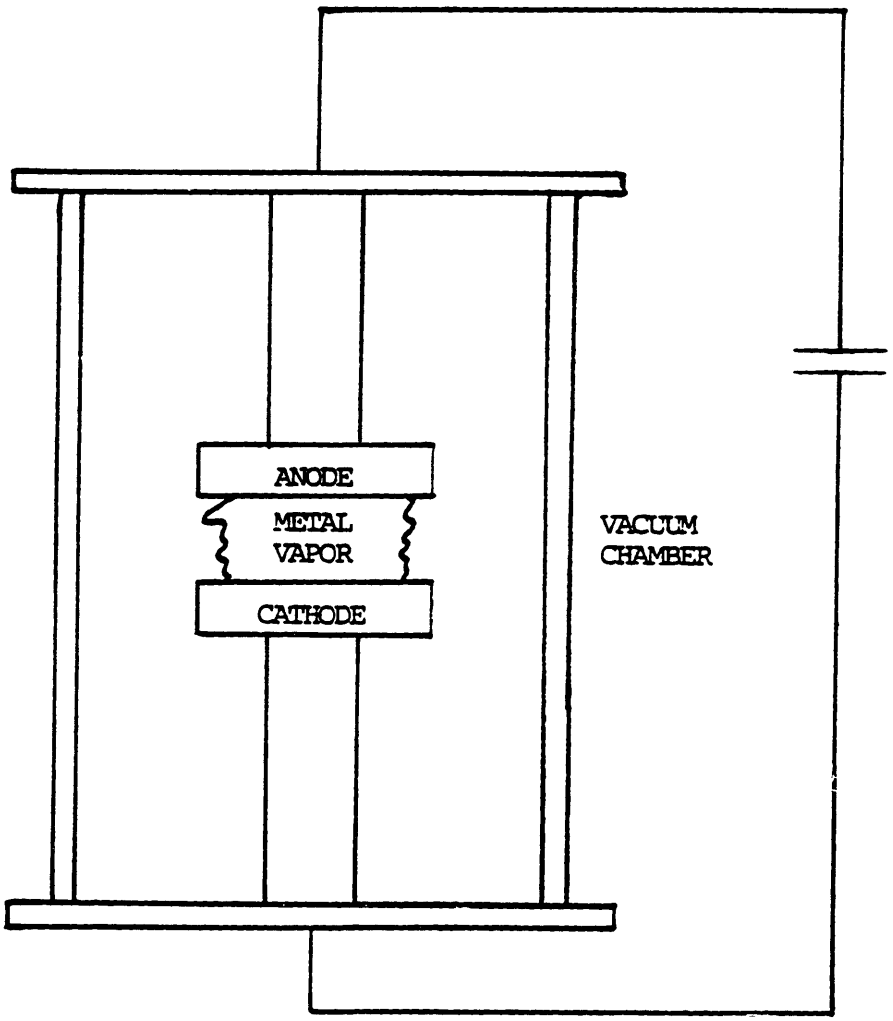

Figure I.2

PHASES OF MVVAS OPERATION

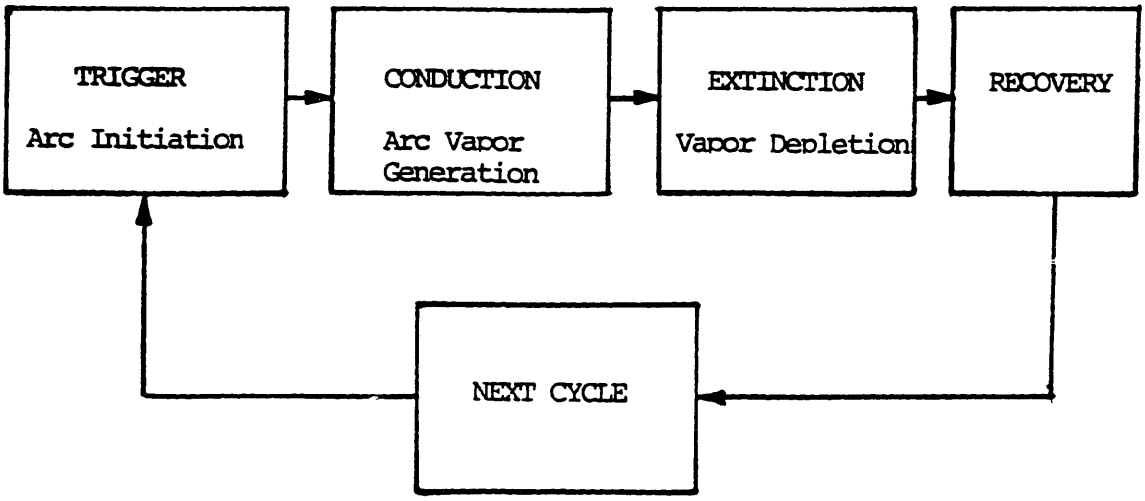

The situation of particle-loss exceeding particle-creation generally happens at a current zero. An alternating current is the most common example of a current waveform with a zero-crossing. If the current is sufficiently near zero for a sufficiently long time the conditions for current interruption have then been satisfied and the chances for actual interruption are quite good. The particle loss mechanism is that of plasma recombination on any surfaces present, particularly the electrode surfaces. The essential necesary condition for current commutation is the elimination of charged particles from the interelectrode region. In an ordinary triggered vacuum gap, the particles are swept clear of the gap by their thermal velocity. These conditions are necessary but

not sufficient for current commutation. Other factors must be considered before a definitive statement on interruption ability may be made. Examples of additional factors are: thermal heating of an electrode, melted metal splatter on insulator surfaces, micro-protrusions, the vacuum gap dimension, and the applied voltage.

The terminology "vacuum arc" is an unfortunate choice. An arc necessarily has a substantial number of high energy ionized particles; it certainly is not a true "vacuum". Similarly, a vacuum will not support any current conduction; an arc is impossible in a high vacuum environment. Rooted in the historical development of these devices, the terminology persists. We take the word "vacuum arc" to mean simply that before there was an arc there existed a reasonably good vacuum environment. Yet, like so many before me, I, too, continue usage of the term vacuum arc.

My thesis is organized according to a format which leads logically from the most general considerations to the most specific. An exhaustive theory of vacuum arcs is followed by a general consideration of apparatus issues. The specific implementation of an experimental device designed according to principles I chiefly established is described next. Data I observed is presented and my intrepretation of the data is given.

My original, creative work involved in this thesis is presented in the particular section which is most logically determined by the established format. I have presented the details of the electrode power balance for the first time (to my knowledge) in a coherent, compact and intelligible manner. Of course, I relied upon prior art of vacuum arcs, but never before has such an encompassing, definitive discussion been published.

In the course of this thesis I derived the mathematical equations and elucidated the physical understanding of the magnetic interruption analysis presented in this thesis.

The entire Theoretical Extension section represents exclusively original work. The increased understanding offered by this section is a direct result of my creative thinking.

A further example of novel work is my design of the experimental device. Innovative features such as the method of gap variation and slotted electrodes are described in detail.

I have supplemented this whole body of original work with the results of other researchers. Thus, I have put my own work into perspective with work done by others.

II. THEORY OF ARCS

A detailed account of the theory of arcs is presented in this chapter.

A. Electrodes: Power Balance

Introduction

The principal physical basis of an arc discharge is governed by an energy equation. In its most common representation, when applied to the cathode, the energy equation becomes:

$$P_{cathode} = M\ Cp\ dT/dt.$$

The notation is as follows:

$P_{cathode}$ = power to the cathode [Watts]

M = effective cathode mass [kg]

Cp = heat capacity of the cathode [J/kg K]

T = cathode temperature [K]

t = time [s]

The task is to evaluate $P_{cathode}$. A list of various energy-relevant processes appears in Figure II.A.1. These processes, according to our present understanding, in combination with specific material properties, contain the relevant macroscopic physics of an arc discharge. It is the richness of these phenomena which makes for rewarding

research.

Convective heat transfer is notable by its absence from Figure II.A.1. Shown in Figure II.A.1 is a column giving the algebraic sign of the effect which the process has upon the cathode temperature. A (+) sign indicates that the effect will tend to increase the cathode temperature. A (-) sign means a tendency to decrease the cathode temperature.

Figure II.A.1

ENERGETIC PROCESSES

Cathode Effect	Process
+	(1) charged particle bombardment
+	(2) neutral particle bombardment
+	(3) ohmic (resistive) heating
+	(4) plasma radiation
+	(5) plasma recombination
-	(6) plasma ionization
-	(7) bulk metal radiation
-	(8) bulk thermal conductivity
-	(9) electrode phase change
-	(10) work function escape energy
-	(11) electronic heat capacity

A brief description is given below for each of the parameters listed in Figure II.A.1.

II.A.1 Charged Particle Bombardment

Charged particle bombardment is simply the result of the deposition of the kinetic energy acquired by charged particles as they fall down the electric-potential well. Essentially the particles convert this potential energy to thermal energy of the respective electrode. Assuming an accommodation coefficient of unity, the total energy delivered to the electrode surface is the sum of the cathode-fall potential, the kinetic energy of the particle, and the ionization energy.

The ionic kinetic energy is greater than the total voltage drop from anode to cathode. This phenomenon is due to the existence of a "potential hump". Figure II.A.2 shows the form of a potential hump. The possibility of a potential hump was first discussed by Compton [Compton, 1931] and Tanberg and Berkey [Tanberg and Berkey, 1931]. More recently, researchers in the field have made experimental measurements attempting to investigate the structure of the potential hump [Plyutto, Ryzhkov, and Kapin, hereinafter referred to as PR&K,1965; and Davis and Miller, referred to as D&M, 1969]. The results of their work [PR&K, 1965; D&M, 1969] show that ions have an energy greater than the anode potential. The ionic energies vary for different materials,

but range typically from 25 eV [PR&K] to 70 eV [D&M]. For our case, we use a value appropriate to stainless steel of E_i = 29 eV. The total energy deposited per ion is

$$V_i = V_c + E_i + I,$$

where V_c is the cathode-fall voltage, taken to be 7 volts [Cobine, 1955; Reece, 1963], and I is the ionization potential also taken to be 7 volts. Thus, assuming singly charged ions, V_i = 43 volts. (It should be noted that a large fraction of the ionic population is multiply charged [PR&K, 1965; D&M, 1969]. For simplicity we consider only Z = 1 ions.) It is important to note that this energy deposition occurs over a very small area at the cathode. The cathode spot energy fluxes are quite high indeed, as will be discussed later.

The existence of a potential hump is easily seen to be plausible from two different, but related, points of view. An energy balance performed at the cathode cannot be achieved without a potential hump: the cathode becomes colder because the material vaporized and ionized requires a great amount of energy. This assumes the various parameter values of materials and of the arc discharge are correctly obtained. Thus, an increased input power is required at the cathode for a balance to be achieved. The increase in the ion energy due to the hump is precisely

enough for such a balance. The alternative point of view is one of conservation of current. Again, assuming the various parameter values to be correctly obtained, one may calculate the electron current leaving the cathode. Also given the plasma parameters, one may calculate the electron current going to the anode. The paradox arises that the electron current leaving the cathode is less than that arriving at the anode. A potential hump explains the paradox because it generates a space-charge which gives rise to an electric field which accelerates ions and retards electrons. From this point of view, the existence of a potential hump has an effect which is similar to ambipolar diffusion [Gunter Ecker, 1980].

Section II.E.5 presents a theory on potential hump formation.

Figure II.A.2

POTENTIAL HUMP FORM

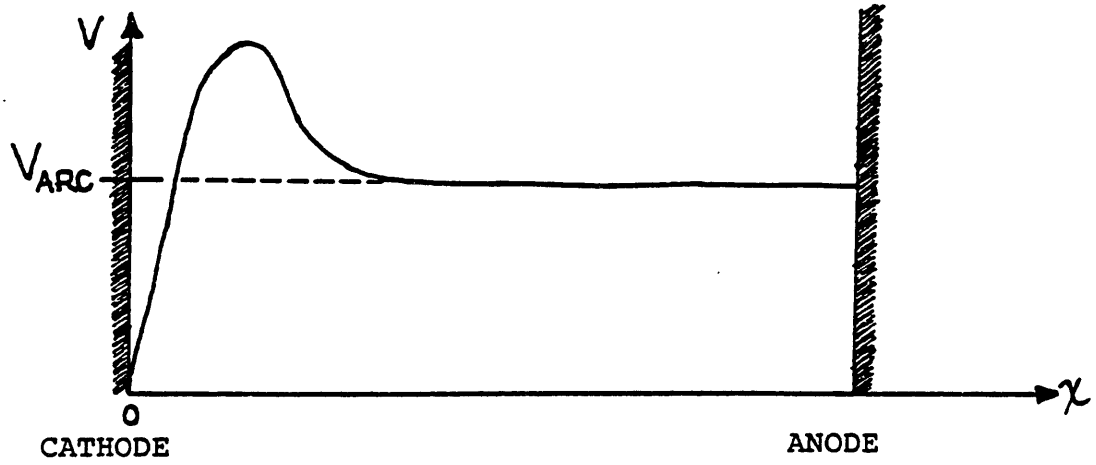

II.A.2 Neutral Particle Bombardment

Neutral particle bombardment represents the energy transferred by particle-surface collisions. During inelastic surface scattering by neutrals some fraction of the initial kinetic energy is deposited on the electrode surface. In this calculation we include charge exchange neutrals. The reaction is $\underline{A}^+ + A \rightarrow \underline{A} + A^+$ where the ionization state is indicated by a (+) sign and the energetic particle is underscored. Note in this case the plasma is optically thick to charge exchange neutrals. The practical effect of this fact is that the metal surface presents a solid angle of 2π to the emitting volume. The scale depth of this volume is $l = 1/n\sigma$, where σ is $\sigma_{CX} + \sigma_I$, i.e. the sum of charge exchange and ionization cross-sections.

II.A.3 Ohmic heating

Ohmic heating is the ordinary result of passing current through a body with a finite resistivity.

II.A.4 Plasma Radiation

The plasma in the inter-electrode region transfers energy by several mechanisms. Plasma radiation is one means by which energy is transferred from the plasma volume to the

electrode surface. The radiation mechanisms include Bremsstrahlung and line radiation. Recombination of electrons and ions occurs in two different environments: volume or near-surface recombination. Simultaneous conservation of energy and momentum requires at least three bodies for recombination to be allowed. In radiative recombination, one of the "bodies" is represented by photons which carry away the excess energy and momentum. The photons which intercept the electrode surface are already accounted for by the plasma radiation. Radiative recombination depends linearly on the electron and ion densities in the volume of plasma.

II.A.5 Plasma Radiation

Three-body recombination, by contrast, is truly a three body event. In addition to the electrons and ions, which recombine as in radiative recombination, neutrals are present which may absorb the excess energy and momentum. The probability, or rate, of three-body recombination is proportional to the densities of the interacting species. There are three principal three-body recombination reactions: ion-ion-neutral, electron-ion-electron and electron-ion-neutral. The ion-ion-neutral reaction has a low probability of occurrence under conditions applicable to vacuum arcs; only at extreme ion densities does this rate become appreciable. The two latter reactions, however,

are significant under arc discharge conditions. These reactions, in fact, are the most important ones for arc extinction. The electron-ion-electron rate is given by Zel'dovich and Razier [Zel'dovich and Razier, 1966]. We have used their three-body recombination rate in our calculations.

Data for the electron-ion-neutral reaction rate is scarce. However, Kimblin [Kimblin, 1971] has measured ion wall currents in vacuum arc discharges. He has suggested this current to be a result of recombination of ions at the walls. Kimblin measured an ion current equal to approximately 10% of the total arc discharge current. We have used this value in our calculations. Hence, the probability for three-body recombination is greatly enhanced near the surface of two classes of objects: (1) condensed matter, where the neutral density is approximately three orders of magnitude higher than the peak neutral density in the plasma, and (2) electron emitting materials, where the density of electrons is high. The electrodes satisfy both conditions, while any exposed material surface satisfies the former condition. Of course, <u>all</u> material surfaces are included, conductor or dielectric. During periodic cleaning of the glass vacuum chamber, we have noticed metallic build-up in the inside

surface. We take care to remove this debris as it would eventually obstruct our view of the discharge.

II.A.6 Plasma Ionization

Ionization of the plasma tends to have a cooling effect on the electrode. This follows under the assumption that the same amount of total energy is available; more energy transferred to the plasma means less allocated to the electrode. This is exactly analogous to the phase change energy. This occurs, for instance, when a stream of incident electrons ionizes a volume of neutral gas; if the gas were not present, the ionization energy would be deposited on the electrode surface as in process II.A.1.

II.A.7 Grey Body Radiation

As the temperature of the electrode increases, the surface will radiate more energy according to the black body relationship, corrected by the emissivity: that is, the surface will radiate as a grey body. In our calculations which follow, we assume the surrounding surfaces to be at zero temperature. This assumption is, of course, false, but it allows simplification of the calculation and the error introduced by this approximation is certainly less than that of other approximations used. In addition, the approximation becomes better and better as the electrode temperature increases. We also ignore the shape factor, F_{ij}

for the solid angle of the opposing electrode.

II.A.8 Thermal Conductivity

Since energy is deposited primarily at the electrode surface, bulk thermal conduction represents a cooling effect of the surface region. Thermal conduction is of most importance early in the discharge. The energy transport rate is proportional to the temperature gradient. This gradient is largest before the energy has had time to "spread out" or diffuse. This concept is closely related to the existence of cathode spots; a detailed discussion is postponed until more background material is given.

II.A.9 Electrode Phase Change

The rate of increase of temperature of the electrode is not precisely steady in time. At various points during the temperature rise, the local temperature remains constant while the input power supplies the energy needed for a phase change. Starting with the solid metal phase and proceeding to the ionized phase we have at least three phase changes. They are: melting, vaporization and single-ionization. Additional phase changes include solid metal internal changes (e.g. alpha to beta phase transformation) and multiple ionization events. Ionization has been taken into account above and so will not be discussed further. A substantial amount of energy is involved in the processes

of melting and vaporization. The effect is listed as a cooling agent in Figure II.A.1. This is true for the region of high energy flux. When condensation occurs, however, on a material surface the energy "stored" as thermal energy of a gas re-appears at the material surface. Hence, in essence, vaporization tends to cool one area but tends to heat another area.

II.A.10 Work Function Escape Energy

Electrons in a metal are in a quantum mechanical potential well. The effective depth of the well is the total depth, W, minus the Fermi energy, e_F, and is called the work function for the particular metal and is designated by ϕ. This effect is a quantum mechanical one, yet it has simple classical analogies. One analogy is that of the simple potential well: a certain amount of energy must be supplied in order to extricate the electron from the well. The amount of energy required varies with the electron's kinetic energy (i.e. temperature) and any external electric field which may be present. The higher the temperature, or the greater the electric field, the less energy required and the more likely it is that the individual electron will escape. The second classical analogy, applicable in the absence of an external electric field, is one of simple electron evaporation from the metal. The net effect is to

cool the metal; the cooling power is approximately equal to $\phi_- I_-$, where I_- is the electron current and ϕ_- represents the average cooling effect per electron. As pointed out by Lee (and others), ϕ_- is numerically different from ϕ [Lee, 1960; Holmes, 1974; and Compton, 1931].

II.A.11 Electronic Heat Capacity

A result of charge neutrality in the closed electrical circuit is the replacement of the electron just "lifted" from the potential well by another electron. This second electron has a maximum energy equal to the Fermi energy of the particular metal plus kinetic energy corresponding to the bulk metal temperature. The lost electron, however, had a greater energy because of its higher temperature. Also, as mentioned above, electrons with a greater energy are more likely to be the ones which escape the potential well. Hence an energy loss has been experienced by the metal equal to the difference in kinetic energy of the two electrons. This is recognized as simply the electronic heat capacity. This effect results in a cooling power equal to $1.5\ k_B(T_H - T_C)I_-/e$, where T_H is the temperature of the hot electron and T_C is the temperature of the cold replacement electron.

Figure II.A.3 shows, in a schematic form, the processes contributing to the energy equation. In Figure II.A.3 the

arrowhead indicates the direction of positive energy flow.

Figure II.A.3

CATHODE ENERGY BALANCE

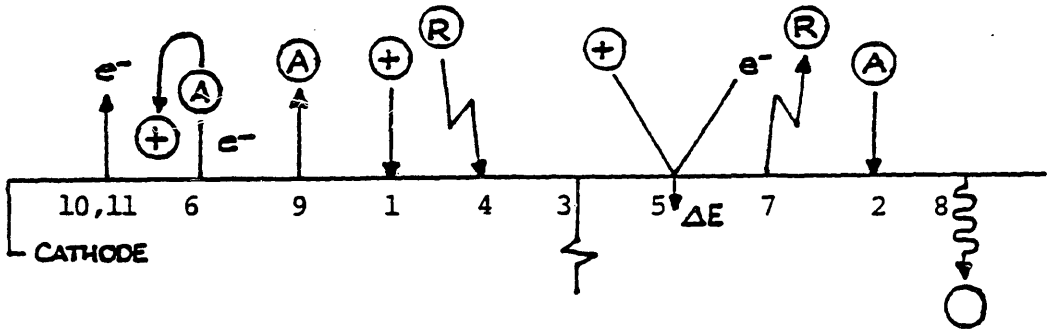

(1) charged particle

(2) neutral particle bombardment

(3) ohmic heating

(4) plasma radiation

(5) plasma recombination

(6) plasma ionization

(7) bulk thermal radiation

(8) bulk thermal conductivity

(9) electrode phase change

(10) work function escape energy

(11) electronic heat capacity

$P_{cathode}$ may be evaluated by writing the expressions for the individual terms and algebraically summing them to obtain a net power transfer.

$$P_{cathode} = P_{charged\ particle} + P_{neutrals} + P_{resistive} + P_{radiation} + P_{recomb} - P_{ioniz} - P_{BB\ rad} - P_{thermal\ cond} - P_{phase\ change} - P_{\phi} - P_{e\ heat\ capacity}$$

where,

(1) $P_{charged\ particle} = \sum V_i I_+$,

(2) $P_{neutrals} = r E_n \dot{N}_n + \langle \sigma_{cx} v_i \rangle n_i n_n e_i V_s$, $(0 < r < 1)$

(3) $P_{resistive} = I^2R$

(4) $P_{plasma\ rad} = \int (P_{recomb\ rad} + P_{Bremsstrahlung} + P_{line})$

(5) $P_{plasma\ recomb} = \alpha_{3B} n_i n_e n_n V_s E$

(6) $P_{plasma\ ioniz} = XI\ E_I/\eta$

(7) $P_{BB\ rad} = \sigma T^4$, $(T > T_{room\ temp})$,

(8) $P_{thermal\ cond} = A\ k\ dT/dx$,

$$(9) \qquad P_{\text{Phase change}} = \begin{cases} H_{\text{fusion}}\, dM/dt, & T = T_{\text{melt}} \\ H_{\text{vaPor}}\, dM/dt, & T = T_{\text{boil}} \\ 0, & \text{otherwise} \end{cases}$$

$$(10) \qquad P_{\phi} = \phi I_{-}$$

$$(11) \qquad P_{e \text{ heat caPacitY}} = 1.5\, k_B (T_H - T_C) I_{-}/e$$

where,

α_{3B} = three body recombination coefficient [cm^6/s]

n_j = number density of species j [cm^{-3}]
(e = electron, i = ion, n = neutral)

V_s = volume of the near-surface interaction [cm^3]

V_p = plasma volume [cm^3]

E_I = ionization potential energy [J]

Z = ionization level of atom.

The above is a generalized framework; we want to specialize to the case at hand, namely that of power balance of a cathode, and, in particular, a cathode spot. Before proceeding we briefly describe the phenomenon of cathode spots.

A cathode spot is a localized region of the electrode where the current density is very high - of order 10^6 - 10^8 A/cm^2. In photographs such spots are easily recognized by the bright light emission. Figure II.A.4 shows several such cathode spots.

Figure II.A.4

OPEN-SHUTTER PHOTOGRAPH OF CATHODE SPOTS

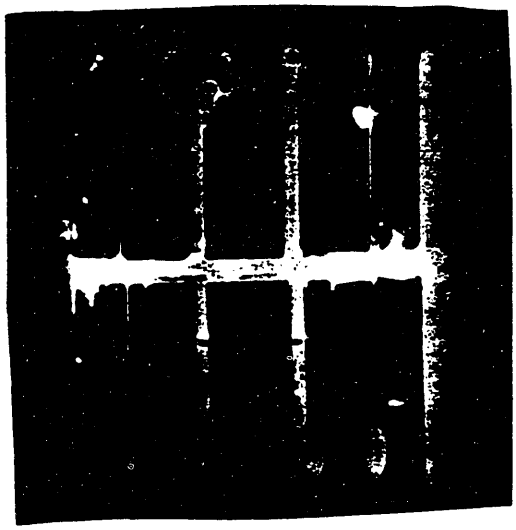

On a microscopic level much remains unknown about cathode spots. What is known is a macroscopic description of cathode spots. Figure II.A.5 gives several of the characteristics of cathode spots.

Figure II.A.5

CATHODE SPOT CHARACTERIISTICS

diameter = 10-50 microns [Robson, 1978]

total spot current = 100 amps (copper) [Kimblin, 1973]

current density = 10^6 - 10^8 amps/cm^2 (copper)

spot temperature = 3300 K (copper) [McGlure, 1974]

spot velocity = 10 m/s [Reece, 1963]

vaporization rate X = 60 ug/C [Kimblin, 1971]

emitted electrons/atom = 10 (copper)

An interesting feature of a cathode spot is the maximum current associated with it. This implies that, refering to Figure II.A.4, for a 200 amp arc discharge to pass between copper electrodes, two (2) cathode spots would be required. The two spots would not coalesce into one-200 amp spot. This further implies a positive slope of the graph of the voltage across the electrodes versus the current passed through them. In short, vacuum arcs have a positive resistance to an increment of current. Thus vacuum arcs will burn in parallel with load sharing among cathode spots assured. Gas gaps and SCRs (silicon controlled rectifiers) are two examples of switches which do not possess this ability. Special considerations must be made for these two latter switching elements when parallel operation is desired.

The existence of cathode spots as areas of intense energy fluxes prompts a numerical tabulation of the total power and the power flux delineated into two columns: one expressly for cathode spots and the other for similar regions that are not cathode spots. Figure II.A.6 lists those processes confined to cathode spots.

Figure II.A.6

CATHODE SPOT PROCESSES

(1) charged particles

(6) ionization

(7) black-body radiation

(8) thermal conduction

(9) phase change energy

(10) work function escape energy

(11) electron heat capacity

Sufficient background material has been given to enable order of magnitude calculations to be made of the several parameters of interest. The various assumptions required to proceed are detailed in Figure II.A.7.

We calculate for the applicable case of a 10 kA arc

current. Given the current the majority of the numerical parameters are available in the published literature either specifically for vacuum arcs or as a material property. The other parameters are a function of geometry or are simply derivable from first principles of physics. The calculation of mean free paths of particles in the interelectrode plasma for the processes of ionization, charge exchange, et cetera are first-principle calculations.

Figure II.A.7

ASSUMPTIONS FOR NUMERICAL CALCULATIONS

I = 10 kA

r = 0.5

V_i = 43 volts [PR&K, 1965; D&M, 1969; see also Section II.A.1]

I_- = 0.9 I [Kimblin, 1971]

$n_i = n_e = 10^{16}$ cm^{-3} [Boxman, 1974; Kaneda, 1981.]

$n_n = 10^{17}$ cm^{-3} [Reece, 1963]

$n_a = 10^{22}$ cm^{-3} [Kittel, 1976]

T_{ev} = 1 ev

V_s = 2.5 cm^3

V_p = 25 cm^3

E = 7.7 ev [copper, Weast, 1974]

T_H = 3300 K

T_C = 300 K

H_f = 250 J/g [Touloukian, 1981]

H_v = 6.3 kJ/g [ibid.]

$dM/dt = XI$

X = 73 ug/C [Kimblin, 1973.]

ϵ = 0.9

k = 0.8 W/cm K

Z = 1

$J = 5 \times 10^6$ A/cm^2 [Cobine, 1955; Ecker, 1980]

$v_n = 9 \times 10^4$ cm/s

ϕ_- = 2.6 eV [Lee, 1960]

The results of the calculations are presented in Figure II.A.8. The details of the actual calculations are given in Appendix A. The notations used is as follows: P_{total} is the surface power density [Watts] of the electrode (cathode), F_{spot} is the power flux [W/cm^2] of the cathode spot, and F_{not} is the power flux of the entire electrode surface.

Figure II.A.8

CATHODE POWER CALCULATION RESULTS

			P_{total}	F_{spot}	F_{not}
(1)	charged particles	(+)	43 kW	21.5 MW/cm2	
(2)	neutral particles	(+)	15 kW		620 W/cm2
(3)	Ohmic heating	(+)	2 kW		
(4)	radiation	(+)	3.3 kW		130 W/cm2
(5)	recombination	(+)	4 kW		160 W/cm2
(6)	ionization	(-)	7 kW	3.5 MW/cm2	
(7)	black-body rad.	(-)	100 W	200 W/cm2	
(8)	thermal cond.	(-)	3.2 kW	1.6 MW/cm2	
(9)	phase change	(-)	6.6 kW	3.3 MW/cm2	
(10)	work function	(-)	23 kW	11.5 MW/cm2	
(11)	e^- heat capacity	(-)	3.5 kW	1.8 MW/cm2	

Several conclusions can be drawn from Figure II.A.8. Addition of the total power column indicates that approximately 24 kW of unbalanced power heats the cathode. This energy gain results in a bulk metal temperature rise rate of about 0.2 K/ms of arc duration. Thus, the great thermal mass of the electrode prevents any appreciable temperature rise of the bulk metal. The cathode spot itself, however, is an entirely different case. The thermal mass of the cathode spot is, by comparison, quite small. Because of this fact, the cathode spot is very nearly always in power balance. As an example, if the spot were out of balance by a net power of 1 kW the resulting temperature rise rate would be approximately 1000 K/us. This, of course, would tend to equalize the input and output power to the spot. In fact, this rise rate is of the order, but less than, the rise rate experienced by the spot itself during its formation. Early in the discharge, before the cooling mechanisms have been activated, the net input power flux is of order 10 MW/cm^2. This flux multiplied by the spot area yields an unbalanced power gain of greater than 1 kW, thus the rise rate of the spot is greater than 1000 K/us. Grissolm and Newton have conducted experiments on anode spots with incident energy fluxes estimated at 10 MW/cm^2. Their observations show the rise time of spots to be of order of 2 us [Grissolm & Newton].

II.B Electrodes: Material Considerations

Phenomena associated with the electrodes can be attributed to either surface or bulk efects. These effects determine criteria for selection of the particular electrode material. A list of selection criteria is given in Figure II.B.1. Following Figure II.B.1 is an explanation of the importance of each criterion. From a more practical point of view, other criteria including material availability, purity, cost, machineability, amount of trapped gases, and ease and safety of handling, are also important considerations.

Surface Effects

II.B.1 Vapor Pressure

The vapor pressure is the pressure associated with a given material at a specific (uniform) temperature at which the liquid phase and vapor phase exhibit detail balancing. The principle of detailed balancing, applied to the issue at hand, is as follows: as many atoms leave the liquid state per unit velocity interval per unit time in transition to the gaseous state

Figure II.B.1

ELECTRODE MATERIAL SELECTION CRITERIA

Characteristic	Desired aspect
Surface Effects	
(1) vapor pressure	low
(2) phase transition temperature	high
(3) erosion rate	low
(4) heats of transformation	high
(5) high voltage standoff	low
Bulk Effects	
(6) work function	low
(7) arc stability	(conditional)
(8) electrical conductivity	high
(9) thermal diffusivity	high
(10) mechanical strength	high

as leave the gaseous state per unit velocity interval per unit time in transition to the liquid state. In the literal sense, detailed balance means each microscopic collision process is balanced by the exact reverse process [Lifshitz and Pitaevskii, 1981]. The vapor pressure is only a function of material and temperature. The importance of material selection in regard to vapor pressure is easily seen if one a considers material such as zinc. At a temperature of 1000 K, well below typical cathode spot temperatures, the vapor pressure of zinc is 0.1 atm. Thus, in violation of our assumptions, this is not a vacuum arc at all; it is, in fact, a relatively high-pressure gaseous arc burning in an ambient atmosphere. The extinguishing capability of a gaseous arc is severly impaired due to the high pressure in the arc. Figure II.B.2 gives the vapor pressure of various metals at temperatures characteristic of cathode spots.

Figure II.B.2

VAPOR PRESSURES OF METALS

Metal	Boiling Point (760 Torr) (K)	Temperature[a] (10^{-6} Torr) (K)
Cd	1040	390
Zn	1185	450
Cu	2840	1120
Fe	3135	1300
Ni	3190	1340
Mo	4880	2080
W	5830	2660

(a) O'Hanlon, 1980

II.B.2 Transition Temperature

A high boiling point will have two related effects: i) the vapor pressure will be lower at a given temperature (see above), and ii) a high boiling point means rapid cooling of the spot because the cooling mechanisms increase as temperatures increase. With respect to the latter, however, thermionic electron emission limits the utility of the refractory metals; in this case the boiling temperature is too high. Rich has noted that the ultimate limiting parameter in vacuum arc operations is anode spot formation [Rich, 1971]. His observations show the critical parameter scales with increasing phase transition (melting)

temperatures.

II.B.3 Erosion Rate

The rate of erosion of the electrodes is central to understanding the performance limits of vacuum switches. Electrode wear appears to be strictly proportional to the total amount of charge which passes through the switch. In other words each atom ablated from the cathode surface generates a characteristic number of primary electrons which carry the actual discharge current. At first thought this might seem contrary to expectations. Erosion is not determined by the spot temperature. This is essentially because the spot is such a small thermal mass (as we have seen) that its temperature is not determined by input power; it is approximately at the boiling point. Figure II.B.3 shows experimental cathodic erosion rates and effective electrons/atom vaporization ratios for a wide variety of metals.

II.B.4 Heats of Transformation

The cooling power per atom ablated is directly proportional to the heat of transformation of the metal. Hence, a material having a high heat of transformation tends to cool the cathode spot more readily than a material with a lower heat of transformation.

Characteristics (1)-(4) are all closely related material parameters; to a large extent they determine the material quasi-steady state response to a high incident energy flux. Section II.E.3 will investigate the steady state response in more detail by introduction of a relatively simple theoretical model describing material ablation.

Figure II.B.3

CATHODE EROSION RATES FOR VACUUM GAPS

Metal	Erosion Rate (ug/C)	Electrons/Atom
Cd	650	1.8
Zn	215	3.2
Mg	35	7.2
Ag	150	7.5
Al	120	2.3
Cu	115	5.2
Cr	40	14
Ni	80	6.9
Fe	73	7.2
Ti	52	9.6
C	16	7.0
Mo	47	21
W	62	31

[Kimblin, 1973; Plyutto, Ryzkhov & Kapin, 1965]

II.B.5 High Voltage Standoff

The ability to withstand high voltage can be summarized by measurements of the electric breakdown strength of a particular material. In order to understand the parameters upon which breakdown strength depends, we review the results of work previously published [Rozanova and Granovskii, 1956].

Rozanova and Granovskii conducted experiments to determine the relative ordering of various anode materials in terms of increasing breakdown voltage. Figure II.B.4 shows the results of their ordering (starting at the lowest breakdown voltage and increasing down the figure). In Figure II.B.4, metals are grouped together if insignificant differences in breakdown voltage were observed. The interpretation of their results lead to the widely quoted conclusion that the electrical strength of a vacuum gap depends on the mechanical strength of the anode, if this strength is characterized by Young's modulus.

Figure II.B.4

METAL BREAKDOWN STRENGTH ORDERING VS. YOUNG'S MODULI
(breakdown strength increasing down the table)

Metal	Young's Modulus[a]
C, graphite	1 x 10^6 psi
Al	10
Cu	16
Fe, Ni	30
Mo, W	55

(a) Machine Design, 1983 Material Reference Issue, 14 April 1983.

Other work has tended to support this conclusion [Erven, et al, 1970]. Experiments on metals of the same composition but differing mechanical strengths have also verified the above conclusion [McCoy, et al, 1964]. McCoy, et al, used stainless steel 304 in the hot-rolled condition (76 on the Rockwell B scale) and the cold rolled and annealed condition (92 Rockwell B). The harder metal consistently had a higher breakdown strength.

It should be noted that this phenomenon is not systematically related to the electric field-enhanced electron emission characteristics of metals [Farrall, 1980]. Figure II.B.5 shows metals listed according to

increasing critical field values for electron emission and the critical electric fields. It is beyond the scope of this thesis to investigate field-enhanced emission; the results are listed simply to complete the discussion of metal electrical breakdown strength. Note that the relative order of Figure II.B.4 has little bearing on the order of Figure II.B.5.

Figure II.B.5

CRITICAL-FIELD ORDERING FOR METAL ELECTRON EMISSION
[after Farrall, 1980]

Metal	Relative Electric Field
Mo	1.0
Stainless steel	1.1
W	1.2
Cu	1.3
Ni	1.9

The above description applies to un-arced electrodes. Electrodes which have been subjected to high current arcing will have suffered asperite formation. Asperite formation is an important process because excessive formation implies a reduced interruption capability. The mechanism is Fowler-Nordheim electron emission due to surface features with a scale radius of order 0.1 micron. The formation of these microprotrusions is a poorly understood process. This surface roughness, however, can be significantly reduced by electrode conditioning. This is usually accomplished by ion bombardment and can increase the initial breakdown voltage by a factor of 2 or more [Farrall, 1980]. Unfortunately, protrusion growth seems to be a result of processes initiated during the arc discharge. Consequently conditioning of repetition-rated devices is not a trivial matter. As a final word concerning high voltage standoff, it is noteworthy that the results of a conditioning process are observed to deteriorate in time [Farrall, 1980].

Bulk Effects

II.B.6 Work Function

The work function plays an important role in the cathode spot scenario. A large work function implies a relatively large cooling effect on the spot during electron emission

(assuming non-thermionic emmission). As we shall see in Section II.E.4, a model of arc stability is developed in which the work function is related to the minimum anode potential. This model indicates that an arc will be more stable on a material of a lower work function.

II.B.7 Arc Stability

Arc stability is to be interpreted as the ability of the arc to continue carrying current. Vacuum arcs become unstable, i.e. interrupt, when they lose the ability to continue the fundamental emission processes which supply current-carrying particles from the cathode [Farrall, 1980]. Arc interruption must be controllable to be useful. Thus, we wish the arc to be reliably stable until the instant of interruption. Associated with arc instability is a large fluctuating anode voltage drop. Minimization of this fluctuating voltage is also obtained by a low work function material. As mentioned, these two topics are closely intertwined. More detail is provided in the appropriate section.

Various experiments have been conducted with the aim of determining the average arc lifetime as a function of current. Figure II.B.6 shows the results of such experiments [Farrall, 1980]. As pointed out by Farrall, the

metals appear in nearly the same order, left to right, as they do in the vapor pressure plot, Figure II.B.7. These plots strongly suggest that arc stability is closely related to the ease with which vapor is produced from a metal [Farrall, 1980].

Figure II.B.6

AVERAGE ARC LIFETIME AS A FUNCTION OF CURRENT
[Farrall, 1980]

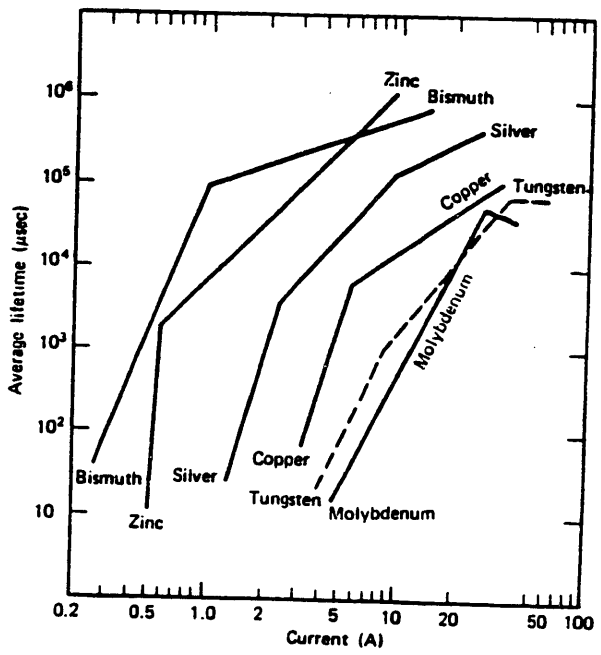

Figure II.B.7

VAPOR PRESSURE AS A FUNCTION OF TEMPERATURE
[Farrall, 1980]

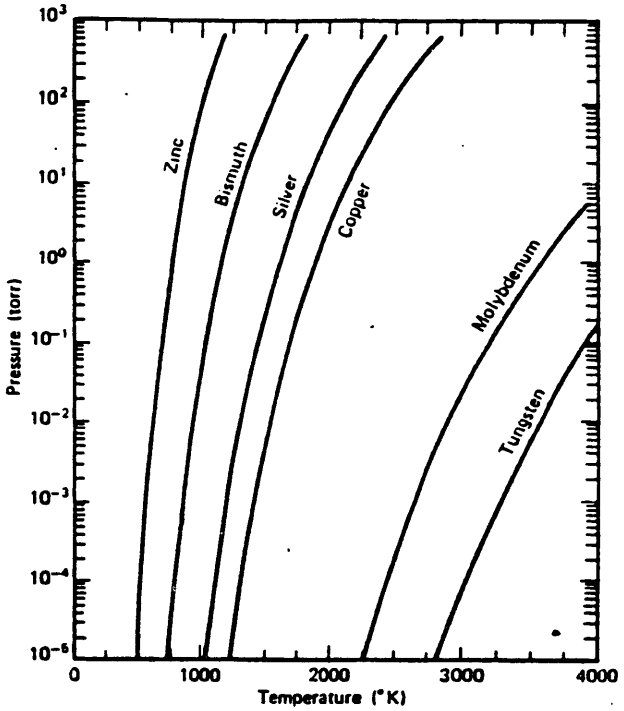

We have seen, in Figure II.B.6, that the arc lifetime is strongly dependent on the arc current. As the arc current approaches zero in a normal sinusoidal fashion, a point in time exists when the time until the sinusoidal zero is obtained is greater than the arc lifetime as shown in Figure II.B.6. Figure II.B.8 shows this schematically. In this figure we have drawn a sinusoidal half cycle of arc current with horizontal lines whose length is proportional to the average arc lifetime at the specific current level. The length of the lines was derived from Figure II.B.6.

On average, when a certain amount of time equal to the arc lifetime passes, the arc suddenly interrupts: that is the meaning of the arc lifetime. The sudden arc interruption is the phenomenon of a current chop. In an otherwise sinusoidal current, when the value of the current reaches a sufficiently low value, the current drops abruptly to zero: it "chops" to zero, hence the name. The importance of this parameter lies in the inductive voltage rise associated with a sudden change in current. The inductive voltage is: $V = L\, dI/dt$, assuming values for the circuit inductance of $L = 100$ uH and current rate of change $dI/dt = 10$ A/us gives a voltage of $V = 1000$ volts, well above the value of the anode-cathode drop voltage.

In the absence of chopping phenomena, the plasma would decay with the diminshing sinusoidal current. At a normal current zero, this plasma would disperse due to its thermal energy and time of flight characteristics. Two different scenarios can subsequently occur; neither is desirable. When a current chop event occurs, a large voltage can appear across a plasma which has not had time to decay with the normal sinusoidal current. The net result is plasma re-ignition and current interruption is not achieved. The second scenario is the case where the arc current <u>does</u> interrupt. This forces the inductive voltage to appear across equipment which may not have been designed to

withstand a high voltage. This, obviously, is a safety hazard.

The two important parameters in a chopping event are (1) the electrode material, and (2) dI/dt near a current zero. For the specified material, the latter parameter allows estimation of the expected time remaining in the discharge which is to be compared to the arc lifetime at the chosen current level. This process converges to a "chop current" in a non-linear fashion due to the sharp dependence on current exhibited by the arc lifetime, as shown in Figure II.B.6. It should be remembered that the rate of change of the current is intimately connected with the chopping event; however, for estimation purposes, the order of magnitude of chopping current is roughly 10 A at a frequency of 60 Hz.

Figure II.B.8

ARC LIFETIME SIGNIFICANCE

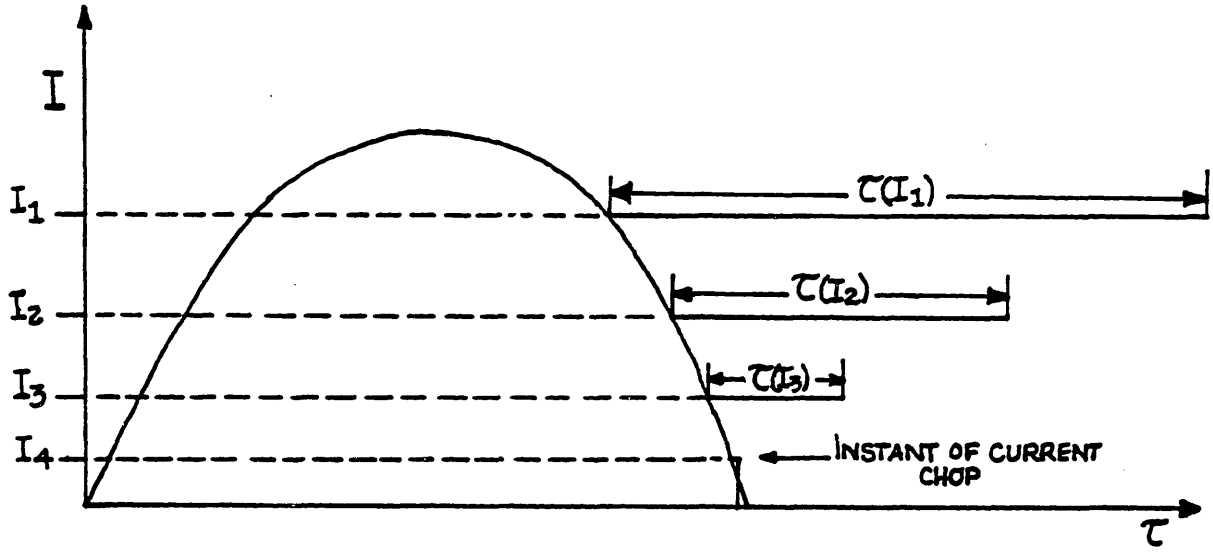

II.B.8 Electrical Conductivity

Resistive power is dissipated in the electrode proportionately to the reciprocal conductivity. Although this is a minor factor in the power balance for ordinary metals, it prevents some more exotic materials from useful implementation.

II.B.9 Thermal Diffusivity

The ability of the bulk electrode internally to distribute the intense energy flux deposited at the electrode surface depends on the thermal diffusivity. Hence, cool-down between single shots or burst of shots could conceivably be limited by the diffusivity. A correlation between a thermal parameter and gross anode melting has been noted by Rich

[Rich, et al, 1971]. That research group found, for a fixed geometry and frequency, the critical current (i.e. that current which caused bulk melting) increased roughly proportional to the thermal "goodness" parameter $k_{th} T_m/(\alpha)^{1/2}$.

II.B.10 Mechanical Strength

We have seen that the electrical breakdown strength has been related to the mechanical strength through the Young's moduli. There are, however, other reasons to use a high strength material. Large Lorentz forces may be generated by interaction of the substantial currents and either self- or externally-generated magnetic fields. In our particular device the electrode has been slotted along the z-axis to improve the interruption characteristics as discussed in section III.D. The result is cantilevered "fingers" which carry the current. In designs such as ours, choosing a material with good mechanical characteristics is an important consideration.

II. Plasma Physics

II.C.1 Plasma Processes

To a large measure the arc properties are determined by the cathode processes and material. As one increases the discharge current, however, the plasma, which envelopes the cathode spots, plays an ever more important role in the evolution of the arc. Taken to an extreme, this can easily be seen by considering atmospheric, or even higher pressure, gas gaps. The essential difference is the lack (or presence) of an ambient environment which can contribute current carrying (ionized) particles. As the desire and capability to use greater and greater current grows, the field of arc discharges will enjoy renewed attention. Therefore, in this section we consider the various plasma properties and processes.

The plasma surrounding a metal vapor arc has long been a source of experimental uncertainty. Compton, in early arc discharge work [Compton, 1931], performed experiments in order to investigate plasma properties in an arc. Much has been done since then, yet, the field is still in somewhat of a confused state. The lack of effective information transfer from the realm of the physicist to the hands of the engineer is, in my view, the primary cause of this confusion. Therefore, to the end of improving the transfer

of information, a rather fundamental viewpoint is taken in this section so that the salient points do not become bogged down in details.

Plasma Definition

A plasma may be defined as a collection of particles of which a substantial fraction have a net electrical charge. A further qualification of plasma is that there must be a large number of charge-carrying particles in a sphere of radius equal to the Debye length. The Debye length is discussed shortly. Electric and magnetic fields exert forces on the plasma particles in proportion to the net particle charge.

Coulomb Force

Fundamental to plasma physics is the Coulomb force. The Coulomb force is the force experienced by a charged particle (simply referred to as a "charge") as a result of an electric field. This is true whatever the source of the field: an external source or another charged particle. An isolated charge will affect another charge anywhere in infinite space. The Coulomb force is said to have an infinite range, that is, charges very far away from each other can influence one another. This aspect of plasmas, which causes long range organized plasma oscillations, allows them to behave in seemingly strange ways. Collective

motions of the plasma are ubiquitous; much theoretical work has been done in order to understand the collective modes of plasma. It is beyond the scope of this section to present the results of the work concerning plasma collective modes.

Debye Length

The response of charged particles to an electric field is to "shield" or cloak the source of the field from the rest of the plasma. This phenomenon occurs over a certain spatial scale and a certain temporal scale. The spatial scale is called the Debye length, which is, roughly, a measure of the sphere of influence of a plasma particle. The reciprocal of the temporal scale is called the plasma frequency. The plasma frequency is the maximum oscillation frequency of a plasma; any slight charge imbalance is nullified in a time of order 1/(plasma frequency). The product of the Debye length and the plasma frequency is the characteristic particle velocity.

Even at this early point in the development of the description of plasma there appears to be contradiction. On one hand the Coulomb force is of long range, and, on the other hand, the Debye length limits the sphere of influence of a charge. These concepts are not contradictory, of

course, but complimentary. In response to an electric field, caused by a charge imbalance placed in a plasma, an amount of charge equal in magnitude but opposite in sign to the imbalance localizes near the source of the imbalance. Hence, when viewed from a distance greater than the Debye length from a charge imbalance, no imbalance is detected: the plasma has "shielded" the imbalance. Figure II.C.1 schematically shows this shielding phenomenon. It is important to note that we have not depended on mechanical collisions with any particle of any kind; the particles need be aware of each other solely by the existence of their pervading electric fields.

Figure II.C.1

DEBYE SHIELDING

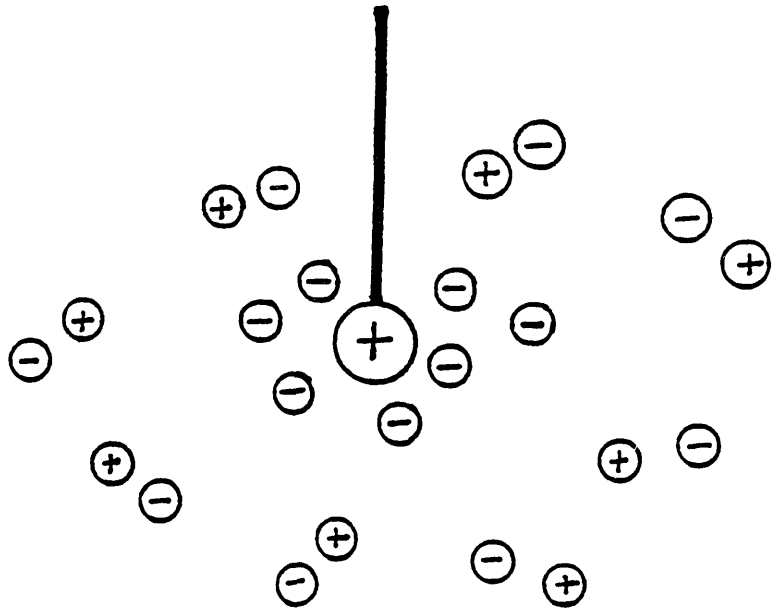

The equation for the Debye length is given below:

$$L_D = \sqrt{\frac{kT}{4\pi ne^2}}.$$

We briefly discuss the parameter dependence of the Debye length. (Because the electrons perform the majority of the shielding function due to their smaller mass we confine ourselves to discussing electron parameters.) From Maxwell's equations we know Div E = 4 ne^2. For order of magnitude purposes, E = V/L_D (we have anticipated the identification of the scale length with the Debye length L_D). Then Div E = V/L_D^2. Using the equation for L_D we find the order of magnitude of voltage is V = kT/e.

This represents the (scale) voltage variation which may occur over distances of order L_D; if we attempt to impose externally a voltage greater than kT/e, the plasma shields the voltage within a distance of L_D. This has a very important implication for vacuum arcs: the potential differences which occur in the arc column occur in a distance of order L_D. Calculation for typical arc parameters shows that L_D is quite small - typically of order 10^{-5} cm. Since the arc column itself is much longer

than L_D, the majority of the voltage drop occurs over a comparatively small distance and only a small voltage drop occurs over the bulk of the distance. Hence, only a small electric field exists over most of the arc column. Early experimenters seemed quite intrigued by this result [Compton, 1931]. A large electric field at the plasma edge results from the concentration of the voltage drop over a relatively short distance. As we have mentioned in Section II.B, this has implications for field-enhanced electron emission for electrode materials.

The other significant parameter in the formula for the Debye length is the plasma density n. As n increases the Debye length decreases; physically the explanation is that more electrons are available in a given volume to take part in the shielding and so shielding occurs in a shorter distance. As a parenthetical note it may be noticed that the charge of the shielding particle enters the expression for L_D. Particles with a greater charge shield more effectively.

In summary, the plasma shields an externally imposed voltage in a distance of order L_D.

Ionization

Ionization occurs when an electron from a previously

neutral particle obtains sufficient energy to overcome the ionization potential. The departure of one electron leaves a net charge of +1 on the new ion. Ionization can occur multiple times in order to create particles with net charges of +2 or +3 and so on. Accumulation of sufficient energy to overcome the ionization barrier need not occur in a single collision. In fact, it can be shown [Zel'dovich and Razier, 1966] that atoms initially pass through excited states. Hence, it is subsequent collisions of excited atoms with energetic electrons which produce ionized particles [Compton, 1931]. This process can be schematically written as in Figure II.C.2.

Figure II.C.2

PLASMA COLLISIONAL PROCESSES

$A + \underline{e}$	$\rightarrow A^+ + 2e$	(ionization)
$A^* + e$	$\rightarrow A^+ + 2e$	(excited atom ionization)
$A^+ + e$	$\rightarrow A + h\nu$	(radiative recombination)
$A^+ + e + e$	$\rightarrow A + e$	(ion-electron-electron recomb)
$A^+ + B + e$	$\rightarrow A + B$	(ion-neutral-electron recomb)
$\underline{A}^+ + A$	$\rightarrow A^+ + \underline{A}$	(charge exchange)

The charge state of the ion is indicated by the (+). An energetic particle is underscored, and an atom in an excited state is denoted by an asterisk.

Recombination

The process of ionization has a logical reverse process: that of recombination. As discussed in Section II.A, different types of recombination are of differing relative importance in different regimes of the plasma parameters. Three types of recombination are shown in Figure II.C.2. At material surfaces the ion-neutral-electron recombination is most important and in the plasma volume the radiative and ion-electron-electron recombination are most important.

Charge Exchange

The charge exchange process is schematically shown in Figure II.C.2. In contrast to ionization and recombination, charge exchange does not change the relative populations of the interacting species. Instead, charge exchange changes the energy distribution of the species. As indicated by the underscore in Figure II.C.2, an energetic ion collides with a neutral and gives the neutral the excess energy. Alternatively, an electron leaves the neutral and attaches itself to the ion. In either event, the result is to produce an energetic neutral and a low energy ion. We mention this process because in the discussion of the potential hump the lack of observed charge exchange neutrals [Davis and Miller, 1969] has implications on the

spatial volume occupied by the high energy ions.

Radiation

The power balance aspects of radiation have already been discussed in Section II.A. What has not been discussed is the emission process.

Bremsstrahlung is the radiation produced by charged particles. A particle with a net charge radiates energy when accelerated. When two charged particles influence each other through their Coulomb fields they radiate according to their acceleration. The most common example is the attractive force between an assumed stationary ion and a moving electron. The electron is deflected from a straight-line path due to the Coulomb force, hence is accelerated and hence radiates energy.

The existence of excited atoms implies radiation at specific wavelengths according to the particular excited neutral atom. This type of radiation is called line radiation because only specific lines or wavelengths are emitted. If the excited atoms radiate too quickly, they are not in an excited state long enough for a subsequent collision to ionize them. If the excited atom attains a meta-stable state then the intensity of radiation will be small because the transition rate is small. Hence, the

significance of radiation will vary according to the characteristics of particular atoms. Because such atoms originate at any available surface they are frequently impurities and the resulting radiation is called impurity radiation.

Any material at a finite temperature radiates energy according to the black-body formula. The plasma temperature is in excess of 12,000 K. Thus, the reader may assume the radiation emitted would be quite large. However, because the arc-plasma is optically thin, the amount of black-body radiation is almost insignificant; if the plasma were optically thick, black-body radiation would be a significant arc cooling mechanism.

Collisionless-Collisional Effects

Interruption of vacuum arcs is observed to occur very quickly when an already low current density arc passes through a zero value of current [Lafferty, 1966]. This observation is in contrast to the relatively lengthy interruption time for gas gap switches.

A high pressure gas gap arc must rely upon volume recombination in order to quench the plasma. Essentially, the charged particles have a lifetime which is several milliseconds long. Voltage recovery must await the extinction of the charge carriers, else the arc re-ignites.

As stated previously, the metal vapor vacuum arc switch relies upon surface recombination in order to quench the vacuum arc. Two physically distinct processes must occur for this surface recombination to extinguish the arc on a time scale faster than gas gap extinction.

The first process which must occur before vacuum arc extinction is the transport of the plasma to a material surface. This fundamentally can happen in an ordinary collisional process or it can happen as a time-of-flight process. In the low density plasma (as opposed to the dense cathode spot regions) the mean free path for atoms can be greater than 1 mm. This means that the plasma has roughly

ten collisions tranversing the 1 cm electrode gap. This can be described by either a collisionless or collisional theory. Because the number of collisions is small, the results of the two theories do not differ greatly. Essentially, then, particles leave the interelectrode gap with nearly the time-of-flight speed [Miller, 1971]. The thermal velocity is of order 10^6 cm/s [PR&K, 1965; and D&M, 1969]. Thus approximately 1 us is required for the plasma to vacate the gap. Our model of the arc as a quasi-collisionless plasma therefore accounts for the experimentally observed extinction times. Moreover, similar gas gap calculations clearly show the effect of a diffusion dominated process. Figure II.C.3 shows the comparitive calculation for a collisionless theory and collisional theory for vacuum arcs, and the collisional theory for gas gaps.

Figure II.C.3

COLLISIONLESS AND COLLISIONAL THEORETICAL RESULTS

<u>Vacuum Arcs</u> ($n = 10^{16}$ cm^{-3}, $v = 10^6$ cm/s)

$t_{collisionless} = d/v = 1$ us

$t_{collisional} = d^2/4D = 2$ us

<u>Gas Gaps</u> ($n = 10^{19}$ cm^{-3}, $T = 1000$ K)

$t_{collisional} = d^2/4D = 1$ ms

Another aspect of interparticle collisions is that of collisions between different species. We have already seen Bremsstrahlung radiation as an example of inter-species collisions.

A logical question, then, concerns the length of time between collisions for the plasma particles. If we assume, temporarily, that the plasma is 100% ionized (no neutrals to worry about) then there are three important collision times: (1) electron-electron collision time, (2) ion-ion collision time, and (3) electron-ion collision time. The above times are listed in increasing order. The large mass ratio of m_i/m_e is responsible for the variation in collision times. The time scale of interest determines the significance of the relative collision times.

The important events of a vacuum arc occur in times of order magnitude microsecond. Cathode spot formation and arc extinction, as we shall see, are examples of events which occur in a few microseconds. The electron-electron and ion-ion collision times are substantially less than a microsecond for typical plasma parameters. The electron-ion collision time, however, is of order microseconds. This has

the implication that the electrons and ions have reached an equilibrium state individually, but they are not in equilibrium with each other. The energy and momentum states of the electron and ion distribution functions are not yet coupled on these time scales: the different species have not had time to "know" about the other species.

As a result, the electrons and ions have quite different energy distribution functions. The electrons have a very fast collision time and so are described approximately by a Maxwellian distribution function with a well-defined temperature. The ions, having a collision time varying as the square of the mass ratio, have a quite different distribution function. However, it is not a Maxwellian distribution function [PR&K, 1965]. Thus the temperature of the ions is not well-defined. The average energy per ion is still a valid concept and it is to this that one must refer for meaningful information concerning the ions. The next section gives approximate collision times in order to give the reader a feeling for the times involved.

Potential Humps

Tanberg [Tanberg, 1930] was the first researcher to systematically investigate the flux of high energy ions from a vacuum arc. More recently, PR&K [PR&K, 1965] and Davis and Miller [D&M, 1969] conducted extensive studies of high

energy ions. They measured ionic states of several different ions, finding multiple ionization states. They also measured the energy of the ions. The existence of a source of high energy ions, therefore, seems well established. It has been suggested [PR&K, 1965] that a localized region of high potential exists which supplies these ions. The concept of a potential "hump" offers an explanation of the existence of high energy ions. A sketch of the potential hump profile is shown in Figure II.C.4.

Figure II.C.4

POTENTIAL HUMP PROFILE

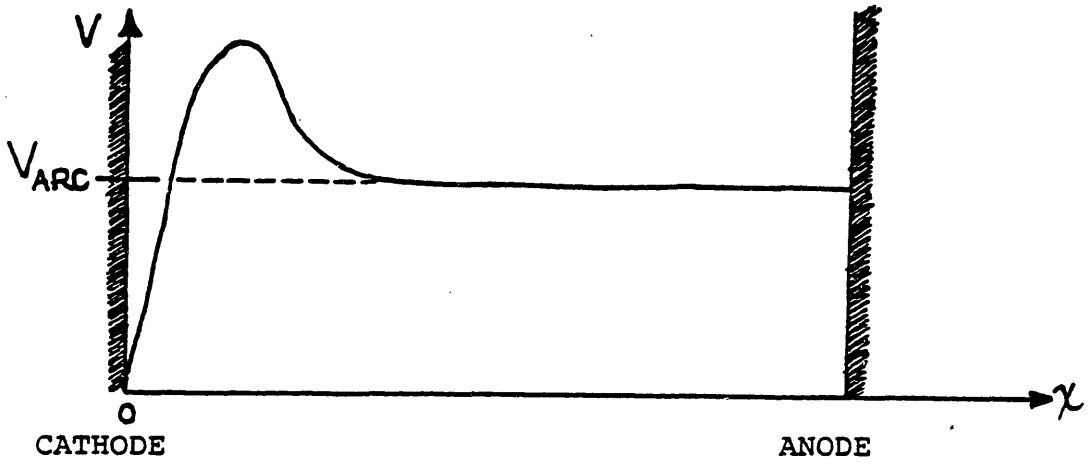

As the current is increased, the formation of an anode potential hump seems possible and has been suggested by PR&K [PR&K, 1965]. Figure II.C.5 shows schematically the form for an anode potential hump.

Figure II.C.5

ANODE POTENTIAL HUMP FORM

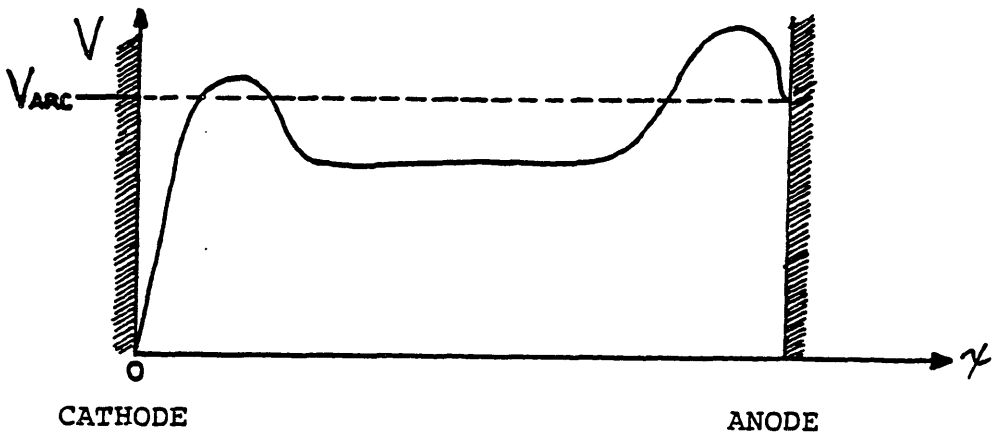

According to Mitchell [Mitchell, 1970], when the arc voltage is greater than the ion kinetic energy, cathodic ions are prevented from reaching the anode. "Ion starvation" results and the arc voltage rises. This creates a region of intense ionization immediately in front of the anode. This mechanism would [Mitchell, 1970] cause an anode potential hump.

We should emphasize that corroborating evidence for anode potential humps is required before their presence is assured.

In Section II.E.5 we give a theory of potential humps in some detail. Two cases of quasi-collisionless and collisional plasma are considered in that section.

II.C.2 Plasma Characteristics

In this section we list the numerical values typical of vacuum arc plasmas. The rationale for doing this is to give the reader some idea of the order of magnitude of the parameters and also to indicate that there is a wide variation of these parameters (orders of magnitude, in some cases) in different regions of the arc. Examples of widely varying parameters are the neutral density, and the cathode energy fluxes.

Figure II.C.6 shows some typical plasma parameters. Note that, where appropriate, we specify the region of applicability.

Figure II.C.6

VACUUM ARC PLASMA PARAMETERS

electron temperature - 2 ev (20,000 K)
ion energy (averaged) - 30 eV
electron-electron collision time - 0.2 ns
ion-ion collision time - 10 ns
electron-ion collision time - 200 ns
Debye length - 10^{-5} cm
plasma frequency - 300 GHz
plasma density - near electrode - 10^{18} cm^{-3}
- in gap - 10^{16} cm^{-3}
gap mass density - 10^{-5} g/cm^3
current density - 5×10^6 A/cm^2

Thus, in a microsecond, an average electron would have had

5000 collisions with other electrons; an average ion would have had 100 collisions with others ions; but the average electron and ion would have collided only 5 times. Note that these collision times scale roughly as the square root of the mass ratio [Braginskii, 1965].

II.D Interruption Mechanics

II.D.1 Natural Commutation

Metal vapor vacuum arcs will naturally tend to interrupt themselves by a variety of processes unless the plasma is continually being regenerated due to power dissipation in the switch. Some of these interruption processes are: ion recombination, surface recombination, gas dispersion, etc. Once the switch current has gone to zero, either by forced commutation or a natural current zero, power dissipation in the switch instantly vanishes. Switch interruption is then simply a matter of the charge carriers re-depositing on the electrodes or other surrounding surfaces before bulk power dissipation and subsequent plasma generation has a chance to recover. This can be thought of as a simple thermal inertia problem. The thermal inertia of the plasma must be dispersed before a new conduction cycle starts in order to interrupt successfully the switch. For precisely the same reasons that a metal vapor vacuum switch has low losses, it has a very low thermal capacity. This is exactly why a metal vapor vacuum switch has interruption times about three orders of magnitude less than a gas gap switch. Figure II.D.1 summarizes the effects that influence the innate ability of a vacuum switch to interrupt.

Figure II.D.1

FACTORS INFLUENCING NATURAL VOLTAGE RECOVERY

Factor	Effect
vapor pressure	high vapor pressure implies copious vapor emission
peak current	increase in erosion products
electrode purity	thermal expulsion of trapped contaminant gases
current duration	bulk heating of electrode decreases cooling by thermal conduction
$T_m(k\rho Cp)^{1/2}$	increase of erosion products
time rates of change of current and voltage	allowable escape time decreases as rates of change increase
electrode separation	required escape distance increases, condensation solid angle decreases
thermionic emission	emission through current zero, may provide initial electrons which re-ignites plasma
asperite formation	enhanced Fowler-Nordheim field emission
small atomic mass	increased particle velocity

[Farrall, 1980; Kamakshaiah and Rau, 1977, Miller and Farrall, 1965; Rich and Farrall, 1973]

II.D.2 Magnetic Interruption

Instead of relying completely on passive means for plasma

dissipation one can consider using some active means for removing the metal plasma from the gap. Magnetic fields appear to be the ideal way of accomplishing this. Magnetic fields can exert extremely high forces in very short time scales. For example, in our lab we have generated in excess of 100,000 pounds thrust in a five microsecond period [Mongeau, 1981]. Furthermore, magnetic fields can exert these forces at a distance thus avoiding the problems of obstructing the arc during normal conduction or of contaminating the vacuum environment. In addition, electrical control allows active intervention with precise timing.

Most work to date with metal vapor vacuum arcs in magnetic fields has involved the use of quasi-steady state fields [Graneau, 1981; Poeffel, 1980; Heberlein and Gorman, 1980; Gilmour, 1980]. The background magnetic field is generally used to spread and distribute the arc over the entire electrode surface area thus preventing intense heat spots and so postponing the formation of arc channels and the consequent creation of gross melting. The background field extends the current-carrying capabilities of the switch beyond passive interruption levels of operation.

A much more dramatic use of magnetic fields involves the literal removal of the metal plasma from the gap during

commutation. In this mode Lorentz forces ("J cross B") act on the plasma directly, either simply evacuating the gap region or increasing the arc length if there is a vestigial current flow and thereby increasing the effective voltage drop of the gap. Since this arc manipulation is desirable only during the interruption phase, one must use pulsed magnetic fields to achieve the desired interruption time.

All Lorentz forces require both a current and a magnetic field. In a vacuum arc, one can use the normal discharge current as the source current and the self-field it generates as the source field. This is the mechanism used in the "instability" interrupted switches [Schoenbach, 1981]. Alternatively, currents can be generated by inducing an additional current in the switch-plasma that does not in itself contribute to the switch current. Similarly, source fields can be generated by external coils which do not rely on the self field of the switch. Four combinations of J cross B forces can be generated depending on whether the current J is an arc current or an induced current, and the field is either a self field or an external one. Figure II.D.2 summarizes these four approaches for the coaxial geometry where the electrodes are like two cups facing each other.

One should keep in mind from the figure that for the cases employing the normal arc or self field, the Lorentz force will go to zero during a natural current zero. This is useful for interrupters which interrupt near a current peak. However, such a mode of operation is unfeasible for normal commutation. Therefore the only configuration in Figure II.D.2 which can operate as a commutator is case 4 where both the source current and field are not dependent on the main arc discharge conduction current, being generated by an outside coil. This is the configuration on which we have elected to experimentally concentrate. Although there are other geometries which can magnetically commutate (such as rectilinear) the coaxial one appears to be best because of its structural simplicity and high strength.

Figure II.D.2

MAGNETIC-INTERACTION CONFIGURATIONS

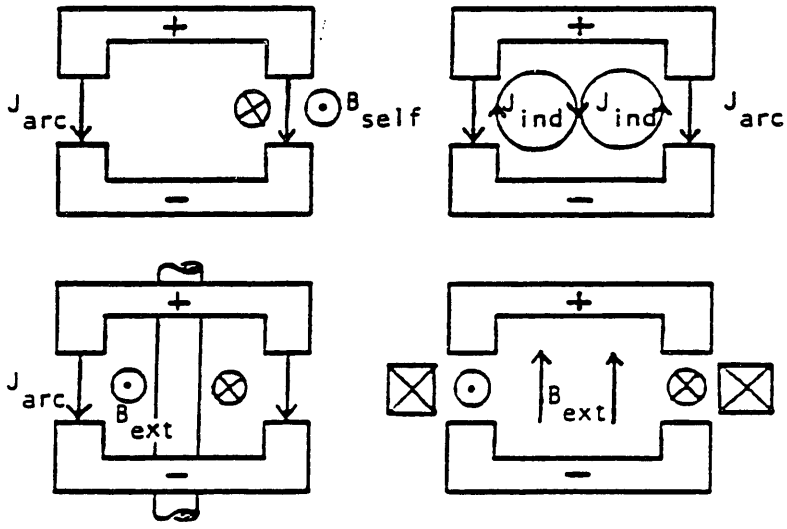

II.D.3 Kinematic Interruption Analysis

Given a complete detailed design of the final experimental configuration and all the relevant parameters, it is relatively straightforward to analyze the exact kinematic response of the gap plasma in response to a pulsed magnetic field. An electrical schematic of the magnetically aided switch system is shown in Figure II.D.3. A simplified calculation is very informative and is presented for purposes of introduction. Appendix C presents a more detailed calculation; the present calculation, however, contains the fundamental physics. Essentially, the analysis is equivalent to finding the induced current in a shorted transformer secondary which in our case is the gap plasma. Once the current is established we simply apply the Lorentz force generated by the pulse coil to find the time it takes for the plasma to be swept clear of the gap region. Using characteristic plasma parameters we find a sweep time of less than ten microseconds can be accomplished with a field of about one kiloGauss.

Figure II.D.3

SIMPLIFIED SWITCH SCHEMATIC

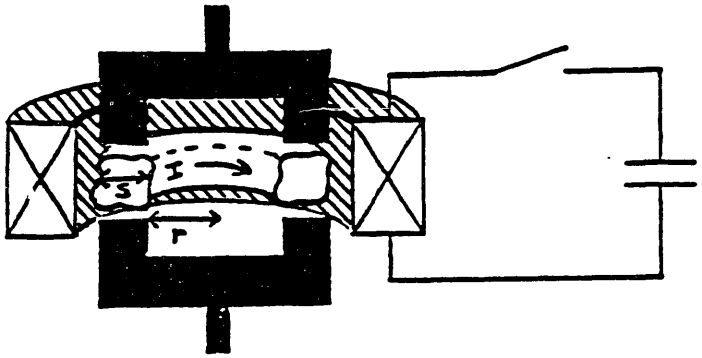

The pulse coil is driven by an auxiliary capacitor bank. The voltage induced in the secondary, which in this case is the plasma itself, can be expressed as:

$$V = d\phi/dt = \frac{\pi r^2}{C} dB/dt \ .$$

Assuming a sinusoidal excitation frequency ($w = 2\pi f$), the complex amplitudes are:

$$V_O = \pi r^2 \, wB_O k$$

This voltage generates an induced current:

$$V_O = I_O \, Z \ .$$

Z is the complex impedance expressed as:

$$Z = \sqrt{R^2 + (wL)^2} \ ,$$

where R and L are the plasma torus resistance and inductance, respectively. The radial force density acting on the plasma is:

$$f = \rho a = J \times B/c = IB/(s^2 c) .$$

For the "back of the envelope" calculation it is sufficient to assume an average acceleration equal to one-half the peak acceleration. (Appendix C does not make this assumption; an allowance is made for radial variation of several of the above parameters.) Assuming a constant average acceleration, the distance, d, the plasma is accelerated in a time t is:

$$d = I_0 B_0 t^2/(4\rho s^2 c).$$

Combining the above equations we arrive at the minimum magnetic field amplitude B_0 necessary to displace the arc in the specified interruption time:

$$B_0 = \frac{2}{t}\left[\rho d s^2 c^2 \sqrt{R^2 + (wL)^2}/\pi r^2 w\right]^{1/2} .$$

This minimum field is plotted as a function of excitation frequency with interruption time as a parameter in Figure II.D.4. At large frequencies the minimum field reaches an asymptotic limit of:

$$B_o = \frac{2}{t}\left[\frac{\rho ds^2}{\pi r^2}\right]^{0.5} .$$

Figure II.D.4

MAGNETIC FIELD REQUIREMENT

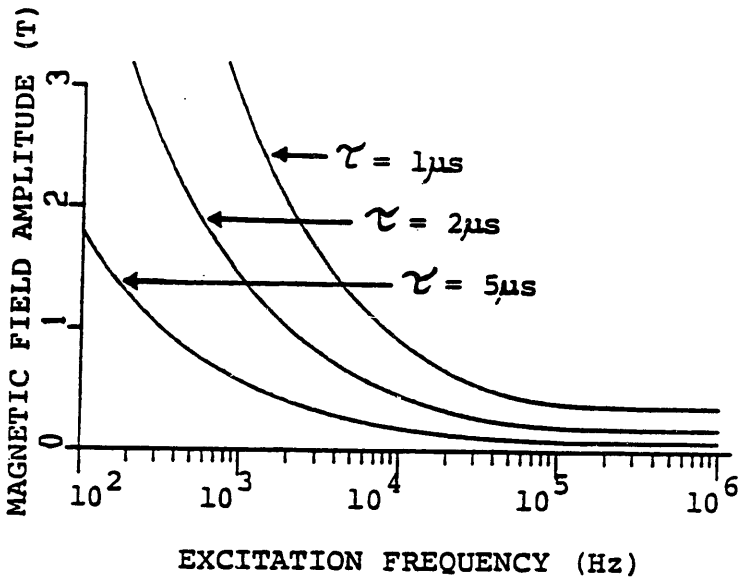

These asymptotic fields are of order of a few kilogauss and are readily generated externally.

II.E Theoretical Extension

In this chapter we inveatigate several aspects of the theory of arcs. We attempt to explain phenomena which either have not previously been explained or we provide alternative explanations for phenomena for which confusing or unphysical explanations exist.

Because, in a particular situation, we wish to create as simple a model as possible yet retain the essential physics inherent in the situation, we frequently rely on well-established experimental results. An example is our use of the experimentally observed average cathode spot current for metals. We use this information to demonstrate the usefulness of our model, by, for instance, showing agreement between theoretically predicted results and experimental results.

The topics chosen include one time-dependent phenomenon which occurs very early in the discharge, two phenomena which are quasi-static, and a final phenomenon which occurs during extinction of the discharge. In essence, this section amounts to examing four special cases of the power balance discussed in Section II.A. We consider the different physical conditions which dominate each situation.

II.E.1 Cathode Spot Radius and Formation Time

We postulate adiabatic heating of the cathode spot. Adoption of a simple one dimensional model leads to the following equation for energy balance:

$$U = P\ t = M_{spot}\ Cp\ T,$$

where, $M_{spot} = \rho V = \rho A\ x.$

The scale distance (i.e. the spot radius) is x. Figure II.E.1 shows the one dimensional model. The distance at which a specified temperature is obtained is denoted by x_T.

Figure II.E.1

ONE DIMENSIONAL MODEL FOR CALCULATIONS

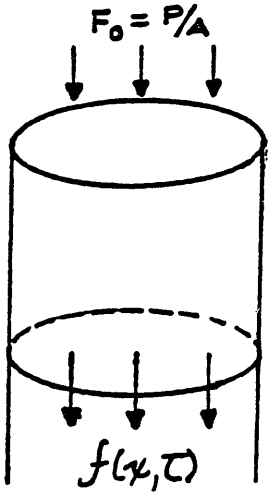

The above equation applies immediately after the arc initiation; before other loss mechanisms become

significant. The one dimensional model is applicable to the extent that:

$$x < \sqrt{(A/\pi)} \ .$$

The heat flux at the spot surface is assumed constant and equal to $F_O = V_i J_+ = V_i I_+ / A$.

The one dimensional solution for the heat flux is given by Carslaw and Jaeger [Carslaw and Jaeger, 1980]:

$$f(x,t) = F_O \ \mathrm{erfc}(x / 2\sqrt{(\alpha t)})$$

where, $\alpha = k/\rho Cp$.

This equation shows that at $x_D = 2\sqrt{(\alpha t)}$, $f(x_D) = 0.16\ F_O$. The scale distance for Diffusion is x_D. A graph of erfc(z) is shown in Figure II.E.2.

Figure II.E.2

GRAPH OF $f(x,t)/F_O = \mathrm{erfc}(z)$

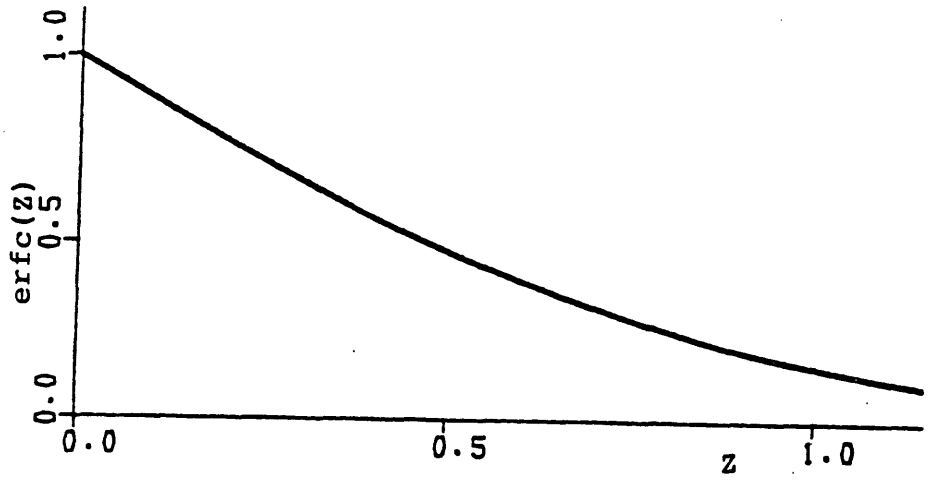

As a reasonable approximation to the temperature T we use the material boiling temperature under one atmosphere of pressure: when $T = T_B$; then $x_T = x_B$.

The condition of adiabatic heating to the boiling point imposes the constraint that $x_B \geq x_D$. However, if $x_B > x_D$ we must include the energy involved in the latent heat of vaporization, which is the largest contributor to the phase change energy. We do not include the latent heat of vaporization in this calculation - we merely heat the material up to the boiling point. In sum, our requirement is:

$$x_B = x_D = x_{crit} \text{ ; this occurs at time } t_{crit}.$$

Our two equations in two unkowns (x_{crit} and t_{crit}) are:

$$x_{crit} = 2\sqrt{(\alpha t_{crit})},$$

and

$$t_{crit} V_i J_+ = x_{crit} \rho Cp(T_B - T_{amb}).$$

These equations are graphed in Figure II.E.3

Figure II.E.3

DIFFUSION AND BOILING DISTANCES VS. TIME
(ONE DIMENSIONAL MODEL)

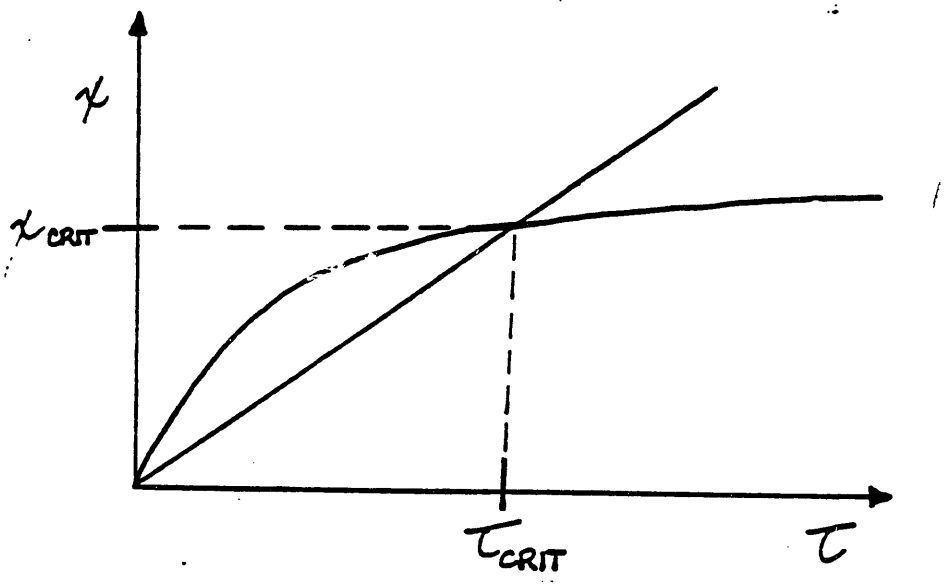

The solution to these equations is:

$$x_{crit} = 2\alpha\left[-\rho\frac{C_p\Delta T}{V_i J_+}\right],$$

$$t_{crit} = 2\alpha\left[-\rho\frac{C_p\Delta T}{V_i J_+}\right]^2.$$

We identify $x_{crit} = r_{spot}$; that is the spot radius is determined by adiabatic heating. Beyond the critical radius (within the constraints of a one dimensional model) the metal tends to boil away faster than the heat diffuses to it - hence we have adiabatic heating. The time scale of spot formation predicted by our model is t_{crit}. Figure

II.E.4 shows x_{crit} and t_{crit} for a variety of metals. The input energy flux is that which is experimentally observed. Hence, our analysis is self consistent - given experimentally observed input parameters, we are able to predict other parameters which are also experimentally observed. This strongly suggests that our model does actually apply to the real physical situation.

Figure II.E.4

TABLE OF CRITICAL DISTANCES AND TIMES
(ONE DIMENSIONAL MODEL)

Metal	x_{crit}	t_{crit}
Al	10 um	0.6 us
Ag	20 um	1.0 us
Cu	20 um	1.7 us
Fe	5 um	0.4 us
Ni	5 um	0.6 us
W	15 um	2.0 us

The results of this simplified calculation allow significant conclusions in spite of the limitations of the model. If the identification of x_{crit} as the spot radius is made, the agreement with the experimental cathode spot radii is quite close. (See Figure II.A.5 for characteristic cathode spot parameters.) Furthermore, if the identification of the spot formation time is taken as

t_{crit}, then the times listed in Figure II.E.4 are of the correct order of magnitude, but are too small by a factor of roughly 2 to 3 compared to observations made by Grissolm and Newton [Grissolm and Newton, 1974]. Although they were investigating anode spots, they calculated an energy flux of 10 mega-Watts per square centimeter incident upon the surface of the electrode. This is the same magnitude of flux used in our case; our one dimensional model does not distinguish between an anode spot (radius of order 1 cm) and a cathode spot (radius of order 10^{-3} cm) when they have the same input energy flux. Agreement to within this factor is considered acceptable. The physical interpretation of this too-rapid spot formation is the lack of appropriate spot cooling mechanisms. This stems from the limitations imposed, for simplicity, on the model. If one were to extend the model to include all time-varying cooling mechanism, then the spot formation time would certainly be larger than that given in Figure II.E.4. This physical model, however, has validity and its beauty lies in its simplicity. Additionally, the results of the model are actually in reasonable agreement with experimental measurements.

In summary, we consider the application of a constant energy flux to a localized area. Initially the thermal heat

flux via conduction is large; however, as time progresses the rate of advancement of heat flux slows: after a time t the flux has diffused a distance $x_D = 2(\alpha t)^{0.5}$. The total energy deposited on the area increases linearly in time. This energy raises the temperature of the thermally active material to approximately the boiling point. Because the total energy increase linearly in time but the volume of heated material increases only as the square root of time, the heated volume increases in temperature. If, at time t_1 the volume averaged temperature is T_1, then at time $4t_1$ the volume averaged temperature is $2T_1$. This process continues until the temperature of the heated region reaches the boiling point. This state is described by x_{crit} and t_{crit}.

A parallel situation commonly encountered in the home occurs when a stick of butter is pushed into a hot frying pan. The butter heats adiabatically - not by heat conduction through the mass of butter.

II.E.2 Ablation Theory

We have developed a simple theory describing material loss from the cathode due to an intense energy flux. It is essentially a steady-state energy balance. Mathematically, the model is formulated in a coordinate frame moving with the receding surface. This has the effect of producing a temperature profile which appears stationary to the moving observer.

Analyses of this type are quite common in problems where there is relative motion of a "fluid" (the ablating surface) and a lab coordinate system. Specifically, the model is mathematically identical to the space craft re-entry problem. In the re-entry problem the heat shield is designed to ablate as a cooling mechanism for either the spacecraft's occupants or instruments. In the vacuum arc problem, the cathode material ablates as a cooling mechanism to the cathode spot. As we shall see, the one dimensional model predicts the surface recession velocity. The surface recession velocity allows calculation of an effective ablation coefficient. The theoretical ablation coefficient may then be compared with experimental ablation coefficients. The ablation coefficient multiplied by the

number of Coulombs passed through the device yields the amount of removed material. In general, the results show reasonably good agreement for all metals except refractories. The reasons for discrepancies concerning the refractories stem from the simplifying assumptions of the model and are discussed.

We assume an intense energy flux. The problem is idealized as a one dimensional steady state model. The energy "reservoir" is the total enthalpy change experienced by the metal. The total enthalpy change includes the temperature rise of the metal, the phase change energies of the metal, and the ionization of the ablated vapor from the cathode spot.

Figure II.E.5 shows the model used for calculations.

Figure II.E.5

SCHEMATIC FOR ABLATION CALCULATIONS

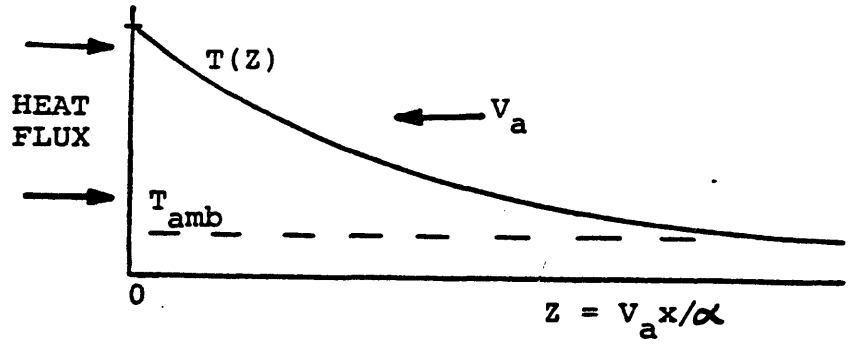

The one dimensional heat equation is:

$$\rho C_p \frac{dT}{dt} = \rho C_p \left(\frac{dT}{dt} - V_a \frac{dT}{dx} \right) = \frac{d}{dx} k \frac{dT}{dx}$$

In steady state we have:

$$\frac{d}{dx} k \frac{dT}{dx} = -V_a \rho C_p \frac{dT}{dx}$$

Applicable boundary conditions are:

$$T(x=0) \leq T_{boil} , \quad T(x=\infty) = T_{amb} ,$$

$$dT(x=\infty)/dx = 0 .$$

Integrating the steady state heat equation once we find:

$$k \frac{dT}{dt} = -V_a \rho C_p T + C_1$$

The boundary condition at $x=\infty$ allows evaluation of C_1:

$$C_1 = T_{amb}$$

A second integration yields:

$$ln(T - T_{AMB}) = \frac{-V_a x}{\alpha} + C_2$$

where $\alpha = k/\rho C_p$.

The boundary condition at x=0 allows evaluation of C_2:

$$C_2 = \ln (T_{boil} - T_{amb}) .$$

The expression for T(x) can then be written as:

$$T(x) - T_{amb} = (T_{boil} - T_{amb}) \exp(-V_a x/\alpha).$$

The net heat flux is that in excess of the ablated, vaporized mass:

$$F_{net} = F_0 - \rho V_a H_{abl} = -k\, dT/dx = \rho V_a C_p (T_{boil} - T_{amb})$$

This energy conservation equation can be solved for the surface recession velocity V_a:

$$\rho V_a = F_0/[H_{abl} + C_p(T_b - T_a)].$$

Here $H_{abl} = H_{fg} + fH_I$, where H_{fg} is the phase change energy, H_I is the ionization energy, and f represents the ionized fraction of the evolved vapor.

The quantity ρV_a is numerically equal to the number of grams of ablated material per square centimeter per second. Experimentally one can determine the mass lost from the cathode, X, per Coulomb of charge passed through the device. The value of X is assumed constant for a given material. This is easily understood when the following is realized: (1) several cathode spots burn in parallel with a certain maximum current per spot, and (2) the thermal inertia of the spot is quite small. By (1), increasing the total current merely increases the number of active spots

but has little influence on the spots already established. Point (2) means that for times greater than a few microseconds the spot has reached a quasi-steady stat . Furthermore, it has been demonstrated experimentally that X is approximately a constant for currents less than about 12 kA [Kimblin, 1973; Mitchell, 1970].

The quantities ρV_a and XJ are, then, conceptually identical. Hence, we can determine a theoretical ablation coefficient, X_{th}, and compare it with the experimentally determined coefficient, X_{expt}.

The incident energy flux $F_O = V_i J_+ = 0.1 * V_i * J$, where Kimblin's result of the ratio of ion current to total current was used. The equation which determines X_{th} is:

$$X_{th} = \rho V_a/J = 0.1\ V_i/[Cp(T_b - T_a) + H_{fg} + fH_I],$$

or,

$$X_{th} = 0.1\ V_i/H_{tot}.$$

Parameters required to evaluate X_{th} are given in Figure II.E.6.

Figure II.E.6

EVALUATION PARAMETERS FOR X_{th}

Metal	T_{boil}(K)	V_i(V)	H_{tot}(kJ/g)
Cd	1040	17	3
Zn	1184	13	6
Ag	2436	20	10
Cr	2945	18	33
Cu	2945	20	17
Fe	3135	20	21
Ni	3187	20	22
Ti	3562	20	24
C	4100	20	150
Mo	4880	28	22
W	5828	25	16

Figure II.E.7 details the evaluation of H_{tot}, as given in Figure II.E.6.

Figure II.E.7

ENTHALPY CHANGES FOR ABLATION

Metal	Cp T (kJ/g)	H_{fg} (kJ/g)	fH_I (kJ/g)	H_{tot} (kJ/g)
Cd	0.2	0.94	1.5	3
Zn	0.4	1.9	3.5	6
Ag	0.5	2.4	6.7	10
Cr	1.2	7.0	25	33
Cu	1.0	4.9	11.5	17
Fe	1.3	6.5	13.5	21
Ni	2.9	6.6	12.5	22
Ti	1.7	9.1	13.6	24
C	1.9	60	89	150
Mo	1.2	6.5	14.2	22
W	1.4	4.7	9.4	16

Figure II.E.8 compares the thecretical results with the experimental results for the ablation coefficients of several metals.

Figure II.E.8

ABLATION COMPARISON: THEORY VS. EXPERIMENT

Metal	X_{th} (ug/C)	X_{expt} (ug/C)(a)
Cd	610	650
Zn	225	215
Ag	200	150
Cr	54	40
Cu	120	115
Fe	95	73
Ni	91	80
Ti	80	52
C	13.5	16
Mo	126	47
W	156	62

(a) Kimblin, 1973

Reference to Figure II.E.8 shows that reasonably good agreement obtains between ablation coefficients determined experimentally and ablation coefficients determined theoretically, based on steady state energy balance. The two notable exceptions to agreement are the refractories W

and Mo. It will also be noted that the metals with the lowest boiling point, Cd and Zn, exhibit the most favorable agreement.

The limitations of the model account for this discrepancy. We have neglected the effective work function. Thus, if the electron emission mechanism for typical metals is the so-called "T-F", or field-enhanced thermionic emission [Lee, 1960], and if the temperature required for constant emission current increases with increasing work function, then one may expect the relatively high work function refractories to rely on an electron emission mechanism different than T-F.

Similarly, if the number of emitted electrons increased significantly with respect to the number of ions, then the cooling effect of the effective work function due to these electrons can no longer be ignored. In fact, the experimental data [Kimblin, 1973] indicates electron emission per ablated atom for W and Mo to be about two to three times that of more typical metals (i.e. from roughly 10 electrons/atom to roughly 20 electrons/atom). For brevity, we indicate emitted electrons per atom by the abbreviation e/a. In order to retain the experimentally-determined constant ratio of ion current to total current,

the average ionization state of the ions is also roughly doubled (i.e. from <Z> of about 1 to <Z> of about 2). Because this model does not account for the cooling effect of the work function, it naturally predicts ablation coefficients which are too large for metals which emit a relatively high proportion of electrons. In this case, our predictions are high by about a factor of 2. Comparison of the ratio e/a from Figure II.B.3 with the ablation coefficients of Figure II.E.8, shows improved agreement between our theoretical ablation coefficients and experimental ablation coefficients, as the ratio e/a decreases.

Figure II.E.9 shows this correspondence between e/a and our ablation theory. The figure reveals good agreement between our results and experimental results for an e/a ratio up to 7.0. Fair agreement is obtained for an e/a ratio up to 14.

Figure II.E.9

CORRESPONDENCE OF ABLATION THEORY
AND
EMITTED ELECTRONS PER ATOM

Metal	e/a	X_{th}/X_{exPt}
Cd	1.8	0.94
Zn	3.2	1.05
Cu	5.2	1.05
Ni	6.9	1.14
C	7.0	0.84
Fe	7.2	1.3
Ag	7.9	1.3
Ti	9.6	1.5
Cr	14	1.4
Mo	21	2.7
W	31	2.5

Obviously, a more complicated model could be constructed which would exhibit even better agreement with experimental results. Thus, our model clearly has limitations, but it also has advantages.

The first advantage of the model is its ability to predict theoretical ablation coefficients and obtain good

to fair agreements with experimental results.

The second advantage of the model lies in the model formulation. The model is analogous to spacecraft re-entry ablation models. By formulating the cathode erosion in this way, it is hoped that the essential physics is self-evident and, further, that a useful analytical technique can be transfered between the disciplines of science and engineering.

A third advantage is the additional insight afforded by the model. For instance, Figure II.E.7 shows that the largest contribution to the enthalpy change is that due to ionization. The average ionization state of the plasma clearly has an impact on the magnitude of the energy required for ionization.

Kimblin [Kimblin, 1973] showed that for metals with a wide range of physical properties, the ratio of ion current to total current was a constant roughly equal to, but slightly less than, 10%. He defined an ionized fraction, f, of atoms which are ionized:

$$I_+ = efXI/m \ .$$

Kimblin derives values of f for a wide variety of metals from his ablation experiments [Kimblin, 1973].

Unfortunately, Kimblin does not pursue this concept, except to correct f for an average ion charge. The corrected value f_C is:

$$f_C = f/\langle Z \rangle \ .$$

Physical restrictions are: $\langle Z \rangle \geq 1$, $f_C \leq 1$, $0 \leq f \leq \infty$.

Specifically, Kimblin does not tabulate $I_+/I = efX/m$. This would have tended to reinforce his point concerning the constancy of the ratio I_+/I. Moreover, the fact that efX/m = constant can be used for further analyses.

To the extent that the ionization potential dominates the enthalpy change, we can write:

$$H_{tot} = fH_I \ ,$$

where $H_I = E_I/m$ and E_I is the ionization potential per atom (7.7 eV for copper) and m is the ion mass ($64 \times 1.7 \times 10^{-24}$ g for copper). Assuming f = 100%, we have for copper, H_{tot} = 11.5 kJ/g.

Substituting this equation into our previous theoretical result we have:

$$X_{th} = 0.1\ V_i/fH_I \ .$$

Using this in the defining equation for f we get:

$$I_+/I = 0.1 = efX/m = (ef/m)\ (0.1\ V_i/fH_I)$$

Cancelling terms we find the following equation:

$$E_I = eV_i\ .$$

Thus, in steady state, the energy deposited by each incident ion is sufficient to ablate and ionize an atom creating another ion. This is as it should be: in steady state the plasma is able to regenerate itself exactly.

The fact that Kimblin found the ratio of ion current to total current to be constant for a wide variety of metals means that the incident ion energy is approximately constant, independent of current. That this is true is seen as follows.

The equation below expresses charge and energy conservation:

$$I_+/I = \text{constant} = efV_i\ (J_+/J)/[mf(E_I/m)]\ ,$$

or,

$$I_+/I = eV_i\ (J_+/J)/E_I = \text{constant}.$$

Thus, to the extent that the ratio of the relevant areas, A_+ and A, is constant, we find:

$$A_+/A = \text{constant} = eV_i/E_I \ .$$

It must be remembered that E_I represents a weighted average of the ionization potential. Thus since E_I is constant (for constant $\langle Z \rangle$), eV_i, the incident ion energy, is also constant. Moreover, for typical metals, the second ionizational potential, E_2, is greater than, but of order, twice the first ionization potential, E_1: $E_2 = 2E_1 + \Delta E$. Thus, neglecting for a moment the energy ΔE, we expect that up to $\langle Z \rangle = 2$ the ratio of I_+/I will remain constant. The third ionization potential is usually much higher than $3E_1$, thus as current is increased we eventually would expect the production of ions to be reduced relative to the increase of current. At this point, the ratio of ion current to total current would be reduced.

Reece [Reece, 1963] and Mitchell [Mitchell, 1970] have experimentally observed a change in the arc characteristics and erosion rate at currents exceeding 12 kA. Above this current level the arc voltage substantially increases. Mitchell [Mitchell, 1970] has termed the current level at which the arc voltage increases the "ion starvation" current. The concept is the following one: in order for production of ions to increase, more input energy is required. The ions receive the increased energy by falling down the larger potential well. The increased arc voltage,

which creates the potential well in this model, is a direct result of "ion starvation."

In summary, we have developed a steady state, one dimensional, energy balance model describing cathode erosion. The theoretical results are in fair agreement with experimental results. Taking note of dominating terms in the energy balance has led to an explanation of the constant arc voltage for modest currents, and further, the phenomenon of ion starvation has been discussed in the context of energy balance.

II.E.3 Potential Hump Theory

Ions have been observed to attain energies substantially higher than the anode potential [PR&K, 1965; D&M, 1969]. One explanation for the origin of these energetic particles is the formation of a potential hump in the plasma surrounding the cathode spots.

We have developed a comparatively simple theory which predicts the existence of a potential maximum within the plasma immediately surrounding the cathode spot. The problem is idealized by a one dimensional, steady state model. This model conserves particles and charges. The ion flux to the cathode is determined by the particular collisional regime.

In the quasi-collisionless theory, we assume a particular ionization fraction (of neutral vapor). In this case, the ion flux is directly related to the ablated neutral flux. The ion velocity is determined from the potential distribution, which is given self-consistently from Poisson's equation. Boundary conditions which are required to form a mathematically complete problem are explained in the model. By using perturbation techniques, we obtain an approximate analytical solution. Under certain conditions, the results show formation of a potential

maximum in the space charge region immediately outside the origin of the neutral vapor. In order for hump formation to occur, the ionization mean free path for neutrals must be less than or of order of a Debye length. This restricts the allowable plasma densities which will support a potential hump.

The collisional theory is also based on a one dimensional, steady state model. Particle and charge conservation is obeyed. In the collisional model the ion flux is determined by a balance between the accelerating electric field and the retarding effect of collisions. The electric field is determined by the ambipolar condition. We give an example of an ion density profile which exhibits a local maximum. This allows calculation of the perturbed ion density. The perturbed potential is then calculated and shown to agree with observations.

Quasi-Collisionless Hump Theory

The quasi-collisional theory is based on a one dimensional, steady state model. Particle and charge conservation is obeyed. The ionization fraction depends on the cathode material [Kimblin, 1973; PR&K, 1965]. For greatest utility, we wish to assume a specific ionization fraction which is representative of many electrode materials. An

appropriate choice of the ionization fraction is about 100%. This fraction is representative of materials such as copper, nickel, iron and others.

Because this is a quasi-collisional theory, we assume only sufficient collisions to produce the required ions. This point deserves some comment. Essentially, to satisfy this assumption, single electron impact ionization must occur. It is well known [Cobine, 1955] that the electrons have a temperature which corresponds to an energy less than the ionization potential of most metals. Thus, single impact ionization is quite unlikely except deep in the potential well. For example, if we assume a Boltzmann distribution for the electrons, the fraction of electrons which have the energy E_I is approximately $\exp(-E_I/kT_e)$. If E_I is the value appropriate to copper (7.7 eV) and an electron temperature of 3 eV is assumed, then the percentage of eligible electrons is less than 8%. It has been shown [Zel'dovich and Razier, 1966] that formation of excited atoms through multiple electron collisions is the most expedient way to ionize atoms when the electron temperature is too low for single impact ionization. Hence, this assumption should be regarded with suspicion and considered a possible source of error when detailed comparision with experimental results is performed. Nevertheless, for simplicity, we retain the use of this assumption.

Because the electron flux from the metal is approximately ten times the neutral flux [Kimblin, 1973], we neglect the increased electron flux arising from ionization. We assume the electron flux is roughly constant.

At this point we have established the equality of the neutral flux and the ionic flux. Since the ions and electrons have few collisions, the respective velocities are determined simply by the conservation of energy: $K = U - V$. In this equation K is the kinetic energy, U is the total energy, and $V = V(x)$ is the potential distribution. (For the case of ions, $U = V_0$ is the potential at which the atom was ionized - neglecting the neutral kinetic energy.)

Poisson's equation is the equation which closes the model. This allows self-consistent evaluation of the potential distribution.

Our methodology may be summarized as follows:

(1) the neutral flux determines the ionic flux,

(2) the potential distribution determines the ion velocity,

(3) the ion velocity and the ionic flux determine the ion density,

(4) the ion density determines the potential distribution,

(5) as in an iterative scheme, a self-consistent potential distribution must agree with that used in (2) above.

The time dependent particle conservation equations are:

$$\frac{dn_i}{dt} + \nabla \cdot \Gamma_i = n_e n_n \langle \sigma_I v_e \rangle - n_i n_e \langle \sigma_{REC} v_e \rangle = S$$

$$\frac{dn_e}{dt} + \nabla \cdot \Gamma_e = S$$

$$\frac{dn_A}{dt} + \nabla \cdot \Gamma_A = -S$$

Simplifying to one dimension dependence and assuming steady state conditions we get:

$$\nabla \cdot \Gamma_i = d\Gamma_i / dx = S$$

$$d\Gamma_e / dx = S$$

$$d\Gamma_A / dx = -S$$

Direct integration yields the following results:

$$\Gamma_i = -\Gamma_A$$

$$\Gamma_e = \Gamma_i + \text{constant}$$

We assume a neutral density dependence of:

$$n_A(x) = n_{AO} \exp(-x/R),$$

where, R is the neutral ionization mean free path. Since we have force-free neutrals the neutral velocity v_A is constant.

The particle fluxes are then:

$$\Gamma_A = n_{AO} v_A \exp(-x/R) \qquad \text{(assumed)}$$

$$\Gamma_i = -n_{aO} v_A \exp(-x/R) = n_i(x) v_i(x)$$

$$\Gamma_e = 10 n_{AO} v_A - n_{AO} v_A \exp(-x/R).$$

We have used the condition that the electron flux is ten times that of the ion flux. This condition is based on the results of measuring ion current as a fraction of total current [Kimblin, 1973].

Figure II.E.10 shows a schematic representation of the fluxes.

Figure II.E.10

QUASI-COLLISIONLESS PARTICLE FLUXES

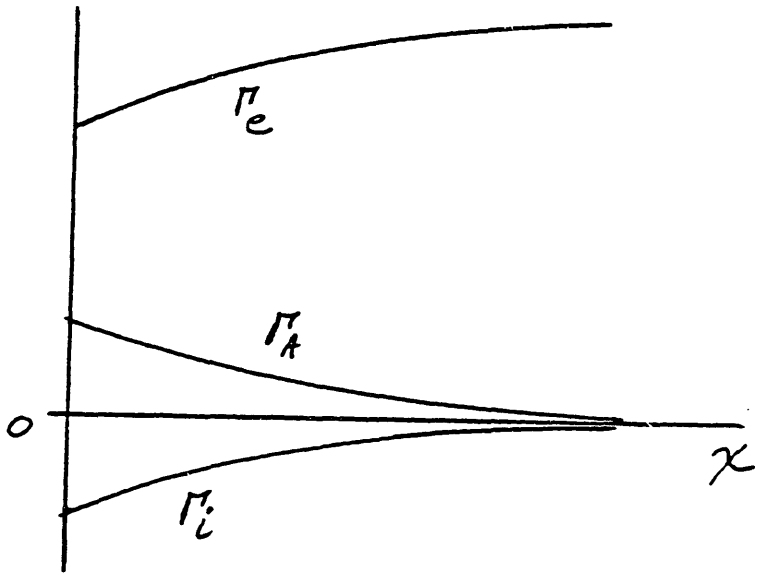

Assuming the electron flux is roughly constant (e.g. 10 >> 1), we neglect the second term in the electron flux equation:

$$\Gamma_e = 10\, n_{AO}\, v_A = n_e(x)\, v_e(x).$$

The electron velocity is given by:

$$v_e = (2V(x)/m)^{0.5} + (kT/m)^{0.5},$$

and the ion velocity is:

$$v_i = (2Z[V_O - V(x)]/M)^{0.5}.$$

Then the ion density is given by:

$$n_i(x) = \sqrt{\frac{M}{22}} \frac{n_{AO} v_A \exp(-x/R)}{[V_O - V(x)]^{0.5}}$$

Poisson's equation is:

$$V'' = d^2V/dx^2 = -4\pi\rho = -4\pi e(Zn_i - n_e).$$

Substitution of n_i and n_e into the above equation allows self-consistent determination of n_i, n_e, and V.

As an illustration of application of this methodology, we analytically solve the equations by a perturbative technique. We use the following boundary conditions on the potential: $V(x=0) = 0$, and $dV(x=0)/dx = -E_{emission}$. The use of the electric field at the boundary x=0 is motivated by the electron emission process. Several authors [Ecker, 1980; Lee, 1959] have estimated the necessary electric field which provides the observed electron current. We use their results here. Numerically, we have $E_{emission} = -2 \times 10^7$ V/cm = - dV/dx.

The equation for V''(x) may be written as:

$$V''(x) = -C\, g(x)$$

where C contains the constants involved. If we define $f(x) = V(x)/V_O$, then:

$$C = 4\pi e\, n_{AO}\, v_A/(2V_O/M)^{0.5},$$

and,

$$g(x) = \sqrt{Z}\, \exp(-x/r)/(1-f(x))^{0.5} - 10\sqrt{m/M}\,(\sqrt{f(x)} + k_e)),$$

where, $k_e = (kT/V_0)^{0.5}$ is the dimensionless electron thermal velocity. We integrate in a straightforward manner from 0 to x, where x is restricted for the present to be small. Since V(x=0) = 0, we may assume f ~ 0 for x sufficiently small. We assume, for simplicity, Z = 1. Then we have:

$$dV/dx - (dV/dx)_{x=0} = C\,[I_1 - 10\,(m/M)^{0.5}\, I_2]\ ,$$

where,

$$I_1 = \int_0^x \exp(-x/R)\, dx = x\ , \qquad (x < R)$$

and,

$$I_2 = \int_0^x dx/k_e = x/k_e\ .$$

Thus,

$$V = \int_0^x dx\ dV/dx$$

$$V = (dV/dx)_{x=0} - 0.5\ C\ x^2\ [1 - 10\ (m/M)^{0.5}/k_e].$$

This is of the form:

$$V = Ax - Bx^2\ ,$$

where, $A = V'(x=0)$.

This form satisfies our boundary conditions (as it must), and furthermore, our approximation $f(x\sim 0) \sim 0$ is justified *a posteriori* for x sufficiently small. Our expansion is valid for $x < R$.

As in quantum mechanics, one may now use the form $V = Ax - Bx^2$ and iterate to a solution. The mathematical details quickly become overwhelming. Resort to numerical methods is the usual recourse. Discussion of numerical methods is beyond the scope of this section.

In summary, we have presented a simplistic quasi-collisionless theory of potential humps. Although it may be argued that the model is not realistic, the basic physics are more easily understood in a simple model. An analytical solution is given which is valid for $x < R$, where R is the neutral ionization mean free path.

In a simple way we can demonstrate conservation of charge. The time dependent equation is:

$$d\rho/dt + \nabla \cdot J = 0.$$

In steady state we have:

$$\nabla \cdot J = \nabla \cdot J_i + \nabla \cdot J_e = 0.$$

For arbitrary x we can write the current densities as:

$$J_i = e\Gamma_i ,$$

and,

$$J_e = -e\Gamma_e .$$

The expression for the total current density is:

$$J_{tot} = J_i + J_e = -10\ e\ n_{AO}\ v_A .$$

Hence, we have $\nabla \cdot J_{tot} = 0$ and J is less than zero, that is, to the left, as it should be for electrons traveling to the right.

Collisional Hump Theory

The theory for the collisional hump is based on a one dimensional, steady state model. The model conserves particles and current. The ion flux is determined by a balance between the accelerating electric field and the retarding effect of collisional drag. The electric field is determined by ambipolar diffusion.

For simplicity we assume only singly ionized particles to be present. Then the increase in the flux of electrons is equal to the increase in ionic flux. Denoting the particle mobilities by μ_j and the diffusion coefficients by D_j, we have the following for the individual fluxes:

$$\Gamma_i = \mu_i n_i E - D_i \nabla n_i,$$

and,

$$\Gamma_e = \mu_e n_e E - D_e \nabla n_e.$$

The condition $\Delta \Gamma_e = \Gamma_i$ leads to the following equation for the electric field E:

$$E = \frac{D_i \nabla n_i - D_e \nabla n_e}{\mu_i n_i - \mu_e n_e}$$

Poisson's equation can be written as:

$$\nabla \cdot E = dE/dx = 4\pi\rho,$$

where, $\rho(x) = e\,(\,n_i(x) - n_e(x)\,)$.

We define $n_1(x)$ as a perturbation to the ion density:

$$n_i(x) = n_e(x) + n_1(x).$$

At this point, we make several simplifying assumptions:

$$\nabla n_1 << \nabla n_i \sim \nabla n_e ,$$

$$D_i << D_e ,$$

$$\mu_i << \mu_e .$$

We consider $n_1/n_i < 1$. Then we have:

$$\frac{d}{dx}\left(\frac{D_e}{\mu_e}\frac{\nabla n}{n}\right) = -4\pi e n_1(x)$$

Neglecting the gradient of the electron temperature, justified by the large electron thermal conductivity, we get:

$$(kT/e)\, d^2(\ln n)/dx^2 = -4\pi e n_1(x)$$

or,

$$kT/(4\pi ne^2)\; n d^2(\ln n)/dx^2 = -L_D^2\; n\; d^2(\ln n)/dx^2 = n_1(x).$$

To recapitulate, we use the ambipolar electric field as a forcing function. The different diffusion rates of ions and electrons cause an electric field which tends to equalize the inter-species loss rate. This gives rise to a density perturbation, $n_1(x)$. The above equation, subject to the

assumptions mentioned, allows calculation of $n_1(x)$.

As an example of use of this theory, let us assume an ion density profile which exhibits a potential hump. We shall calculate $n_1(x)$ and show that the existence of a potential hump results. Thus, although we have chosen a special intitial density profile, the fact that a hump results reinforces the theory.

We assume the following form for n(x):

$$n(x) = n_0 \, (R/x)^{0.5} \, (1 - \exp(-x/R)) \, .$$

The resulting equation for $n_1(x)$ is:

$$n_1(x) = -n(x) \frac{L_D^2}{R} \left\{ \frac{e^{-2s}}{s} + \frac{(1-e^{-s})^2}{4s^2} + \left(\frac{s-1}{s}\right) \frac{e^{-s}}{1-e^{-s}} - \frac{3}{4s^2} \right\}$$

Figure II.E.11 shows these two profiles. The humps are quite evident.

Figure II.E.11

SAMPLE POTENTIAL HUMP DENSITY PROFILES

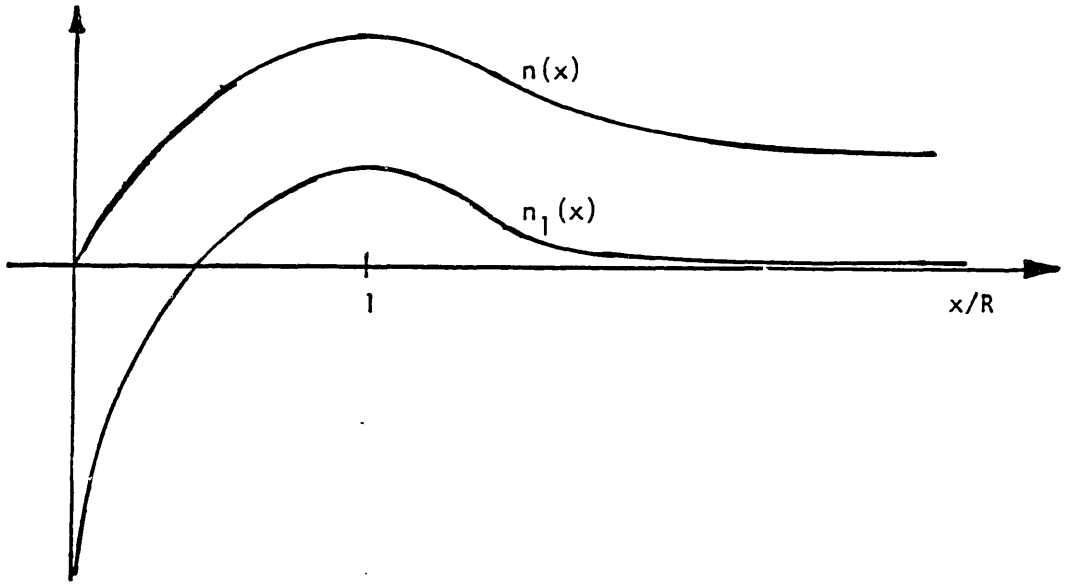

We can estimate the height of the potential maximum. For a rough approximation we can use the following expression for V:

$$V \sim 4\pi e n_{1,max} L^2 ,$$

where, $n_{1,max} = 0.3\, n_0$,

$n_0 \sim 10^{18}$ cm^{-3} ,

$L \sim 6\, L_D \sim 8 \times 10^{-6}$ cm.

The result is V ~ 35 volts. This is the order of magnitude of the experimental results.

Density Restrictions

The region of intense ionization must be less than or of order of a Debye length. This is because the plasma achieves quasi-neutrality over distances of order of the Debye length. This condition puts a restriction on the plasma density which is a necessary condition for hump existence. This condition may be written as:

$$L_D \geq R \ ,$$

where, $R = v_A/(n \sigma v_e)$ is the neutral mean free path,

and, L_D is the Debye length.

Our restriction has now become:

$$n \geq \frac{4\pi e^2}{kT \sigma^2} \left[\frac{v_A}{v_e}\right]^2 .$$

Inserting typical parameters, as given in Figure II.E.12, we find the critical density for hump formation to be:

$$n \geq 6 \times 10^{17} \text{ cm}^{-3} \ .$$

Figure II.E.12

CRITICAL DENSITY PARAMETERS

$kT = 3$ eV

$\sigma \sim 10^{-15}$ cm^2

$v_A/v_e \sim 10^{-3}$

PR&K [PR&K, 1965] have calculated hump densities of order of the above critical density. An interesting observation was made by Davis and Miller [D&M, 1969]. They noted the lack of low energy ions in the particle flux. This implies few charge exchange collisions. Two complimentary explanations exist which explain this observation:

(1) the volume of the hump is quite small - it should be of order L_D^3,

(2) neutrals and ions do not co-exist; the hump has a high (~100%) ionization fraction.

In conclusion, we have presented two theoretical models of potential hump formation in the plasma surrounding the cathode spots. One theory was based on a quasi-collisionless model, while the other was based on a fully collisional model. The results shown indicate that potential humps can easily form. The condition of hump formation establishes a minimum plasma density. Approximate numerical values of hump parameters are in good agreement with observation.

II.E.4. Arc stability

The unique advantage vacuum arcs have over alternative switching mechanisms is the ability to: (1) interrupt currents on faster time scales than other devices with equivalent current ratings, and (2) interrupt larger currents than other devices with comparable interruption time scales.

The mechanism of arc interruption is not fully understood at present. We have seen in Section II.B.2 that phenomenological experimentation has been conducted [Farrall, 1980]. The product of this research has been plots of currents versus average lifetimes for different materials. These plots have then been compared with vapor pressure plots [Farrall, 1980]. Good correspondence has been obtained between the a posteriori observation that high vapor pressure materials can withstand a lower current for a longer period of time than can a low vapor pressure material. No specific model has previously been proposed to explain this correspondence.

The basic reason for interruption of the arc, therefore, remains shrouded in phenomenology. In this section we create a very simple model of energy transfer in an extinguishing arc. Our basic premise is that energy

conservation must be obtained in the arc for the arc to be stable. We rely on the energy transfer mechanisms introduced in Section II.A; we limit ourselves to interractions occurring at the cathode spot.

Refering to Figure II.6 for cathode spots processes yields the following energy balance equation:

$$P_{spot} = P_{charged\ particle} - P_{ioniz} - P_{BB\ rad} - P_{cond} - P_{phase\ change} - P_{\phi} - P_{e\ heat\ cap}.$$

The terms in the equation are as defined in Section II.A. Because we are assuming an extinguishing arc, we suggest that most of the terms on the right hand side of the above equation are negligible.

Specifically, we neglect residual ionization and the phase change energy because the arc simply does not have the excess energy to vaporize and ionize neutrals.

The spot temperature has a time scale of a few microseconds. For all but the fastest rates of change the spot is in a quasi-static state. Thus the spot temperature falls as rapidly as required by energy conservation. Black-body emission, of course, falls as the fourth power and thermal conduction also becomes negligible. (In fact, in an

arc which had previously obtained steady state conduction conditions, thermal conduction from the bulk to the spot can occur due to the falling spot temperature; this may supply needed energy. Our simple model neglects this effect.) Energy to replace the electron heat capacity is ignored because the spot temperature falls rapidly.

In essence, then, we have an energy balance ($P_{spot} = 0$) expressed by:

$$P_{charged\ Particle} = P_{\phi}.$$

The physics expressed by this equation can be stated as follows: the incident charged-particle energy is just sufficient to overcome the effective material cooling work function. Thus, the incoming ions carry enough energy to continue the supply of electrons, albeit near-zero initial velocity electrons.

The dispersion time for the plasma occurs on a time scale of a few microseconds [Lafferty, 1966]. Other researchers [D&M, 1969; Farrall, 1980] have found that collapse of the potential hump also occurs on a time scale of a few microseconds. Thus, the cathode spot, plasma, and potential hump all have roughly the same, quite fast, time scale. The effect this has is (1) the ions impact the cathode (near

arc extinction) with not the potential hump energy, as they do during quasi-steady state conduction, but with merely the anode potential, (2) the plasma is continuously in a recovery phase after a current peak (i.e. more plasma particles exit the arc than enter the arc per unit time interval after a current peak).

Explicit representations for the energy fluxes are as follows:

$$F_{\text{charged particle}} = V_i J_+,$$

$$F_{\phi} = \phi_{eff} J_-.$$

Kimblin [Kimblin, 1973] has done a rather complete study of the fraction of current carried by ions. His results show that approximately 10% of the total current is ion current, independent of current. Applying his results to the case at hand provides the following relation between the anode potential and the effective cooling function:

$$V_i \geq 9\phi_{eff}.$$

This relation states that the minimum anode potential should be directly proportional to the effective cooling work function. Furthermore, higher potentials are more likely to be unstable than lower potentials. Thus, we would

expect higher work function materials to be more unstable with respect to low energy inputs. An alternative point of view is to use the general, non-linear, V-I relationship to determine V at a given I. If this $V < 9\phi_{eff}$ then arc continuation is energetically unfavorable and the arc will spontaneously interrupt. For a positive V-I relationship, a material with a larger effective work function will extinguish more quickly than a material with a smaller effective work function.

Lee [Lee, 1960] has determined the effective cooling work function as a function of temperature, field, and work function. His results show that the effective cooling work function is approximately 2 eV less than the ordinary work function under representative conditions.

Figure II.E.13 shows a tabulation of the results of comparison of the above simple theoretical explanation for arc chopping at low currents - and hence low voltages.

Figure II.E.13

COMPARISON OF ARC STABILITY THEORY FOR METALS

Metal	Arc Voltage[a]	ϕ_{eff}[b]	(Arc Voltage)/ϕ_{eff}
Cd	11 V	2.1 eV	5.2
Zn	13 V	1.8 eV	7.2
Cu	20 V	2.4 eV	8.3
Ag	20 V	2.3 eV	8.7
W	25 V	2.55eV	9.8
Mo	25 V	2.6 eV	9.6

The theoretical model described in the text predicts (Arc Voltage)/ϕ_{eff} = 9.

(a) Kimblin, 1973
(b) after Lee, 1960; $\phi_{eff} = \phi - 2$ eV

Although the agreement of this simple theory with experiment is, at best, approximate, it does suggest an energy balance is intimately involved with arc instability. Furthermore, a more detailed model is justified to improve the agreement with observation. An examination of the effective cooling work function column in Figure II.E.13 reveals that the metals are again in rough order of arc stability as indicated in Figure II.B.6. It is possible that improved agreement with the above model would be obtained if a more accurate work function correction were used. Phenomenomological models are useful to a limited extent, however, for true understanding to occur, more

physical modeling is necessary.

There is an additional consideration which has not been mentioned in the vacuum arc literature. There is a minimum characteristic size required for existence of different phases. Essentially, the energetically unfavorable process of interface creation must be overcome for a phase transition to occur [Lifshitz and Pitaevskii, 1981]. Surface tension is perhaps the most obvious example of this phenomenon. If a phase transition at the location of a former cathode spot does not persist due to insufficient energy, then the entire electron emission process changes from the "T-F" process [Lee, 1960], also know as the field-enhanced thermionic emission, to pure (quantum mechanical) field-induced emission. The current densities obtainable from field-induced emission decrease quite rapidly with increasing effective work function. The reader should keep in mind that the plasma density decays on the same time scale as the temperature of the cathode spot, hence a space charge-enhanced electric field is not likely. Thus, it seems improbable that the field can intensify to such a degree to produce significant currents, and so the arc is observed to extinguish.

In summary, a physical model has been used to obtain rough agreement with observed low-current instability trends for different metals. The model is a simple one, based on energy conservation, and improved agreement could be expected with a more involved model.

III. APPARATUS ISSUES

III.A Initial Design Requirements

Initial design characteristics were chosen to satisfy the conflicting requirements of achieving significant understanding of and advancement in the field of vacuum arcs in a reasonable amount of time and within a finite budget. A compromise between practicality and idealism was therefore made. Practicality won. Theoretical analyses were performed to determine the minimum range of magnetic fields which would significantly interact with the arc in a metal vapor vacuum arc switch. This range was found to be a few kiloGauss. A preliminary configuration for the field coils was then established which was subsequently substantially modified as the total design evolved.

The very name of metal vapor vacuum arc switch implies some pressure vessel to contain the conduction material. The pressure in the arc itself during conduction is of order Torr, thus, initially it was thought a thermal vacuum of 10^{-4} Torr would be adequate. The requirements on the vacuum system, however, extend throughout the lifetime of the system, and not merely on the pressure during the very short lifetime of the arc. This is due to the build-up of trapped gases on the exposed surfaces. If the vacuum pressure is not sufficiently low, contamination effects due

to impurities internal to the switch will prevent optimum performance. Thus, we determined that operation at a base pressure of less than 10^{-6} Torr was desirable.

As an experimental device, we designed a most flexible and adjustable device in order to optimize the performance of the metal vapor vacuum arc switch. To this end we made seemingly endless design modifications while we were still working on paper. In the final analysis we produced a unit which is very versatile as an experimental device.

III.B Magnetic Field Design

Having previously determined that magnetic fields of order of a few kiloGauss were sufficient to interact with the plasma, we performed analyses to determine a configuration which met this requirement and additionally could be produced from our present stock of equipment. Essentially this meant the various available capacitor banks presented another design constraint. A design consisting of dual two-turn coils of 11 cm radius was chosen. Having two independent coils allowed the possibility of inveatigating two different resulting magnetic fields: an axial field by parallel excitation (the z-direction in cylindrical geometry); and a radial field by anti-parallel excitation of the coils. The resultant coils have an inductance of

1.6 micro-Henries each. When connected in parallel and excited by a 90 microfarad capacitor bank, a period of 54 microseconds results. Ideally this period is much less than the period of the arc discharge so that the arc discharge will appear "frozen" at the instant of application of the magnetic field. This is necessary for maximum effect of the magnetic field. The apparent limitation on the frequency of the arc discharge which will be interrupted is of little concern. A 20 kiloHertz arc discharge is difficult indeed to extinguish!

Initially the coils were constructed from 1/8" inch diameter bare stainless steel wire. As will be discussed later, problems arose associated with the lack of insulation on the wires. An alternative construction called for Teflon insulated wires of the same current-carrying cross-section. See Figure III.B.1

Figure III.B.1

MAGNETIC FIELD COIL CONSTRUCTION

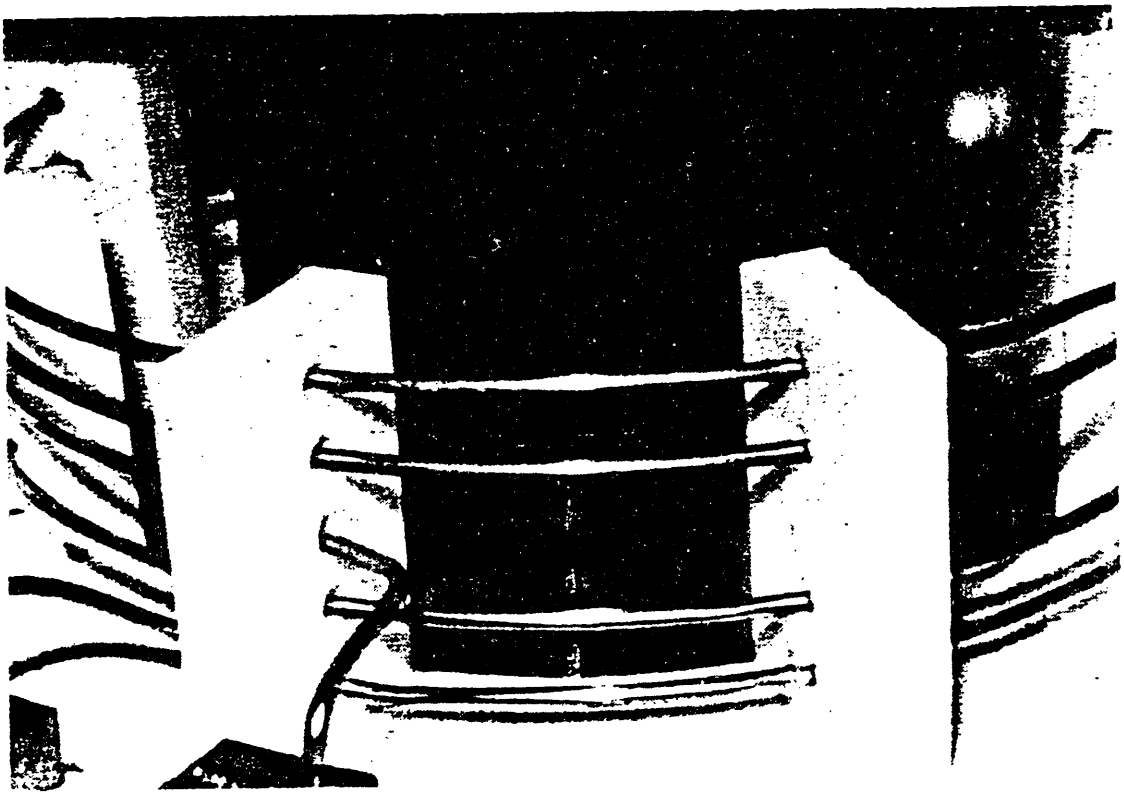

III.C Vacuum Considerations

III.C.1 System viewpoint

The cleanliness of the vacuum environment may ultimately limit the performance of the metal vapor vacuum arc switch. For this reason it is important to understand the pressure vessel from a system point of view. In addition to the desired pressure there are many other, sometimes conflicting, issues to be considered when designing a high performance vacuum system from the very beginning.

Of foremost interest, of course, is the desired operating pressure. The operating pressure is defined, for our purposes, as the pressure below which tests, or shots, are conducted. The pressure may, immediately following a shot, rise above the operating pressure, but as an *a priori* groundrule for consistent results no shots would be initiated while the pressure is above some minimum pressure - the operating pressure.

Flexibility and experimental expediency is provided by a system which is capable of being pumped to a pressure substantially below the actual operating pressure. The fact that the pressure decays in time roughly as an exponential function means an ultimate pressure less than one-third the operating pressure is desirable for the device. The

ultimate pressure chosen implies a restriction on the suitable types of vacuum pumps to accomplish the task. As mentioned above, we determined an operating pressure of 10^{-6} Torr to be an acceptable. Accordingly we designed the system to achieve, under worst case conditions, an ultimate pressure of 3×10^{-7} Torr.

There are several types of vacuum pumps which will achieve the above requirement [O'Hanlon, 1980]. We considered diffusion pumped systems, turbomolecular pumped systems, and ion pumped systems. We had available at essentially no added cost either a turbomolecular pump or an ion pump. We chose the ion pump for reasons of experimental ease and mechanical simplicity.

Figure II.C.1 is a vacuum pumping flowchart. It shows the logical order of the vacuum components from bottom to top.

A mechanical pump is required to rough the pressure down to approximately 1 milliTorr. This process takes about 45 minutes for our system. At this pressure the ion pump can be turned on and the pressure will rapidly fall. The phenomenon of backstreaming prevents one from turning the mechanical roughing pump on and then allowing the pump to work, say, overnight. Oil from the mechanical pump will

Figure II.C.1

VACUUM PUMPING FLOWCHART

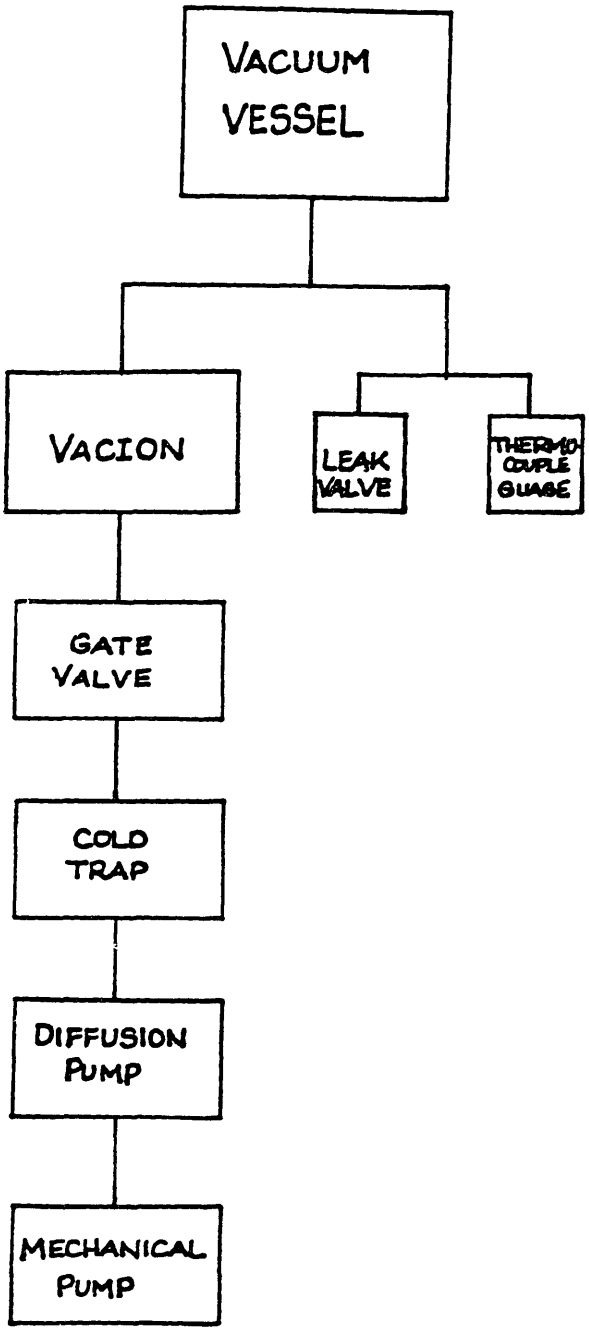

traverse the pumping lines upstream and contaminate the very vacuum chamber one is attemping to evacuate! The oil can accomplish this travel most easily when the pressure is the lowest. This is because the oil molecules are in essentially free flight. The molecules experience no drag effect due to ordinary viscosity. Thus it behooves one to stand watch over the mechanical pump pressure gauge (a thermocouple gauge) in order to close the high vacuum gate valve at the earliest possible moment and then to turn on the ion pump once the mechanical pump has been isolated from the pumping circuit.

II.C.2 General High Vacuum Issues

One of the issues which must be taken into account in a device such as this one, is the choice of various materials to be employed inside the high vacuum environment. In view of the requirements of the device and in light of the physical model of a hot plasma dissipating in the electrode gap, and condensing on the surrounding surfaces, it is very important to use materials with a low vapor pressure under the anticipated conditions. We have seen in Chapter II the importance of material selection for the electrodes. The same problems occur with all surfaces exposed to the plasma environment. The vapor pressure of metals such as copper, silver, tungsten, and stainless steel 304 are low enough at

typically encountered temperatures for these to be the commonly used materials. In a specific application the particular metal chosen will depend on other requirements to be satisfied.

Examples of materials not to be used in a high vacuum environment environment include zinc, cadmium, sulfur and lead. The problem with these materials is their relatively high vapor pressure. Zinc is a component of brass, cadmium and sulfur are found in some types of steels and stainless steels, and lead is a component of most soft solders. As shown in Figure II.B.7, vapor pressure is a rapidly rising function of temperature. Therefore, the above materials must be avoided if they would be subjected to any temperature rise above room temperature; even at room temperature these materials should not be used except for exceptional reasons. Fortunately there exist suitable replacement materials for the above materials.

Diffusion is the transport of one material through another. Gaseous diffusion through the bulk materials which form the sidewall of the vacuum device is one factor which ultimately limits the minimum pressure achievable. The gas pressure on one side of the surface establishes a concentration gradient through the material. It is this

gradient which forces gas atoms and molecules through the solid. Since the internal pressure is negligble compared to the external pressure, approximately the same pressure difference occurs in most high vacuum systems. Hence, using a thick-walled vacuum vessel will reduce the particle concentration gradient, and this, in turn, will result in decreased diffusion transport through the vessel walls.

Permeability is another consideration for high vacuum systems. Permeability is a three-step process [O'Hanlon, 1980] Gas first adsorbs on the outer wall of a vacuum vessel, diffuses through the bulk of the solid and finally desorbs from the interior wall. Steady-state permeation is physically similar to a small, constant leak.

Outgassing is the continous evolution of gases from the vacuum surfaces. The gases become trapped on the surface in a thickness several molecular layers thick. Whether acquired during metal fabrication or exposure to air during assembly, material outgassing has historically plagued the industry unless special precautions were taken. Simple triggered vacuum gaps became a reality once the problem of outgassing was solved by vacuum melting the metal for the electrodes. The central idea of vacuum melting was to eliminate as much gas as possible from the metal during processing.

Other solutions to the outgassing problem include a vacuum bakeout of the entire system while under vacuum pressure. The rate of outgassing is temperature dependent. At elevated temperatures the outgassing is increased over low temperatures. The idea is to "bake off" as much gas as possible during the limited time of the bakeout thereby "cleaning" the system. After cool down, the outgassing rate will presumably be much reduced. A cryogenic cold trap can be used to expedite this bake-out process by preventing back-streaming.

Hence the three concepts of diffusion, permeability, and outgassing are all different but related aspects to achieving and maintaining a high vacuum environment. These three processes occur over over the bulk of solid material. We now investigate the sealing problem at the atmosphere-vacuum interface.

Various access ports were installed in order to supply electrical power to the trigger and coils located interior to the vacuum vessel. The cost of electrical feedthroughs was substantial for the voltages and currents involved in our system. Thus we designed for a minimum number of access ports without reducing the flexibility inherent in

the overall design.

The seals for the vacuum environment received much thought. If one wanted the highest performance system available, the solution is an obvious one: use copper gaskets as the sealing method. If, however, one merely wants a "good" system, while subject to the restriction of a budget, then the answer is not so obvious. The alternative to expensive metal seals is to employ re-usable rubber gaskets.

Of course, throughout the design period we constantly kept in mind the end use for our product. This had the effect of keeping things simple from an implementation point of view, and insured a reasonable compromise between conflicting requirements.

III.C.3 Implementation

The vacuum system in the present form consists of a cylindrical glass vacuum vessel of 18 inches diameter capped at top and bottom by a one-half inch thick stainless steel plate 24 inches in diameter. The 200 l/s Vacion pump operates through a four inch opening in the center of the lower flange. See Figure III.C.2 for a schematic view of the vacuum system.

Figure III.C.2

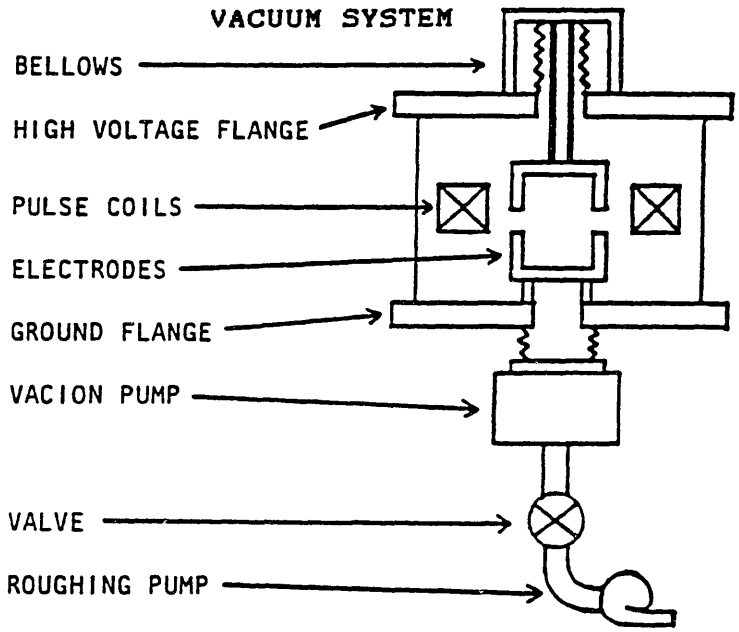

The small diameter access ports are sealed with standard Varian-style copper gaskets. Commercially available electrical feedthroughs were selected for the magnetic field current and the arc discharge trigger lead.

The large (18") diameter vacuum seals are made with Viton-A rubber boot gaskets. These gaskets have proven quite good from a vacuum standpoint, easy to install, and economical because of the ability to re-use them.

We have achieved ultimate pressures of 3×10^{-8} Torr in our system, indicating good system cleanliness, low material outgassing and acceptably low permeability of the glass walls.

III.D Adjustable/Flexible Features

Adjustable features are both difficult to design and evaluate. A device of maximum flexibilty was to be constructed. However, questions such as "Flexible in which way?", "What needs to be adjustable?", et cetera continue to assault the designer.

In fundamental terms, an experimental device is constructed because the knowledge in a particular field has not advanced to the stage where all relevant facts are known. Rational judgment is required to produce an experimental set-up in which flexibility and adjustablity are preserved in all the proper areas, and yet the device is not unwieldy to use. We determined the essential elements which must be allowed to vary for the full range of interest in vacuum arcs to be explored. These elements are described in detail in this section.

III.D.1 Gap Variability

The ability to vary the electrode gap without breaking vacuum was a central design issue. The design chosen was one in which the gap variability is derived from the welded metal bellows attached to the top, cantilevered, electrode. This allows the gap to be varied in excess of 2 inches. The method of alignment is four corner threaded rods. Three

rods are required for movement in three dimensions. The fourth rod serves as a locking rod. This prevents any slow creep of the electrode and also serves as a positive stop when aligning the electrode.

III.D.2 Demountable Electrodes

Demountable electrodes provide the ability to use interchangeable materials and/or geometrical configurations in the device. Initial experiments have been done with stainless steel electrodes, however, we anticipate the use of copper electrodes in the fututre. The lower electrode bolts into position with four stainless steel bolts. These bolts insure good electrical contact between the electrode and its mounting station. The upper electrode is soldered into place with Indium. The soldering is performed after insertion through the adjustable bellows. Electrical contact is assured by the Indium joint. These electrodes can easily be mounted and demounted in a matter of minutes.

There is another, quite unique, aspect of our particular design. During the pulsed application of the primary current (in the magnetic field coil) the plasma acts as a single turn transformer secondary. This is the desired effect. A leakage effect occurs because the electrode cylindrical lip is also a transformer secondary to the primary current. In this configuration the induced circumferential plasma current is electrically in parallel with the induced electrode lip current. This parasitic effect at best dilutes the effort of the pulsed field, and, at worst, may actually make interruption more difficult to

achieve due to the additional Joule deposition of energy in the current carrying electrode.

The electrodes are specifically designed for increased lip-circumferential impedance. This has been accomplished by the use of axial slots in the electrode. These slots are 2-1/2 inches deep, that is, the slot root is approximately a total of three inches from the center plane of the field coil. Figure III.D.1 shows the geometrical situation for the electrodes.

Figure III.D.1

SLOTTED ELECTRODES

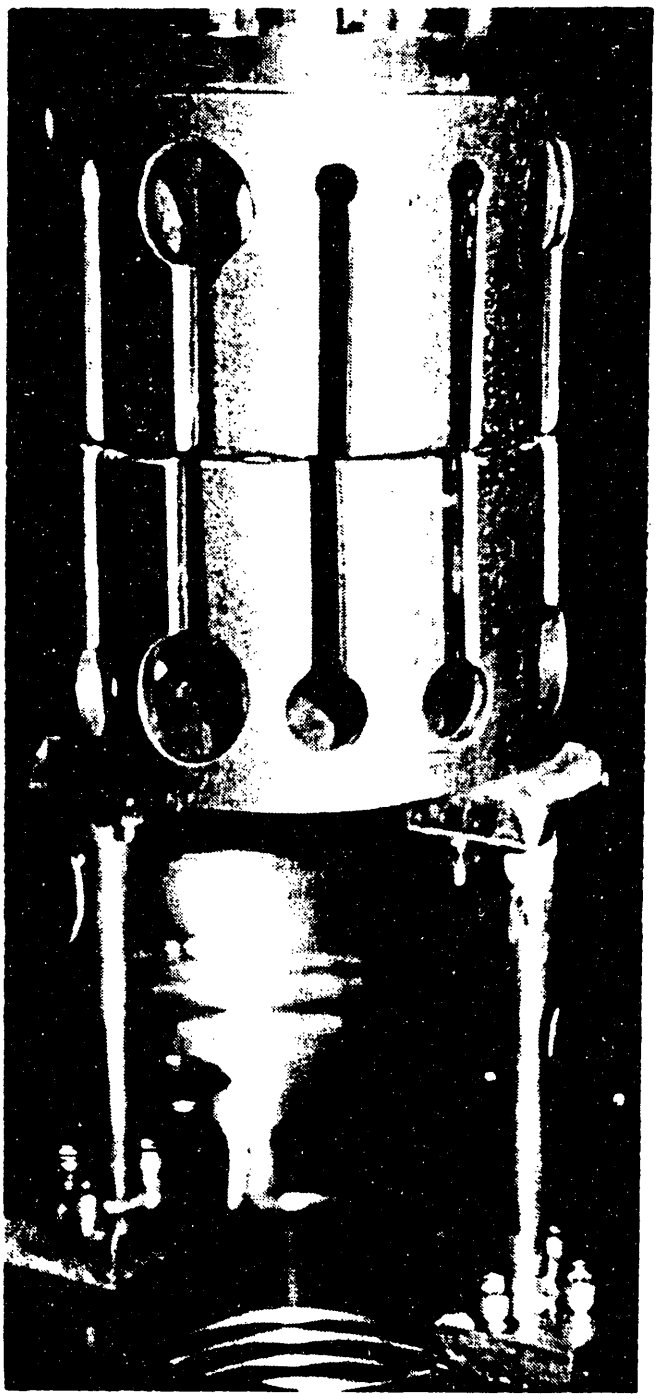

Figure III.D.2 is an assembled view showing the geometrical arrangement of the field coil and slotted electrodes.

Figure III.D.2

SLOTTED ELECTRODE AND COIL GEOMETRY

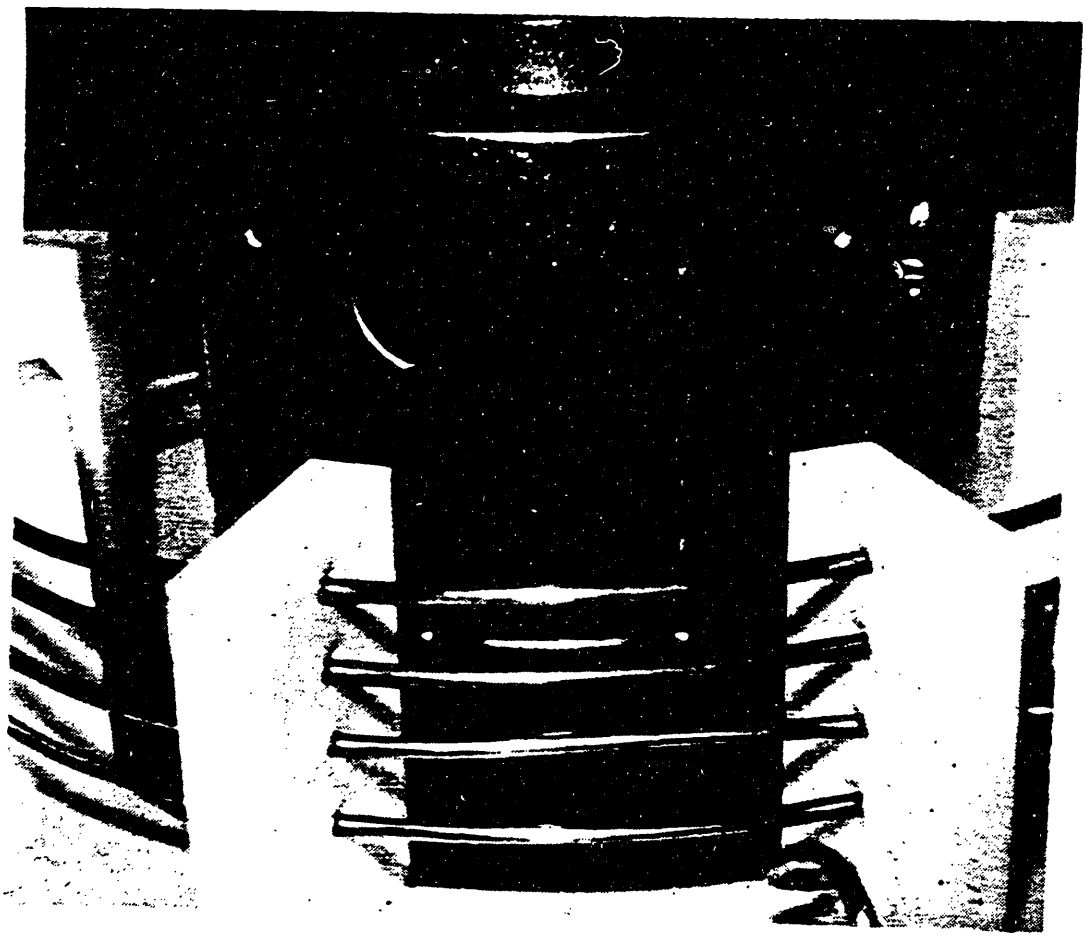

At this point we digress slightly to review the technical issues at hand. Calculations were performed to determine the severity of this leakage current and its effect on the desired plasma current. The problem may be idealized as shown in Figure III.D.3.

Figure III.D.3

IDEALIZED PLASMA MODEL SHOWING LEAKAGE CURRENT

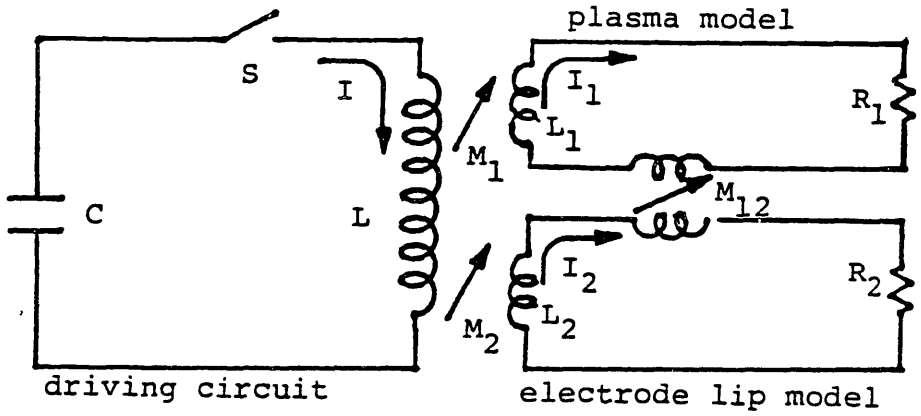

The voltage on the capacitor bank after the switch S is closed is given by (resistance and lead inductance in the primary circuit is neglected for simplicity):

$$V = L\, dI/dt + d(M_1 I_1 + M_2 I_2)/dt$$

The notation used is the following: unsubscripted - primary current parameter; subscripted 1 - plasma parameter;

subscripted 2 - electrode lip parameter.

If we assume flux conservation (i.e. assume that times of interest are less than $(L/R)_1$ or $(L/R)_2$ (for both the plasma circuit and the electrode circuit), we find the following results:

$$\phi_1 = 0 = M_1 I + L_1 I_1 + M_{12} I_2$$

$$\phi_2 = 0 = M_2 I + L_2 I_2 + M_{12} I_1$$

Simultaneous solution of these two equations yields:

$$I_1 = I \left[\frac{-M_1 L_2 + M_2 M_{12}}{L_1 L_2 - M_{12}^2} \right]$$

$$I_2 = I \left[\frac{-M_2 L_1 + M_1 M_{12}}{L_1 L_2 - M_{12}^2} \right]$$

The important point here is the effect M_{12} has on the plasma current. The coupling between the plasma and the electrode lip actually serves to reduce the plasma current. Because of this effect, we have attempted to substantially reduce M_{12} by our slotted electrode design. Essentially, we force the current to traverse a path which is far away from the region of good coupling.

III.D.3 Anode/Cathode Interchangeability

The Vacion pump is connected to the chamber via a four inch diameter formed-bellows tube. This electrically connects the pump to the lower flange. Thus, the lower flange and lower electrode must always remain approximately at ground potential for safety reasons. This in no way, however, restricts the polarity of the upper flange. The top electrode may be either positive high voltage or negative high voltage - in fact in the half cycle discharges the upper electrode in the final state has approximately the same magnitude voltage but opposite in sign to the initial state. The essential point is the interchangeability of anode and cathode in our design.

III.D.4 Flexibility of the Magnetic Field Design

Our design included two autonomous magnetic field coils and a trigger electrode. Thus three vacuum feedthroughs are a minimum for this system. A fourth vacuum access port was added to insure experimental flexibility. Throughout all experiments to date this port has simply been closed or "blanked off." However, we anticipate the possibility at some later date of instrumenting the electrodes, and, at that time, we will require a fourth access port.

By using such a large vacuum vessel we attempted to

mitigate any possible influence of the end effects in our device. An additional advantage of the large vessel is the few geometrical constraints imposed by the surrounding walls.

The flexibility of our approach is emphasized by the incorporation of the magnetic field coil design. Confident that we had sufficient flexibility to implement a coil subsequent to the initial tests, we essentially assembled a triggered vacuum gap. The flexibility inherent in our design allowed us to gain valuable experience with the device much ealier than otherwise possible. Of course, subsequently the field coil has been designed, implemented and suitably modified within the same fixtures.

As mentioned above, we have implemented a glass vacuum vessel. Aside from the vacuum considerations of outgassing and permeability, the use of glass has far-reaching implications. First, as a dielectric the glass is sufficient to hold off the full voltage of the electrodes with a large safety margin. This allows the vacuum flanges to be used as the current feedthroughs. In addition, excellent visibility is afforded by the glass chamber. The expense saved in electrical feedthroughs and indeed in the large vacuum vessel itself is substantial.

Safety when working around the glass vacuum chamber is provided by an encircling piece of Lexan polycarbonate. This not only protects against accidental glass breakage, but also serves as a mechanical support for the top flange should the glass ever break.

IV. EXPERIMENTAL WORK

IV.A Control System Description

IV.A.1 Instrumentation

In addition to the basic systems described in the previous chapter, various control systems are required for effective implementation of the concept of synchronous application of a current-interrupting magnetic field.

a) Electro-pneumatics

Primarily these systems are electronic, especially when timing is of importance. We employ, however, several sub-systems which are not electronic. These systems are: a)the manual shorting crowbars for the capacitors, and b)the electro-pneumatic valves for control of charging two capacitor banks independently and for isolating the charging supply from high voltage surges during an actual discharge.

The manual crowbars operate in a self-evident way and so will not be discussed further. The electro-pneumatic valves also operate in a straightforward way. Because of the safety issues involved and ease of use during the experiment, it is felt worthwhile briefly to discuss the valve operation.

The electrical schematic is shown in Figure IV.A.1. Features of interest include the master safety switch with the indicator light and the four independent electro-pneumatic valves. Supplied with air pressure from a common nitrogen tank, all electrical connections go to a "safed" condition in the event air pressure is lost. The safety issues go beyond one operator; other workers having access to the experimental cell are assured as to their security under all conditions.

Figure IV.A.1

ELECTRICAL SCHEMATIC FOR PNEUMATIC VALVES

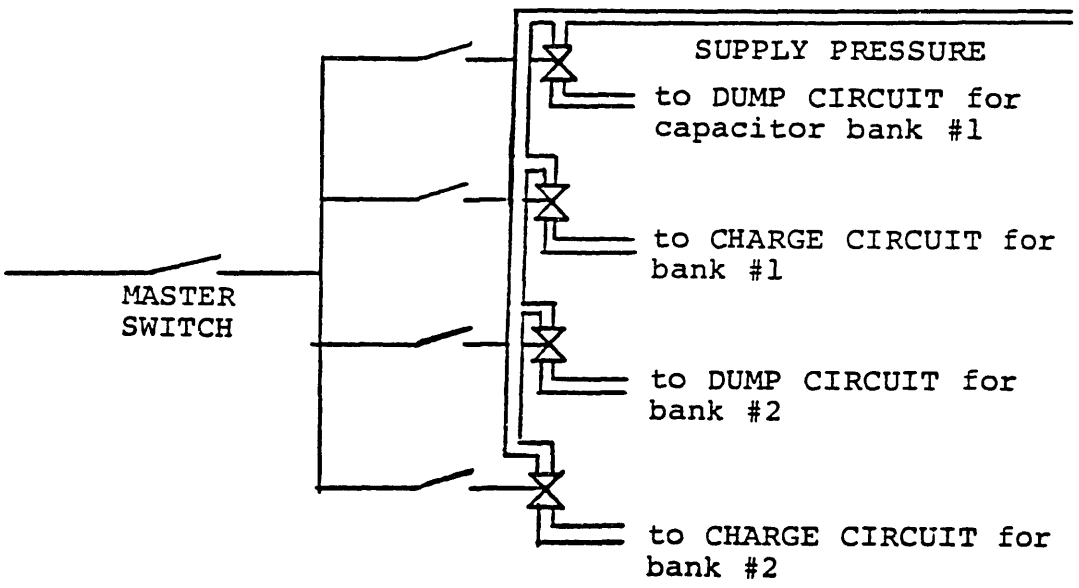

The master safety switch provides the same sense of security as loss of air pressure. The indicator light is wired in series with the master switch. If the master switch is not activated, all electrical connections are "safed." If the indicator light fails for internal reasons, all connections are safed. The indicator light has a logic which means the following: if lit something may be in the "live" condition, under these conditions caution is to be exercised; if the light is extinguished, the system is grounded. Note the system could very well be completely grounded even if the indicator is lit, but it serves as a visible warning that care is to be exercised.

The four other toggle switches control four independent SPST air solenoids. One of the solenoids is for the dump circuit on each of the capacitors, and one is used for the charging circuit for each capacitor. The utility of independent control is the ability to charge the capacitor banks to different voltages. Thus, we have the capability to independently vary the arc discharge current and the magnetic field current.

b) Trigger Boxes

The events to be synchronized are the arc discharge waveform and the application of the pulsed magnetic field.

The currents are initiated by trigger pulses delivered to the respective triggerable gaps. Any timing delays associated with either gap, if significant, would have to be taken into account to determine the actual delay required for synchronous operation.

Providing synchronous timing pulses proved to be no mean task. Many methods were investigated and pursued. Perhaps the easiest method is to use a simple timing delay for the trigger pulses. This is in fact the approach taken. Advantages of this method include the ability to introduce the desired synchronization at an arbitrary time in the arc discharge waveform.

It may turn out that the field-producing current can more accurately or reliably be produced by an electrical circuit which is capable of determining, in real time, the optimum time to initiate the delayed current. For example, a simple circuit could search for a current or voltage extremum. This type of circuit would not add any qualitative ability to the over all performance, but it may improve the reliability.

A simplified control system flow-diagram is given in Figure IV.A.2. A detailed timing diagram indicating the various intrinsic delays associated with the various components is

shown in Figure IV.A.3. From either diagram one can obtain an understanding of the complexity of the process. The latter figure more readily shows the advantages of a passive delay. For instance, even if it were determined that the field should be triggered at a particular moment in time, the time delays inhererent in the remainder of the system must be taken into account for synchronous operation to actually occur. In short, true real-time operation is difficult to achieve.

Figure IV.A.2

SIMPLIFIED CONTROL SIGNAL FLOW DIAGRAM

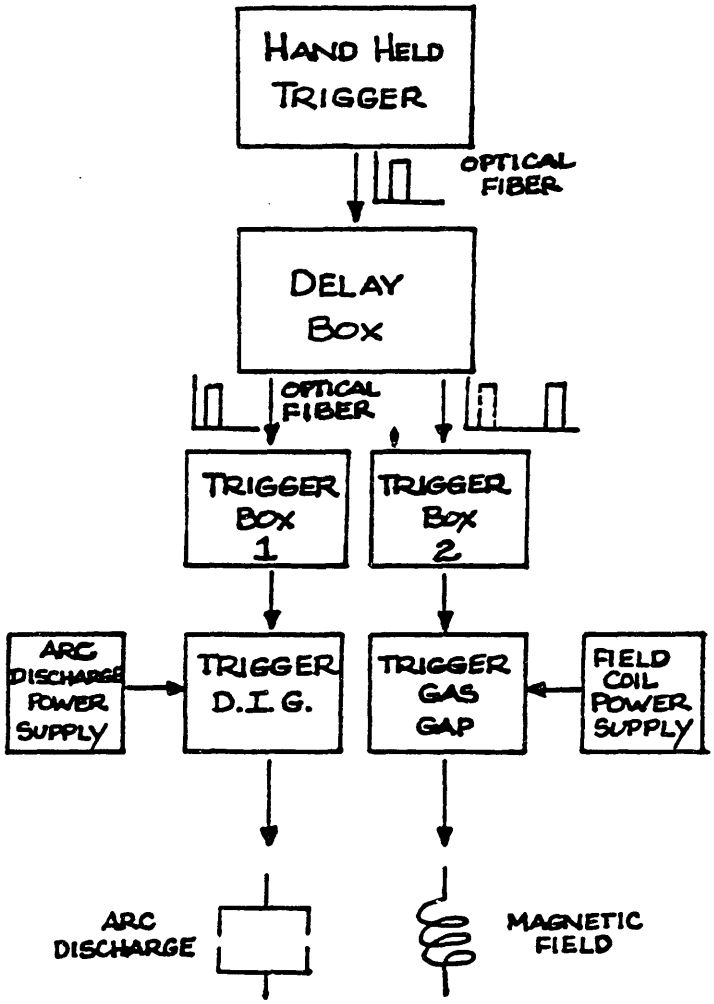

Figure IV.A.3

DETAILED SIGNAL TIMING DIAGRAM

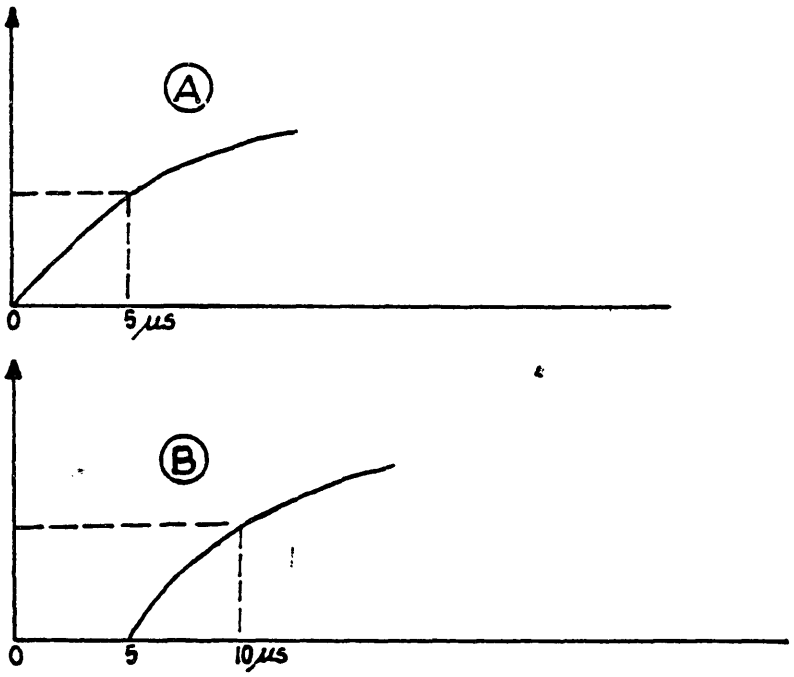

Figure IV.A.3 (cont.)

DETAILED SIGNAL TIMING DIAGRAM

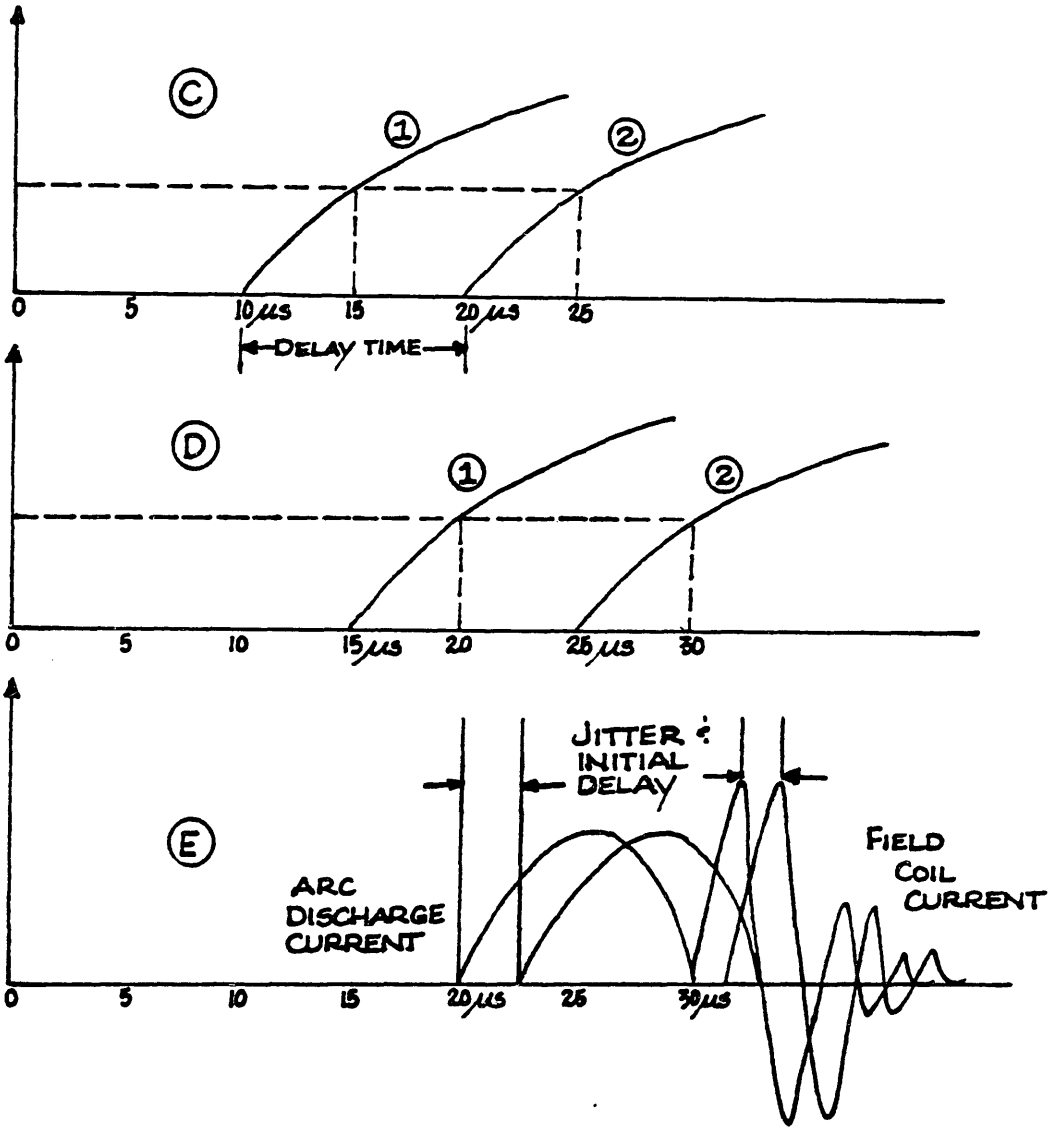

IV. Experimental Work: A. Control System Description

The presence of fiber optics throughout the control system deserves comment. In addition to the omnipresent safety concerns, the ease of implementation of optical fibers makes them a practical answer to the problem of communication with the delay generating electronics. Furthermore, the safety issue, as always, should not be ignored. As indicated in Figure IV.A.2, the high voltage region is isolated from the instrument bench by either, at least, a one megaohm resistor or optical fibers (about five feet long). The instrument bench can be further isolated from the operator by approximately six feet of optical fiber. Thus, the operator is provided an environment safe from any hazards of electrical shock. A nine volt radio battery, which operates the optical emitter, is the only source of current within about eleven feet of the operator.

The circuit implemented for the delay generator is shown in Figure IV.A.4. It shows two outputs which are precisely timed with respect to one another. The first output of the delay box goes to the arc discharge trigger box. This box is shown in electrical schematic in Figure IV.A.5. The second output of the delay box goes to the field-producing trigger box. This box is operationally identical to the arc discharge trigger box.

IV. Experimental Work: A. Control System Description

In essence, the operation is as follows:

1. The hand held trigger emits an optical signal which is detected by the timing box.

2. The timing box gives an output at t=0, and an output some finite time later at $t=T_D$.

3. Each of these outputs, in turn, powers an optical emitter. This signal is detected at the respective trigger box.

4. The receiving photodetector is arranged in a Darlington-type manner with a standard transistor. The resulting current is supplied by a capacitor (introduced for fast response), which triggers a high current SCR.

5. The SCR then shorts one side of the transformer to ground.

At first one may wonder about the wisdom of having the transformer at the primary voltage (600 volts) until the SCR conducts to ground. The reader may be assured that many transistors have been destroyed in attempts to do otherwise. Two alternatives are shown in Figure IV.A.7. When option B was used, we frequently destroyed the second transistor in the Darlington array. The typical breakdown voltage of a transistor (2N3904) is 30 volts. Presumably, the inductance of the transformaer primary caused the SCR to rise high enough in voltage to exceed the reverse-

voltage breakdown rating of the transistor. Option A is presently implemented and no problems have arisen.

Of course, there are many different ways to produce the triggered delay results. It must be said, however, that the trigger pulse provided is quite a robust one. As an example of its utility, the gas gap triggered for the magnetic field has a minimum recommended breakdown voltage (6 KV) far above the value at which we can very reliably operate (2KV). We attribute this circumstance to our particular triggering method.

Figure IV.A.4

DELAY TIMING CIRCUIT

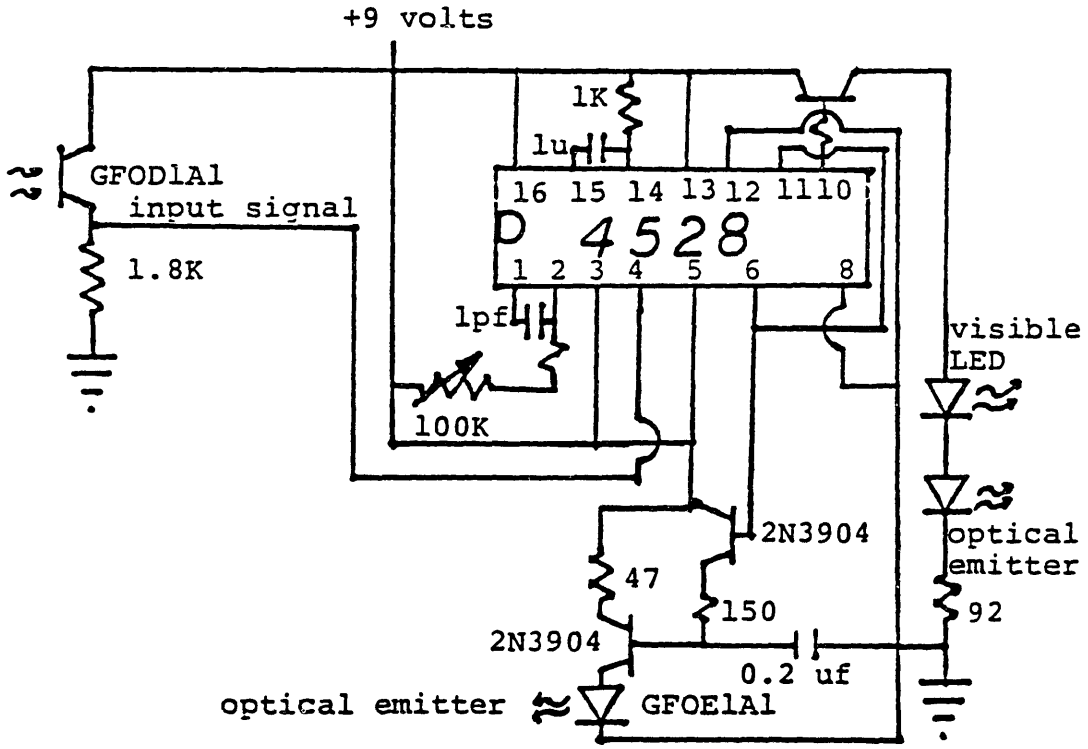

Figure IV.A.5

ARC DISCHARGE AND FIELD COIL TRIGGER BOX

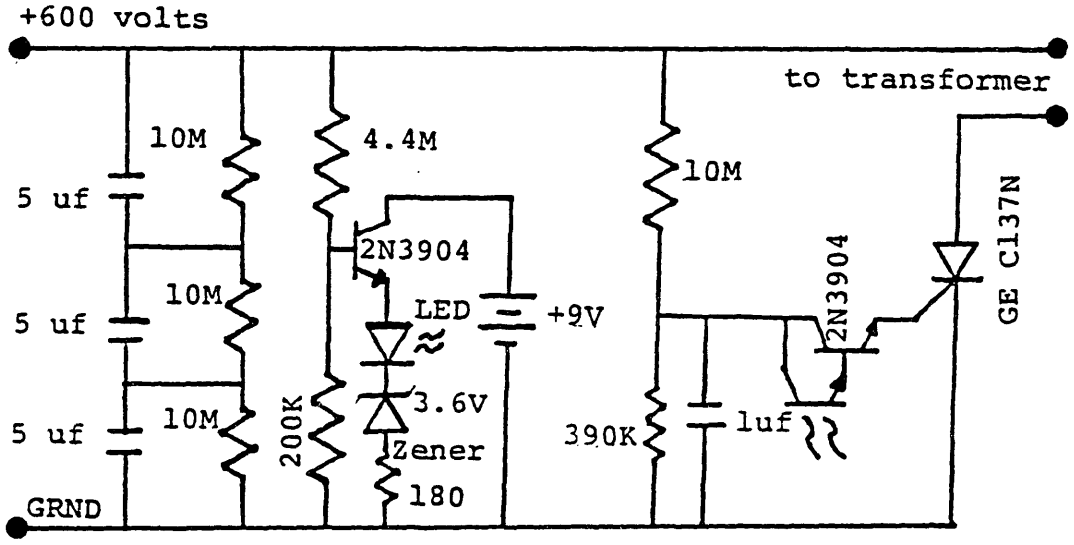

Figure IV.A.6

SCR - TRANSFORMER ALTERNATIVES

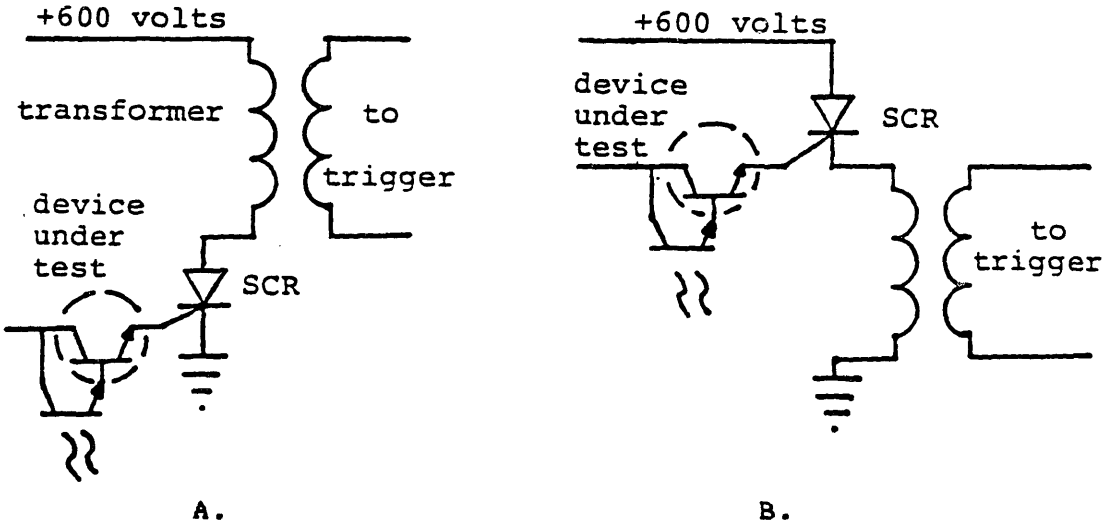

IV.A.2 Diagnostics

In this section we review the type of diagnostics employed through the course of this investigation.

We were primarily interested in gross, macroscopic results. The interruption of a current of order kiloamperes on the first half cycle is the type of event we anticipated. Thus our most important diagnostics were standard tools such as Tektronix high voltage probes, Rogowski coils, and open shutter photographs. The high voltage probes showed the initial charge on the capacitor banks, the final charge on the banks, and the voltage waveforms. The Rogowski coil, when integrated, showed the current as a function of time.

In addition to the obvious use of measuring the arc discharge characteristics, we also conducted control tests with the diagnostics. As an example, when we first installed the magnetic field coil it was bare stainless steel wire. We suspected a discharge was occurring from arc-discharge electrode to coil wire. By use of the Rogowski coil and high voltage probe, we were able to determine the magnitude of the short-circuit current and the parasitic voltage deposited in the field-producing capacitor bank. The effect was actually first noticed on an open shutter photograph which showed tell-tale cathode

spots on the field coil.

As complimentary diagnostics, we employed photodetectors to get an idea of the time history of the light-production from the arc discharge, and Vacion current as an indication of the amount of liberated material from a given shot. Both of these diagnostics aided us tremendously throughout our investigation. As only qualitative information was supplied, however, the usefulness of these methods was limited.

Often over-looked diagnostics, the human visual and aural devices are quite indispensible. Visual indicators ranged from indicator lights to inspections for loose wires or faulty connections. Furthermore, in a darkened room, the existence of corona can visually be detected. One of the first tests performed was the standoff ability of the electrode gap. At 40 KV corona was observed. The maximum operating voltage of 20 KV produced no visible corona. The existence of a small amount of ambient light prevented us from making definitive conclusions from an open shutter photograph, as in performing lower bound measurements on emitted light.

Aural detection of very small arcs due to bad grounding aided us very much during one particular experimental run.

One must exercise caution, however. The human ear is quite sensitive to pressure disturbances. When converted to acoustical energy, the energy of a high voltage capacitor bank can easily permanently deafen an unprotected operator - or anyone else who happens to be in the area at the time of an experimental shot or a fault condition.

IV.A.3 Implementation

Figure IV.A.7 shows an overall electrical schematic of our system. Shown are the pnematic safety valves for the capacitor banks, the hand-held trigger, the optical fibers, the pulse delay box, the two trigger boxes, the vacuum gap, the field coil, and a Rigowskii coil as a current probe.

A variable inductor has been constructed to obtain satifactory time-dependent waveforms. It is constructed of heavy cable wrapped on an insulating mandrel 12 inches in diameter. Typically, we use 20 turns of the cable. This will produce an inductance of 70 uH. With a 37 uf driving capacitor bank, the system has a Z_{eff} of 1.4 .

Figure IV.A.7

OVERALL SYSTEM ELECTRICAL SCHEMATIC

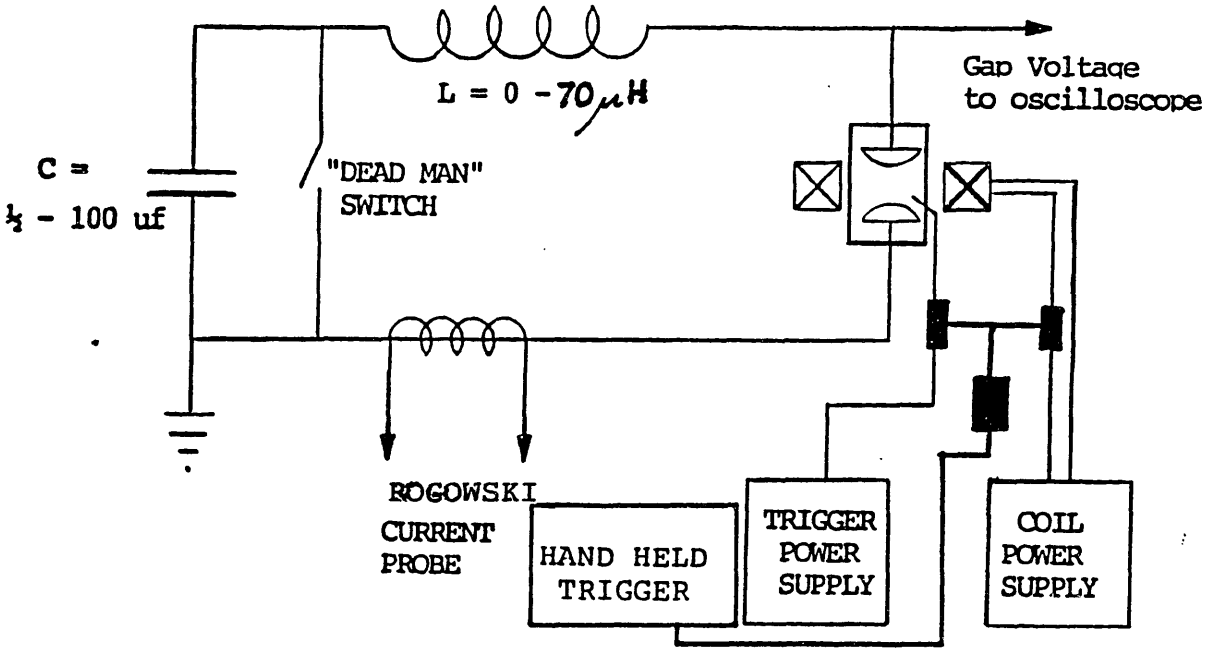

IV.B. Data

In this section we present data obtained from the various diagnostics over the course of the experiment. The data can be conceptually divided according to the type of diagnostic used: prompt is used to describe diagnostics which are monitored on a shot-to-shot basis; periodic is used to describe diagnostics which are meaningful over a relatively long time period.

It should be noted that no external circuit elements were added to enhance the interruption characteristics. Typically, it is common practice for vacuum switch-circuit designers to include capacitors in parallel with the vacuum switch and saturable inductors in series with the switch. These elements improve the interruption performance of the switch. They do not, however, have any effect on the physics of the vacuum switch. Therefore, no experiments were conducted which explored these areas. Obviously, if obtaining maximum results were a concern, the data given below could be improved upon by addition of appropriate external circuit elements.

IV.B.1 Prompt Diagnostics

The high voltage probe, Rogowski coil, photodetector, and open shutter photograph are all prompt diagnostics.

Phenomena such as asymmetry exhibited by the discharge, arc initiation (triggering) effects and interruption characteristics are measured by prompt diagnostics.

It is importnat to note the following definitions concerning electrode polarity. We define the "standard polarity" to be when the upper electrode is the anode and the lower electrode is the cathode. Upon exchange of polarity, we have the "inverted polarity" situation. Inverted polarity has the anode as the lower electrode and the cathode as the upper electrode.

Asymmetry

A striking asymmetric effect was observed to occur in the arc discharge. Out of the several hundred experimental shots, the vast majority had a preferred current half-cycle after which interruption would occur. Specifically, when operating under the standard polarity, interruption would occur almost exclusively after an odd number of current half-cycles. When the electrdoe polarity was inverted, interruption would occur after an even number of half cycles. Figure IV.B.1 schematically illustrates this situation.

An effect related to the interruption half-cycle asymmetry

is the arc-voltage-waveform asymmetry. Operating under standard polarity, the beginning of an even-numbered half-cycle has a much larger transient voltage rise than the beginning of an odd-numbered half-cycle. Similarly, under inverted polarity, the beginning of the even numbered half-cycles exhibits a relatively large transient voltage waveform. A necessary condition for interruption is the transient voltage must exceed the voltage which is re-applied. Essentially, the breakdown strength of the vacuum gap must exceed the applied voltage.

Triggering

Another asymmetric effect observed was the operation of the trigger under anode-cathode inversion. The trigger would initiate a discharge in both circumstances. It required much less energy and current to achieve arc initiation when the trigger assembly was adjacent to the cathode (the so-called "cathode mode"). An increased voltage must be supplied to the trigger box in order to initiate the discharge when the trigger assembly was adjacent to the anode ("anode mode"). The amount of increased voltage required to trigger the discharge depended upon the inter-electrode gap. The design voltage of the trigger box represented a limitation on the maximum allowable gap which would reliably trigger in the anode mode. This circumstance is consistent with the interruption asymmetry discussed

above. Other researchers [Warren, et al, 1981] have noted a similar asymmetry. They also report a difference in operating characteristics for reversal of trigger polarity. We, too, have noticed such effects. The trigger polarity was significant in terms of operating characteristics only under inverted electrode polarity. Because arc initiation was not our emphasis, little quantitative data was recorded.

Interruption

Interruption of AC vacuum switches can be characterized by the peak current in the half-cycle immediately preceding the actual interruption. On this basis we noted the following occurrences:

(1) as mentioned above, the current exhibited an overwhelming tendency to interrupt after an odd or even number of half-cycles, depending upon the electrode polarity, see Figure IV.B.1;

(2) the inter-electrode gap distance had a marked influence on interruption of peak current immediately preceding interruption, see Figure IV.B.2;

(3) gap size influenced the number of half-cycles required to interrupt a given current (the condition of interruption after an odd number of half-cycles for standard electrode polarity persists, and, of course, N_{min}

= 1), see Figure IV.B.3;

(4) smaller discharge frequencies tended to interrupt greater currents (within a modest range), [our experiments did not emphasize this particular aspect, but the tendency was noted];

(5) in multi-half-cycle discharges, the greater the number of half-cycles, the smaller the peak current which immediately preceded interruption, see Figure IV.B.4;

(6) dielectric surfaces in the vicinity of the gap aided interruption, see Figure IV.B.5;

(7) arc re-striking was occassionally observed for temporary interruption times from 1 us to 1 ms, see Figure IV.B.6;

(8) the magnetic field had an effect which tended to reduce the arc recovery-voltage, (to be discussed shortly) see Figure IV.B.7.

(9) for our device and circuit, we have measured recovery parameters of dV/dt = 0.6 kV/us, and dR/dt = 1 Ω/us.

IV.B.2 Periodic Diagnostics

An estimation of the lifetimes of the various components can be determined by inspection of the components after substantial testing. This inspection must, by its very nature, occur only periodically and is somewhat subjective.

The trigger shows serious effects of the plasma environment. Each trigger pulse expels, from the dielectric surface, only a minute quantity of material. The subsequent interaction with the plasma, however, certainly dominates the actual arc intiation event in terms of material loss. The dielectric cylinder surrounding the tungsten pin shows, quite evidently, signs of deterioration and mass loss. It must be said, however, that the dielectric material exhibited deterioration very early in its life (first ~50 shots) and, thus, any subsequent erosion was considered small by comparison. Because the trigger has consistently performed well, it is difficult to make a quantitative estimate of the trigger assembly lifetime at this time; the trigger assembly appears to have an indefinite lifetime. This is likely to be a result of the regeneration of the conductive layer from which the discharge originates. This regeneration occurs primarily as a result of metallic condensation from the previous discharge. The tungsten pin, which is the actual trigger electrode, shows

very little effect of the exposure to the plasma environment. This is to be expected: we selected tungsten as the trigger electrode material precisely because of its low erosion rate.

The electrode lifetime is also expected to be indefintely long. No evidence of bulk or localized melting has been noted. The major effect noted on the electrodes is the familiar cathode tracks, also known as Lichenstein tracks [Graneau, 1981]. These tracks mark areas of the electrodes through which substantial current has passed, as in a cathode spot.

The individual cathode spots, of course, are much too small to observe with the naked eye. One can easily observe, however, the result of repeated arcing. The arcing tends to wear-away any suface impurity which may have been present on the electrodes. The areas which have been effectively "scrubbed" in this manner are demarcated by a smooth, shiny surface. The area on the electrode adjacent to the trigger assembly, especially, is smooth and shiny.

Metallic condensation occurs as a result of each discharge. As mentioned previously, the un-monitored metallic build-up can accumulate until the device is inoperable as an interrupter. The surface nearest the arc serves as a

convenient location for condensation for the metal vapor.

A quick order of magnitude calculation shows that, assuming approximately 500 C have been passed through the device, approximately 10^{21} metal atoms have been ablated from the electrodes. The large surface area of the vacuum vessel means that, for a quasi-uniform spray of vapor over the central region of the vessel walls, approximately a monolayer of metal atoms has formed.

Wiping the inside of the vacuum vessel revealed residue of the arcing process. Teflon, metal atoms, and impurities were the likely components of the residue. When a glass shield was installed immediately surrounding the electrodes, the available surface area for condensation was decreased. Hence, if not periodically cleaned, the thickness of the atom layer could become appreciable within the lifetime of the electrodes.

An additional important observation was the deflection of the magnetic field coils. After dissipating approximately 15 kJ in the field coil (while the coils were electrically connected in parallel), the coils were electrically connected in the anti-parallel mode. Subsequent operation of the coils at current levels of approximately 50 kA

caused a substantial, permanent, yielding of the material. Figure IV.B.8 shows an illustration of the yielding observed. The ability of the coils to produce a magnetic field should not be impaired by this noticeable deformation. The deformation of the coils provides graphic evidence of the existence of a powerful magnetic field.

Figure IV.B.1

ELECTRODE POLARITIES

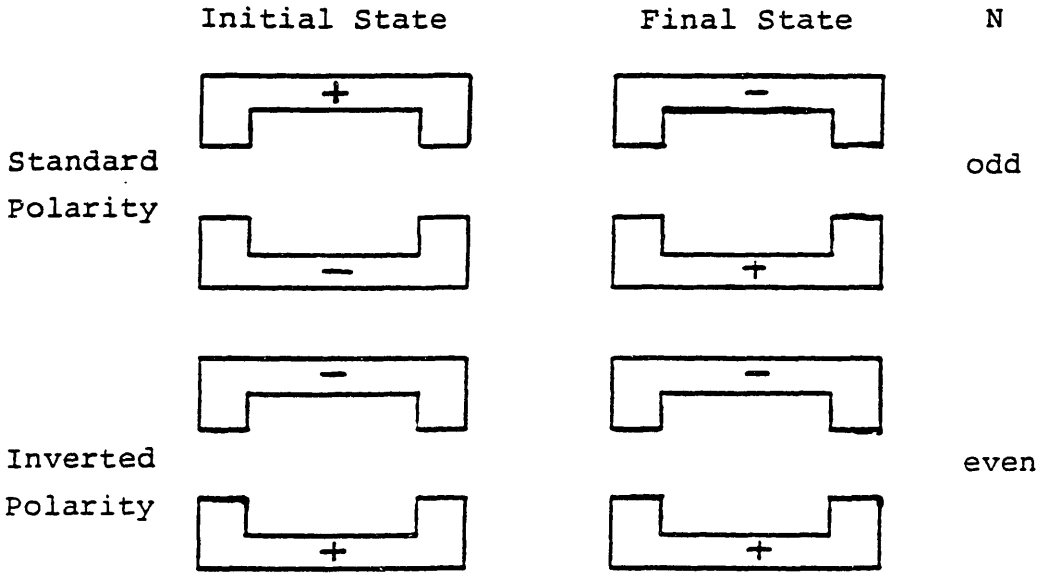

Figure IV.B.2

INTERRUPTING CURRENT VS. GAP SPACING

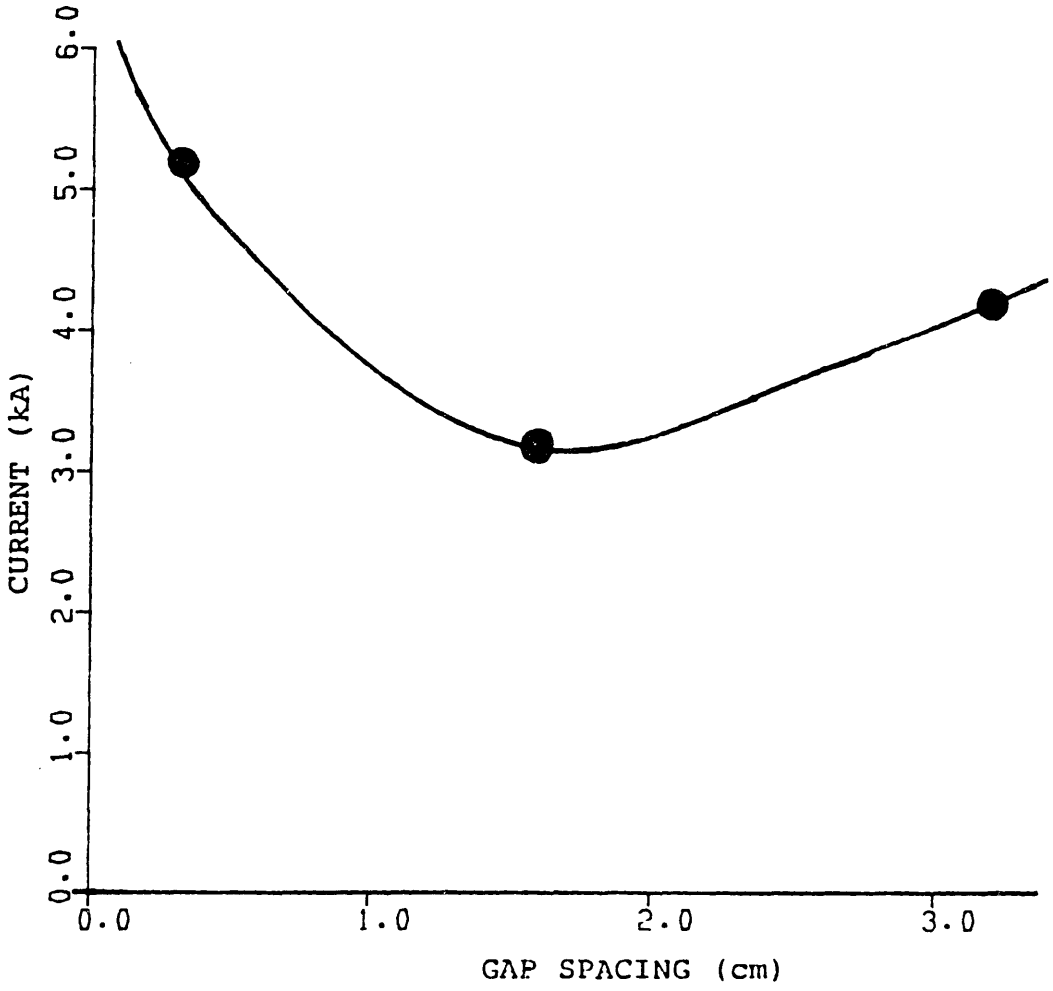

Figure IV.B.3

HALF-CYCLES FOR INTERRUPTION VS. GAP SPACING

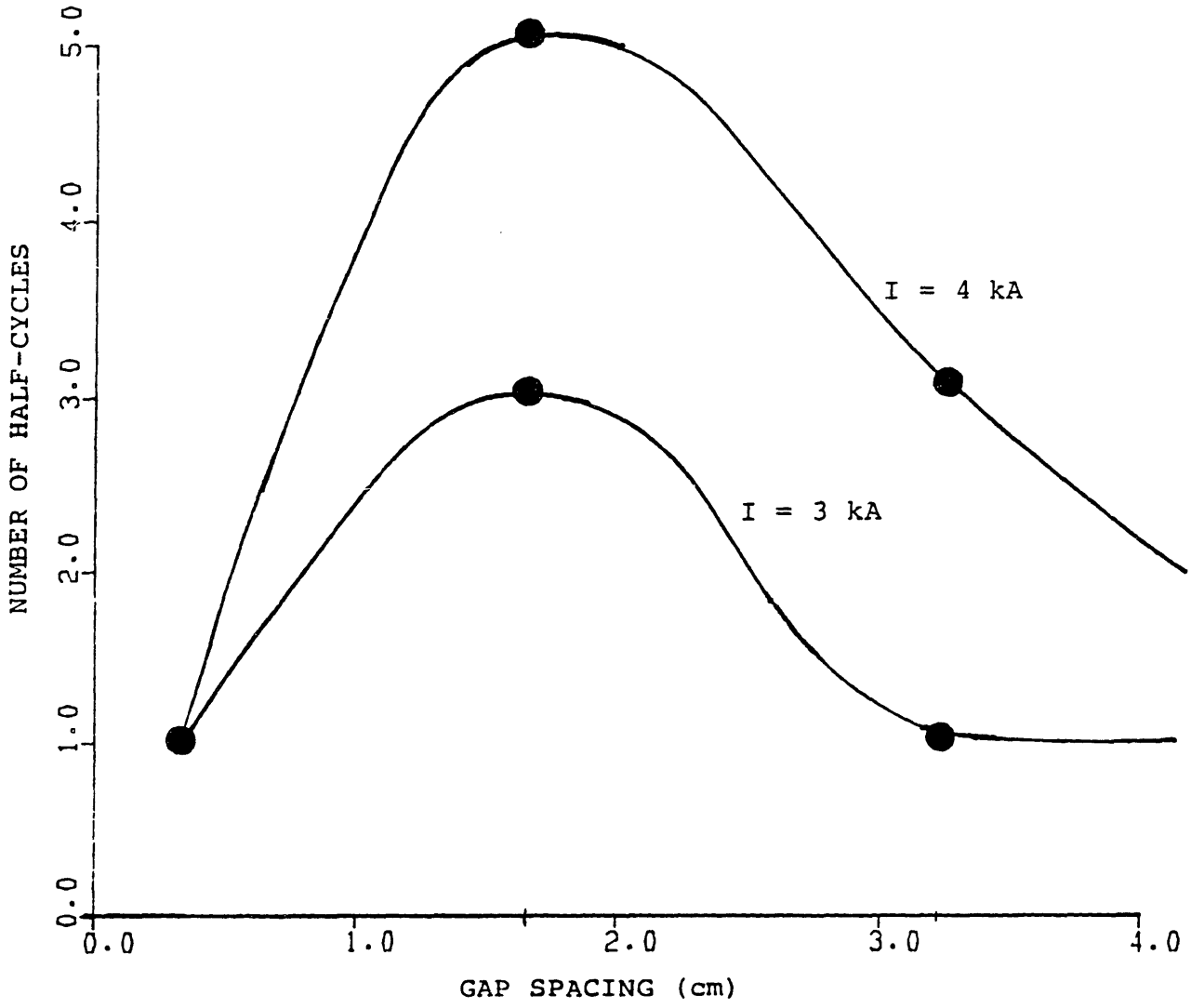

Figure IV.B.4

INTERRUPTION CURRENT VS. NUMBER OF HALF-CYCLES

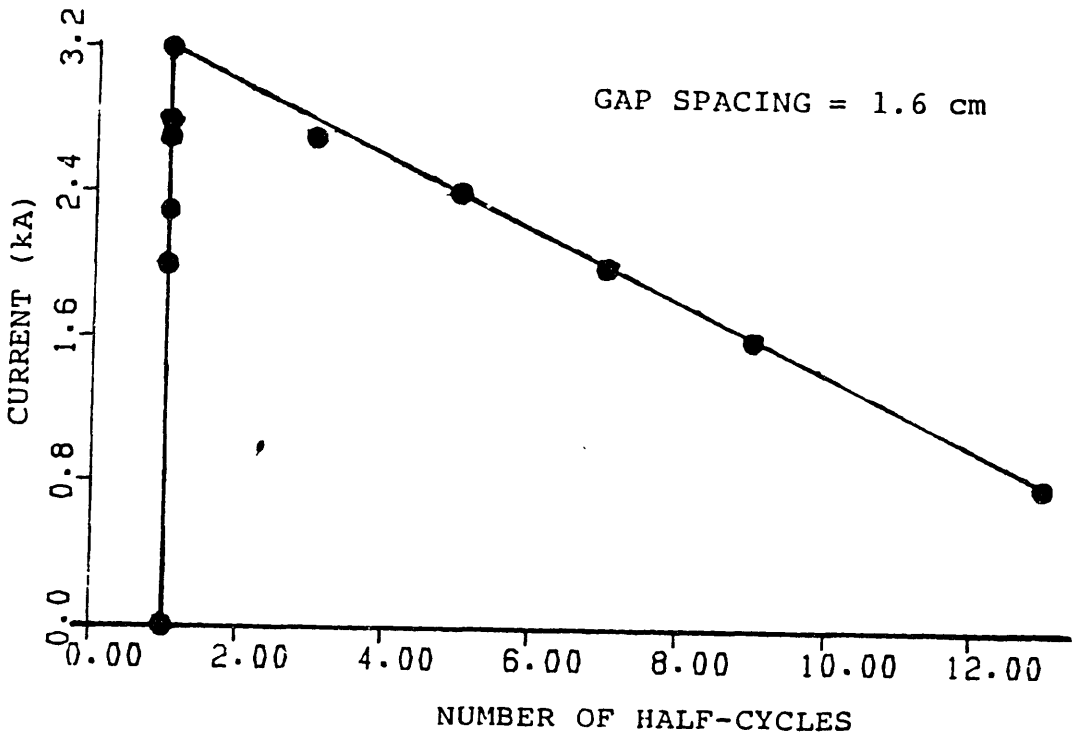

Figure IV.B.5

EFFECT OF DIELECTRIC PROXIMITY

Electrode-Glass Shield Distance	Peak Current Preceding Interruption
16 cm	2.9 kA
4 cm	5.4 kA

Figure IV.B.6

ARC RE-STRIKE

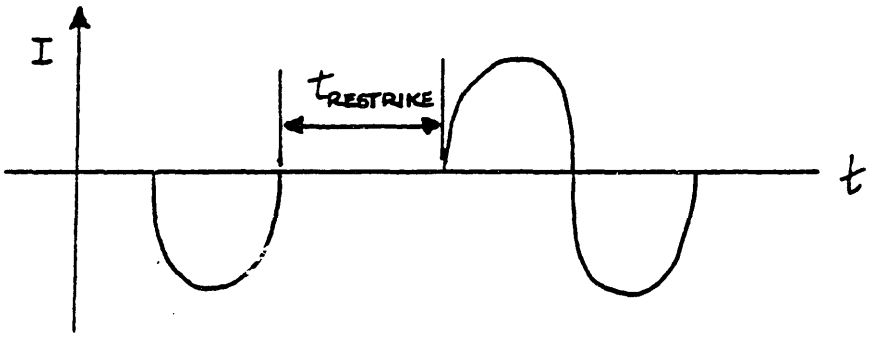

Figure IV.B.7

ARC RECOVERY-VOLTAGE SUPPRESSION

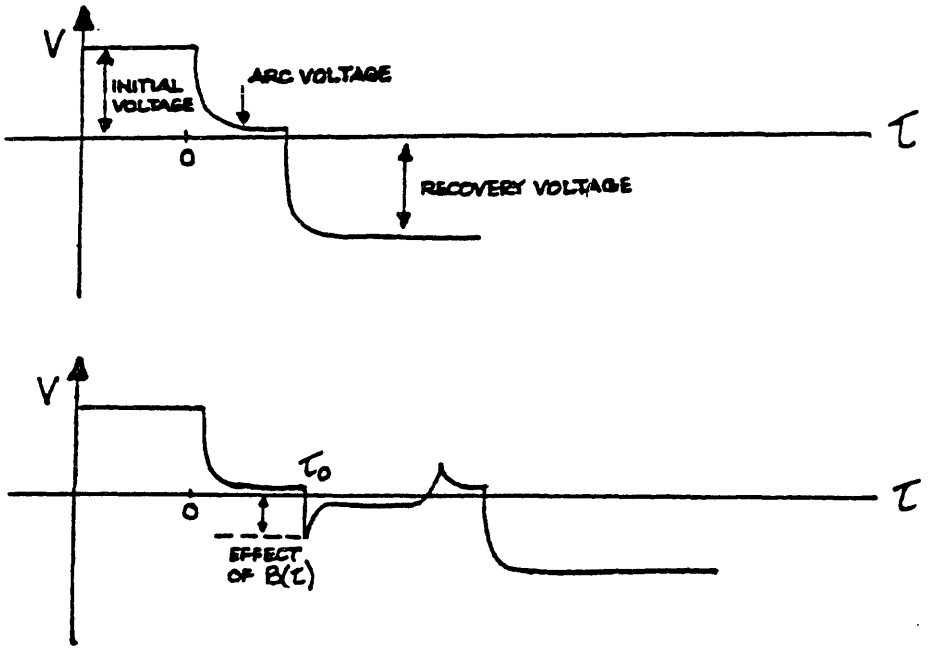

Figure IV.B.8

SCHEMATIC OF FIELD-CAUSED DEFORMATION

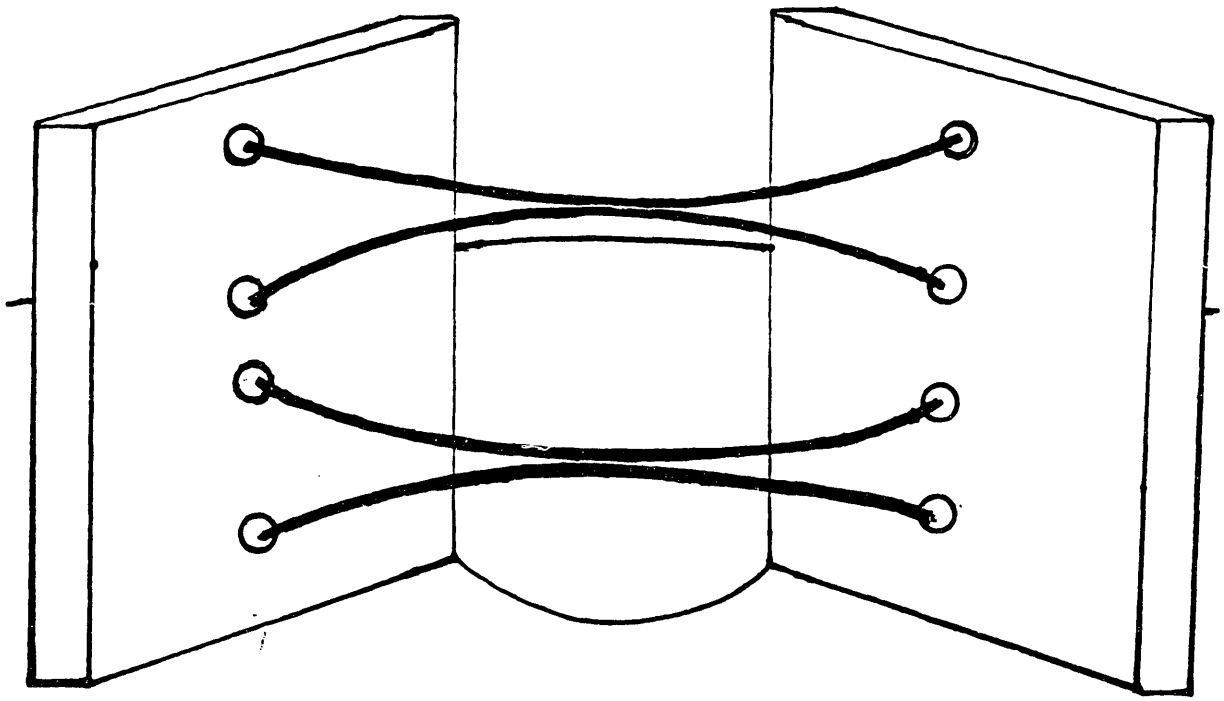

IV.C Interpretation

This section discusses the interpretation of the experimental data presented in Section IV.B. In this section, we focus on the data presented in the figures.

Current dependence on Gap Spacing

Figure IV.B.2 illustrates data representative of the observed trend of the dependence of maximum, single half-cycle current on the gap spacing. In accordance with intuition, beyond a certain gap spacing, increasing the gap increases the maximum interruptable current. This increase results from the well known [Mitchell, 1970; Reece, 1963] increase in arc voltage at larger gap spacing.

An increase in the maximum current also occurs as the gap is reduced below a certain gap spacing. There are two distinct mechanisms at work here. The first mechanism is related to the condensation time of metal vapor in the gap. The condensation time is the time required for the metal vapor to condense on a surrounding surface. As the gap is reduced, the electrode surfaces represent a larger solid angle from the point of view of the plasma. Thus, the time to condense on such surfaces is reduced. The second mechanism, occurring simultaneously with the first mechanism, is similar to the left hand branch of the

Paschen Voltage-pd curve. As the gap decreases, Townsend avalanche conditions become harder to satisfy. The mean free path for ionization becomes greater than the gap. Hence, ionizing particles simply traverse the gap before initiating an ionization event.

As shown by Boxman [Boxman, 1974], the plasma density is proportional to the arc current. The plasma pressure is, of course, directly related to the plasma density. Operation at fixed circuit parameters (L,C) means higher currents require higher voltages. Justification for interpretation of Figure IV.B.2 as a Paschen-type phenomenon is given by plotting the voltage against the product of the current and the gap spacing. In Figure IV.C.1 such a plot is diagrammed. When interpreted in this light, the terminology "vacuum arc" is quite misleading, indeed.

Figure IV.C.1

APPLIED VOLTAGE VS. CURRENT-GAP PRODUCT

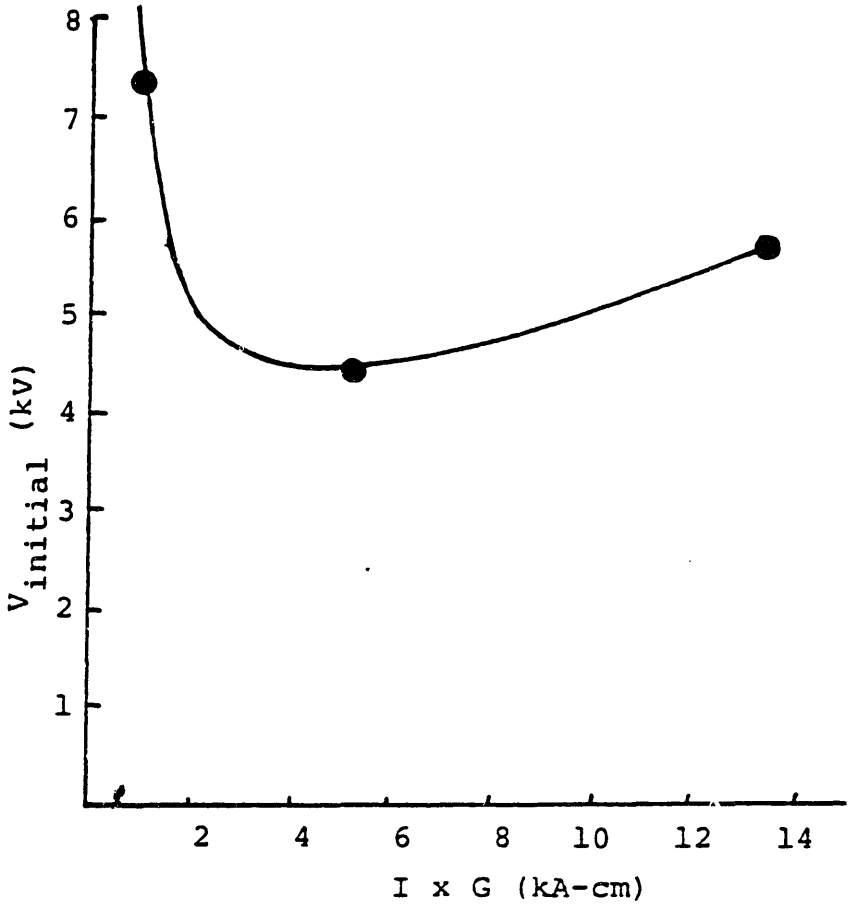

Interruption-Current dependence on Half-Cycles

Increasing the current beyond the maximum interruptable current for the particular gap spacing causes arc re-ignition to occur at the first current zero. Thus, the current executes another two half-cycles (and the total half-cycle number remains odd numbered). The peak current which immediately precedes interruption is observed to decrease with an increase in the number of half-cycles.

Thermal effects occurring to the electrodes cause this reduction in interruptable current. As shown in Figure IV.B.3, this reduction effect is roughly proportional to the actual number of half-cycles executed for the gap spacing noted. (We observed different characteristics for different gap spacings.)

Each subsequent full period of conduction deposits more energy on at the electrode surface. This heats the metal, and causes an increased ablation rate. The presence of the increased neutral gas impairs the interruption capability of the switch. The plasma density must be proportionately reduced if interruption is to occur.

This interpretation is justified by Section II.E.2. In that section it is demonstrated theoretically that the number of ablated atoms depends linearly on the energy input. Thus, to the extent that the energy input per full-cycle is the same for subsequent full-cycle conduction periods, our theoretical and experimental models are consistent. Because the arc current is actually a damped sinusoid, the assumption of constant energy input per period is not strictly true and must be taken as approximate. The current decays only a few hundred amps per period (less than 10% of the total arc current), however, the approximation is quite

accurate.

Presence of Dielectric Surfaces

We have emphasized surface condensation as the quenching mechanism of vacuum arcs. A clear demonstration of this effect occurred as a circumstance of the method of isolation of the field coils from the arc discharge. When operated in a triggered vacuum gap mode, improved interruption capabilities were observed following installation of a second glass cylinder surrounding the electrodes. This cylinder physically separated the electrodes from the field coil.

Originally the nearest vertical surface, on which plasma could condense, was the vacuum vessel wall. The distance from the electrodes to the chamber wall is approximately 16 cm. We installed an additional glass cylinder which effectively isolated the electrodes from the other surfaces on which vapor might condense. The reasons for doing this are discussed shortly. The net result of this isolation-dielectric surface closer to the gap resulted in improved interruption characteristics. Figure IV.B.4 shows a table comparing the electrode-glass shield distance and the peak single-half-cycle currents which were subsequently interrupted.

Teflon has many qualities desirable from an experimental viewpoint. Easy machinability, good dielectric properties, acceptable vacuum properties, and lack of carbon by-products are all characteristics which make Teflon a very attractive material. Accordingly, Teflon was employed as a material for several key components in our system.

Contact of Teflon with the plasma tends to ablate the Teflon. This phase change is preferred to carbonization, a process which occurs to most plastics, as carbonization leaves a conductive residue. A disadvantage of this transformation is the release of ionizable material into the discharge volume. Thus, we believe the improved interruption performance, associated with the installation of the glass shield, may partially be a result of separation of the plasma from contact with Teflon.

Arc-Restrike

Occassionally, it has been observed that the arc will temporarily interrupt for a period of time ranging from 1 us to 1 ms, although it may subsequently re-strike. The exact breakdown mechanism is not known. It is believed that thermal processes and T-F electron emission play a role in breakdown of the temporarily recovered gap. Figure IV.B.5 shows a typical arc re-striking event.

It has been mentioned that no evidence of macroscopic melting has been observed. Cathode spots certainly exist, however, there is no reason to rule-out the continued evolution of metal vapor from a hot localized surface region which previously may have been a cathode spot. Alternatively, residual trapped gas may be outgassing either from the actual electrodes or from the surrounding surfaces. The accomodation coefficient is not exactly unity; this implies reflection of vapor from solid surfaces. Thus, there are several sources of extraneous vapor which may occupy the gap volume.

Microprotrusions, resulting from solidification of cathode spots, have radii of only a few microns. Hence, average electric fields of only a few kilovolts per centimeter can be magnified several thousand times, to values which may cause substantial electron emission current. This emission current will be greater for higher temperatures of the emitting region.

The emission current may directly ionize the residual gas in the gap volume. Alternatively, energy deposition at the electrode may cause gas to evolve from the surface. This evolved gas may subsequently become ionized.

It is important to recall that the electrodes exchange polarity in an AC discharge. That is, the former cathode (electron emitter) is the new anode (electron receiver). Thus, microprotrusions formed during the previous half-cycle are field-enhanced "targets" during the ensuing cycle.

Magnetic Field Effects

Before we detail the observed effects of the magnetic field, we describe some of the problems experienced as a result of our unique mode of operation.

We observed unanticipated interactions of the arc plasma and the exposed wire of the coil which produced the magnetic field. These interactions produced an electrical short of the high voltage electrode to ground through the field coil winding. In open shutter photographs, we observed several brightly illuminated cathode spots on the magnetic field coils. These photographs prompted a more thorough investigation into the phenomenon.

The results of the investigation proved that substantial currents were indeed flowing through the coils to ground. We tested the coils under two conditions: both sides of the field-coil-capacitor shorted to ground, and one side of the capacitor electrically floating. In the former case we

observed a current of 200 Amps to ground. The latter case showed a short circuit current of 400 Amps. Although we did not observe a turn-to-turn short of the coil, we considered it feasible and so we re-designed the coil.

The new design called for 8 gauge copper wire inserted through 7 gauge Teflon tubing. The Teflon tubing was chosen to have a thickness sufficient to prevent recurrence of the short circuit.

A continuous length of tubing was used for each of the two coils. This amounted to a tubing length of approximately two meters per coil. This represented an engineering trade-off between good electrical isolation and good high-vacuum practice. The vacuum pump had to evacuate the full length of tubing if this design were to be effective. The mid-point was one meter from either end. The pumping aperature was effectively one-half of the difference in diameter between standard 7 gauge and 8 gauge items. This aperature was approximately 20 mils. After an appropriately long vacuum pump-down, it was determined that the implementation was ready to be tested.

The tubing worked precisely as designed. The plasma no longer shorted to the coil wire itself. End effects,

however, still persisted in supporting a short circuit. The plasma, essentially, took the path of next least resistance. Instead of shorting directly to the wire, the plasma shorted to the exposed end connections.

This prompted a total field-coil design review. Intermediate solutions, obviously, were not going to work. An all-encompassing solution was finally implemented. It consisted of a vertically mounted glass cylinder totally surrounding the electrodes, with exceptions being allowed for vacuum pumping of the electrode volume. This almost total physical separation of electrodes from the rest of the chamber significantly increased the impedance between different elements of any potential short circuit. Figure IV.C.2 shows a schematic drawing of the solution implemented.

Another possible explanation for the apparent effect of the magnetic field was the actual breakdown of the coil leads. This effect was periodically checked and the usual result was negative: no effect. We noticed, however, that impurities have accumulated at the coil junctions. One of the latest experiments demonstrated high-voltage breakdown of these impurities. Although the periodic checks rule out this effect for all experimental runs, the possibility of a spurious discharge caused by impurity breakdown must be

taken into consideration, especially at higher voltages.

Figure IV.C.2

ELECTRODE ISOLATION CYLINDER

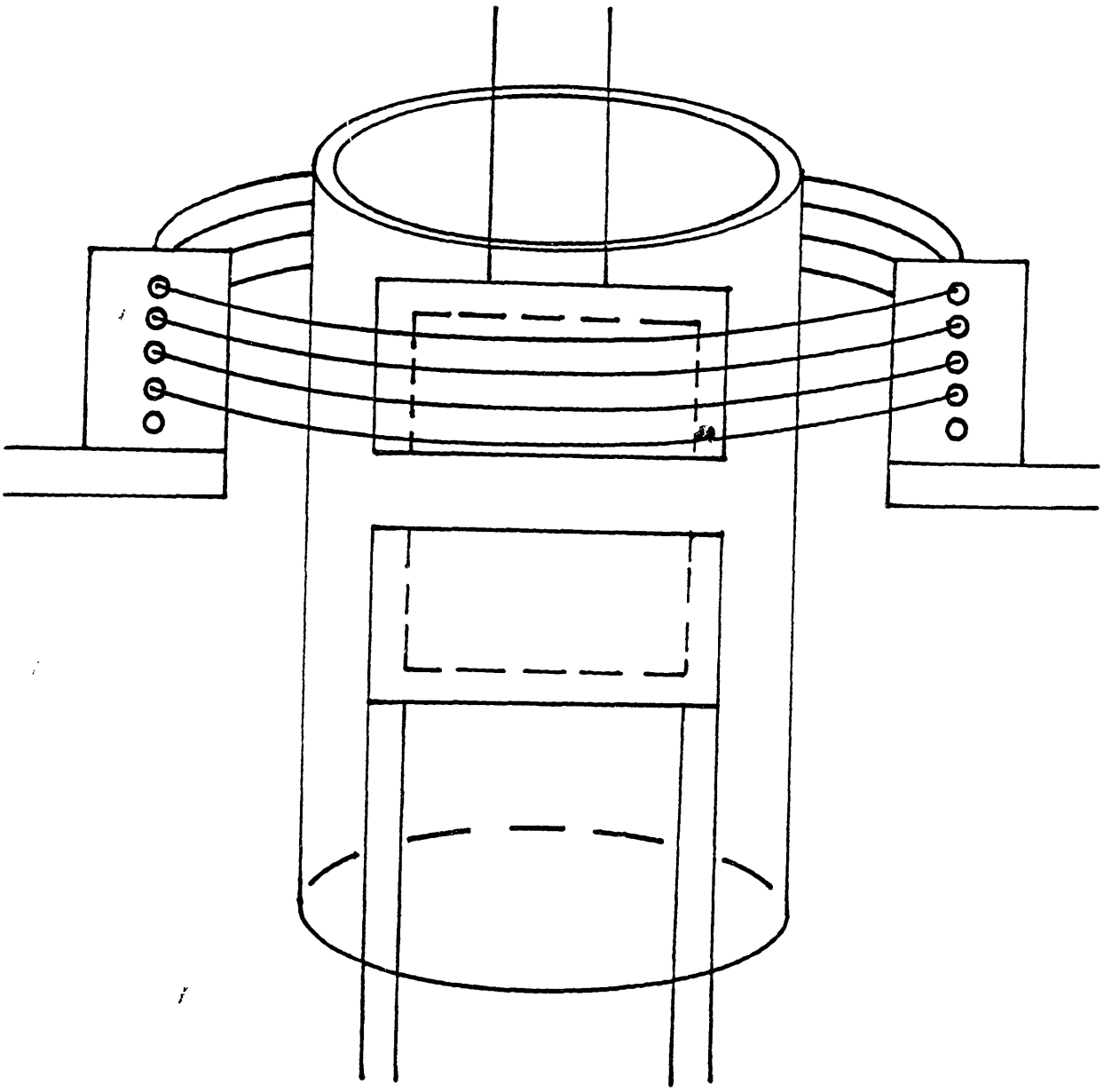

A mounting jig was arranged which held the cylinder, but allowed for vertical movement of the cylinder. This was necessary due to the effect of the expected metallic condensation on the glass walls. The glass can be periodically adjusted up or down to provide a fresh dielectic surface for condensation. Visual observation of the discharge is also aided by moving the obstructing condensed material out of the gap line-of-sight.

As mentioned in the data section, we observed recovery parameters of dV/dt = 0.6 kV/us and dR/dt = 1 Ω/us. These figures apply in the absence of an applied magnetic field. Application of the magnetic field produced a somewhat surprising effect on the interruption parameters. We observed a reduction in the parameters which would accompany interruption when the field was applied. This phenomenon is illustrated in Figure IV.B.6; the field decreased the breakdown voltage.

It appears as if the magnetic field better confined the plasma. Magnetic confinement of plasma is the central idea behind many experimental fusion devices. The topology of our device resembles a particular class of magnetic confinement schemes: the torodoidal fusion devices, or Tokamaks. Because of this topological similarity we consider it possible that the applied field is, indeed,

acting to confine the plasma. Figure IV.C.3 shows an idealized representation of the magnetic fields.

Figure IV.C.3

SCHEMATIC REPRESENTATION OF PULSED MAGNETIC FIELDS

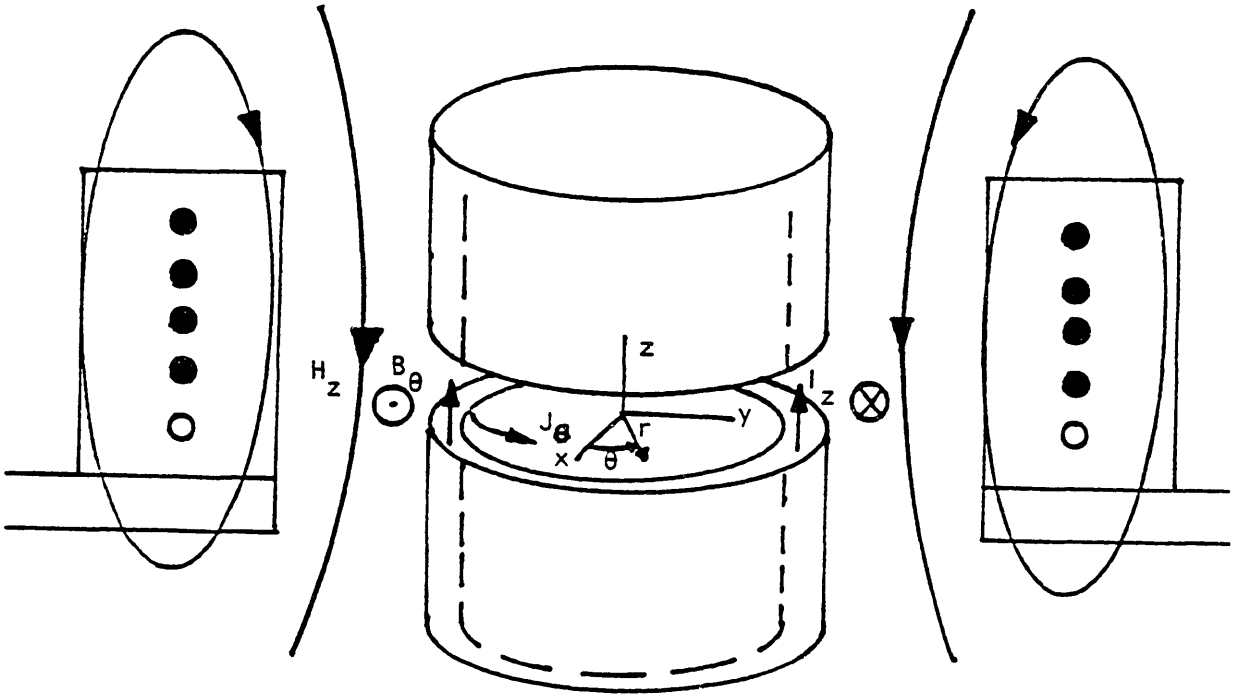

PRESENT DEVICE	TOKAMAK
J_θ	plasma current
B_θ	torodial field
H_z	vertical magnetic field

Our interpretation of this phenomenon is the following: the Lorentz force, which acts to constrict the diameter of the plasma ring, also acts to confine the plasma while the contraction occurs. However, the possibility of spurious, parasitic discharges must be considered.

Hence, we have an ironic twist of events: The same mechanism that moves the plasma also holds the plasma together while it is being moved. Simply increasing the magnitude of the magnetic field does not produce any change in this chain of events. Although a greater force acts on the plasma, a greater confining force is also present.

IV.D. Summary

This thesis has investigated the physics of vacuum arcs and examined how characteristics of vacuum arcs are applicable to vacuum switches. Specifically, four distinct areas have been discussed in-depth. They are the following: (1) Theory of vacuum arcs, including several new theoretical approaches; (2) Description of our device, this amounts to a transfer of technology from our group to the public domain; (3) Data obtained by the device, including some interesting results; and (4) Interpretation of the data, which binds together the theory, device, and the data.

Theory of Arcs

A generalized power balance of vacuum arcs has been examined in detail. Original theoretical extensions have been provided in four separate areas. The cathode spot radius and formation time were theoretically predicted and these predictions agreed well with experimental observations. The quasi-steady state phenomena of electrode ablation and plasma potential hump formation were examined in detail. These original theoretical results again were in good agreement with experimental results. The phenomenon of arc stability during arc extinction was also investigated. It was found that a model based on electrode energy

conservation fit the available experimental data. This physically more-appealing model is in contrast to a previous, heuristic model of arc stability based on electrode material vapor pressure.

In each of the above cases, theoretical models were developed which were quite simple and emphasized the physics of the particular situation. Good agreement was obtained between predictions of the theoretical models and experimental results. The theory could be extended to improve the agreement, however, the essential physics is clearer in a simplified presentation.

The characteristics of materials, such as vapor pressure, outgassing rate, and erosion rate, which must be considered for use in vacuum switches are discussed. Because there is such a wide variation in properties of materials, various engineering trade-offs must be made. For instance, dielectrics commonly do not exhibit both good machining and good vacuum outgassing characteristics. Another trade-off example is provided by Tungsten. The undesirable thermionic electron emission characteristics must be considered as well as the desirable high melting point of Tungsten.

Basic plasma physics has been included to provide the fundamental knowledge necessary to understand the issues of vacuum arc switches. This type of transfer of technology,

methodology, and information from theory to practice is an important result of solutions to applied physics problems.

The mechanics of interruption have been discussed. Magnetically aided interruption was covered on two levels of rigor: a very simplified kinematic model with constant plasma properties, and another, more complete, model which took into account radial dependence of plasma parameters.

Device

The team at MIT/EML has helped me in the formulation of several design criteria for the experimental device. Details of design and construction of our particular device have been given. Many unique uses of materials and techniques have been used. Examples of such uses include the implementation of Teflon structures and re-usable rubber vacuum gaskets. We have built an experimental device that imposes few restrictions on the experiment itself. The ability to modify an experiment based on intermediate results has a value which cannot be over-estimated.

Data and Interpretation

The device has been operated in two modes: a triggered vacuum gap (TVG) mode, and a magnetically augmented TVG mode. The results for the TVG mode are in good agreement with the results of other researchers (in terms of

interruption times, currents, and voltages) and present a baseline for the magnetically augmented results. The results of magnetic augmentation show that magnetic fields can be used to manipulate the arc plasma. The results further show, however, that the plasma is quite difficult to control precisely. We have been able to apply a magnetic field which constricts and confines the plasma, yet becaused the plasma is confined, arc extinction does not immediately occur.

Over 200 experimental shots have been fired. Benchmark results are: single-half-cycle peak current interruption of 5.2 kA, recovery voltage of 7 kV, and an interruption time of approximately 10 us.

Future Work

The idea of a plasma baffle was conceived prior to construction of the device. It was decided, however, that for simplicity the device would be constructed without it. Surface metal-vapor condensation will have immediate application to improved field-augmented plasma extinction. Baffles can be installed on which the field-confined and field-driven plasma will condense. The baffle design will likely resemble that of ordinary gas-arc chutes. The open cylinder-electrode design of the device will allow for installation of such a baffle.

Appendix A

Numerical Power Calculations

In this appendix the numerical details of the results presented in Figure II.A.8 are given. Descriptions of the various processes can be found beginning in Section II.A.1. Other numerical assumptions necessary for these calculations are presented in Figure II.A.7. P is the total power in Watts and F is the surface power density in Watts/cm^2. The subscript "spot" indicates the effective area is the cathode spot area; the subscript "ave" indicates the effective area is the entire surface area of cathode.

(1) charged particles: $P = ZV_iI_+ = 1 \times 43V \times 0.1 \times 10kA$

$P = 43\ kW,$

$F_{spot} = ZV_iJ_+ = 1 \times 43V \times .1 \times 5x10^6\ a/cm^2$

$F_{spot} = 21.5\ MW/cm^2.$

(2) neutral particles: $P = \pi r[E_n \Gamma_n A + \langle\sigma_{cx}v_i\rangle n_i\ n_n\ E_i\ A\ dl]$

$P = .5\ [3.8x10^{-20}J \times 3x10^{21}cm^{-2}s^{-1} \times 25 +$

$10^{-16}cm^2x10^6cm/sx10^{16}cm^{-3}x10^{17}cm^{-3}x1.6x10^{-19}Jx25cm^2x.07cm]$

$P = 15\ kW$

$F_{ave} = P/A = 620\ W/cm^2.$

(3) ohmic heating: $P = I^2R$; $R = 73x10^{-6} \times 7cm/\ 25\ cm^2$;

P = 2 kW.

(4) radiation: $P_{rad} = \Omega [P_{rad\ recomb} + P_{Brem} + P_{line}]$

$P_{recomb} = \alpha_r n_e n_i V_p E$ = 6 kW; F_{rec} = 240 W/cm^2,

$\alpha_r = 10^{-11}$ cm^3/s,

$P_{Brem} = 1.7 \times 10^{-32} n_e n_i T^{0.5} V_p$ = 425 W;

F_{Brem} = 20W/cm^2,

$P_{line} = \sum_n \sum_m A_{nm} E_{nm} N_n$ = 4 kW; F_{line} = 160 W/cm^2,

Ω = 0.3 strd,

P_{rad} = 3.3 kW; F_{ave} = 130 W/cm^2.

(5) recombination (three body): $P_{3B} = \alpha_{3B} (n_e)^2 n_i V_s \Delta E$

P = 4 kW,

ΔE = 1 eV

$\alpha_{3B} = 9 \times 10^{-27} T^{-4.5}$ cm^6/s = 10^{-26} cm^6/s,

F_{ave} = 160 W/cm^2.

(6) ionization: $P_{ioniz} = XI\ E/m$ = 7 kW,

F_{sPot} = 3.5 MW/cm^2.

(7) grey body rad.: $P_{BB} = [\sigma (T_{sPot})^4 A_{sPot} + \sigma (T_{bulk})^4 A_{bulk}] \epsilon$

P = 100 W

$F_{sPot} = \sigma (T_{sPot}^4 + T_{bulk}^4)$ = 200W/cm^2.

(8) thermal conduction: $P = A_{sPot}\ k\ dT/dx$ = 3.2 kW,

$F_{sPot} = P/A = 1.6\ MW/cm^2$.

(9) phase change: $P = (H_{fusion} + H_{vaPor})\ XI = 6.6\ kW$,

$F_{sPot} = (H_f + H_v)\ XJ = 3.3\ MW/cm^2$.

(10) work function cooling: $P_{\phi-} = \phi_- I_- = .9\ \phi_-\ I = 23\ kW$,

$F_{sPot} = \phi_-\ J_- = 11.5\ MW/cm^2$.

(11) electron heat capacity: $P = 1.5\ k_B(T_H - T_C)\ I_-/e$

$P = 3.5\ kW$,

$F_{sPot} = 1.5\ k_B(T_H - T_C)\ J_-/e = 1.8\ MW/cm^2$.

Appendix B Application Considerations

V.B Mega Amp Issues

As in most fundamental experimental investigations, we were interested in the parameters which ultimately limit the performance level of a metal vapor vacuum arc switch. Primarily, we were concerned with limitations imposed by increasing the arc discharge current. More specifically, the question is whether operation at mega-ampere current levels is feasible. If a metal vapor vacuum arc switch could trigger, conduct, and interrupt at the mega-ampere current level it would be a very attractive device for a number of applications. However, several limiting areas must be considered carefully before an experimental program is undertaken to achieve this capability. The operating characteristics of vacuum arcs offer so many unique advantages (rapid commutation, low losses, very high voltage operation) that in the future such an effort should certainly be considered.

Electrode Erosion

Electrode erosion is the most serious concern of high current operation. This is due to bulk metal removable caused by the very great currents and deposition on surrounding surfaces. Because lifetime considerations imply a volume erosion, Figure V.B.1 shows erosion

characteristics of several in terms of cubic centimeter eroded per Coulomb of current passed.

Figure V.B.1

MATERIAL VOLUME EROSION CHARACTERISTICS

Metal	Erosion rate (ucm^3/C)
Cd	76
Zn	30
Mg	20
Ag	14
Al	44
Cu	13
Cr	5.6
Ni	11
Fe	8
Ti	11.6
C	7.6
Mo	4.6
W	3.2

In addition to overall cycle lifetime consideration, however, erosion has other implications. As mention above, plasma condensation on surrounding surface occurs during

current interruption. Unless the switch has been properly designed to take this condensation into account, the build-up of metal may lead to an internal short circuit of the device and subsequent disposal of the inoperative device. If this build-up occurs un-monitored, one must consider the devices as disposable after a certain number of cycles or risk catastrophic failure of the device once the condensed metal reaches a critical level. It is common design practice to shield critical components from condensation of low current erosion by blocking the solid angle of the component as seen from the eroding metal. However, for high current operation, it is not sufficient to merely shield components from the line of sight of the electrode in order to prevent exposure to condensation.

Erosion in droplet form has been observed by several researchers [Daalder, 1976; Jenkins, et al, 1975; Tuma, et al, 1978]. Tuma, et al [Tuma, et al, 1978] have observed condensation on parts of their apparatus which were not exposed to the eroding surface. In particular, the back side of the cathode received a flux of metal particles which subsequently condensed in situ. Two explanations arise. One, suggested by Jenkins, et al [Jenkins, et al, 1975], is that macroparticles of the eroding surface have been ejected with a substanial velocity in an arbitrary

direction. As the macroparticle continues along its flight it continuously emits vapor (as when boiling). This results in sending neutral atoms (and molecules, if present) along another line of sight. The second explanation relies on collisions to re-distribute the particle flux [Tuma, et al 1978]. Essentially, then, the metal atoms have executed an "end run" around shields installed for the purpose of protecting build-up of metal condensate.

At high current levels anode spot formation is observed. In contrast to cathode spots, anode spots are bulk liquid-metal areas. Typically of a few centimeters in diameter, the anode spots represent a more difficult challenge to extinguish than cathode spots. This is primarily a result of the large thermal inertia of the gross melting area which continues to release vapor during a current zero, and partly because, in an AC discharge, the former anode becomes the new cathode and as such it is susceptible to electron emission by the "T-F" mechanism [Lee, 1960].

As mentioned in the materials section (Section II.B) of this thesis, Rich [Rich, 1971] experimentally investigated anode spots. He found that for a given geometry and frequency situation, metals differed widely according to the peak current which could be drawn without anode spot formation. The peak current achieved without anode spot

formation is called the critical current. He correlated the critical current dependence with a thermal goodness parameter $T_m(k\rho Cp)^{0.5}$. His results for a variety of metals appear in Figure V.B.2. (Rich used electrodes 5.7 cm in diameter.)

Figure V.B.2

CRITICAL CURRENT VS. THERMAL "GOODNESS" PARAMETER
[Rich, 1971]

Metal	Critical Current	$T_m(k\rho Cp)^{0.5}$
Sn	2.3 kA	57
Al	6.8 kA	383
Ag	9.7 kA	723
Cu	10.3 kA	954
Mo	13.6 kA	1204
W	13.8 kA	1693

By using the same material in a variety of geometrical configurations, Rich further found geometry to make a significant difference in the critical current. Kamakshaiah and Rau [Kamakshaiah and Rau, 1977] concluded that the arcing time, electrode surface conditions, and contact separations also factor into anode spot formation.

Thus, a variety of guidelines are available to the switch designer which enable him to design higher performance switches.

Current Sharing

The Introduction contains a list of vacuum arc properties. Included in this list is the condition of positive voltage-current relationship. The discussion of cathode spots also mentioned this feature of vacuum switches. The practical implication of a positive voltage-current characteristic is the stable parallel operation of vacuum arcs. Unlike gas gaps, the voltage across the electrode gap of a vacuum arc increases roughly linearly as current increases. Hence, these devices share current evenly among all available arcs.

Since most of the cost of a vacuum switch is the cost of a vacuum vessel and associated high voltage/current feedthroughs, it is quite possible to combine several electrode pairs in the same vacuum vessel all using the same high current feedthrough. On a small scale, this is exactly what occurs for cathode spots. As interest in the commercial application of high current devices grows, more activity is expected in engineering improvements such as the above extrapolation.

Magnetic Forces

The introduction of a large current into confined device implies the existence of a rather large magnetic field. Even though the current executes a simple single-pass through the device, the forces generated can be quite significant. Present-day railguns are an example of a single-turn large-current device. The performance levels of these devices illustrate the existence of large forces which switches must contain. Moreover, the field generated will exert large forces on all current carrying members. Hence, even if interior to the vacuum vessel the current divides into parallel segments, proper design must account for the forces generated.

The plasma-current interaction also is a consideration. The plasma arc channel must be in quasi-equilibrium; hence, the internal plasma pressure must be equal to the magnetic field pressure generated by the current. Figure V.B.3 shows a schematic of the arc channel.

Figure V.B.3

ARC CHANNEL SCHEMATIC

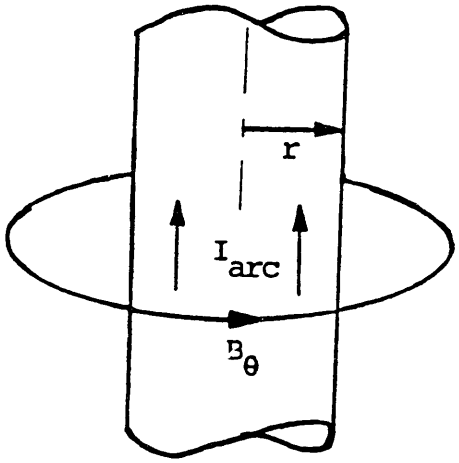

The field at the surface of the arc channel is:

$$B = u_0 I/2\pi r.$$

This field produces a pressure:

$$P = B^2/2u_0.$$

If the magnetic field pressure were greater than that of the plasma (P = nkT), the arc channel radius would decrease. If, on the other hand, the plasma pressure were greater than the magnetic pressure, the arc channel would tend to increase in radius. The condition of quasi-equilibrium is frequently called the Bennet pinch condition.

We can use this simple analysis to predict the arc channel radius. The resulting expression for the radius is:

$$r = \frac{I}{2\pi}\sqrt{\frac{\mu_0}{2nkT}}\,.$$

For copper at an oberved arc channel current of 100 amps, the critical channel radius is about one millimeter. This value agrees with experimental observation [Reece, 1963; Mitchell, 1970; Heberlein, 1980].

As the current in the device increases the resulting magnetic pressure will increase as $B^2 \propto I^2$. For quasi-equilibrium to obtain, the plasma pressure must also scale as I^2: this means that $nkT \propto I^2$. Under present-day conditions it is observed that $n \propto I$, thus as the current increases either n must increase faster than linear, or kT must increase approximately linearly with current. This has important implications for the overall energy balance of vacuum switches, in general, and the surrounding vacuum vessel walls (which presumably must receive the increased heat flux), in particular.

Summary

In addition to the actual performance levels attainable with metal vapor vacuum arc switches, more practical considerations will be necessary for effective, widespread implementation of them.

There appears no fundamental current limitation to metal vapor vacuum arc switches. However, because there are current density limits (even at present-day current levels) proper design engineering will be required to reach desired interruption performance levels. Parallel operation of several current carrying arc channels seems entirely feasible, but there has been little experimental research accomplished in this area. Containment of the increased magnetic forces as a direct result of an increased current will require a suitable mechanical support structure.

V. Appendix C Interruption Kinetics

This appendix presents a mathematically more detailed analysis of the interruption kinetics introduced in Section II.D.3. We assume the magneto-hydrodynamic equations are valid.

For completeness we repeat the introductory analysis given in Section II.D.3. Figure V.C.1 is a simplified switch schematic showing the physical parameters needed for this analysis.

Figure V.C.1

SIMPLIFIED SWITCH SCHEMATIC

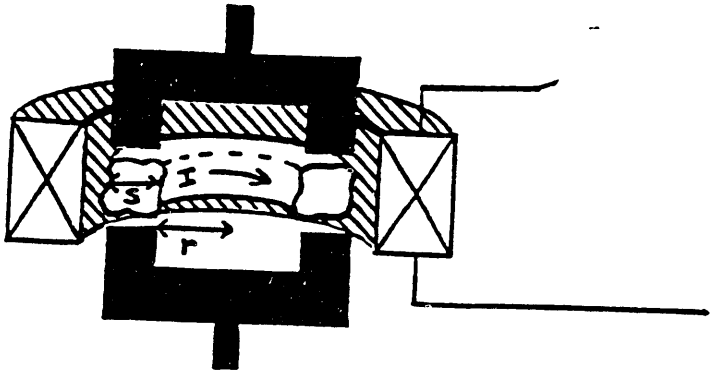

The pulse coil is driven by an auxiliary capacitor bank. The voltage induced in the secondary, which in this case is the plasma itself, can be expressed as:

$$V = d\phi/dt = \pi r^2 \, dB/dt \ .$$

Assuming a sinusoidal excitation frequency ($w = 2\pi f$), the complex amplitudes are:

$$V_0 = \pi r^2 \, wB_0 \ .$$

This voltage generates an induced current:

$$V_0 = I_0 \, Z \ .$$

Z is the complex impedance expressed as:

$$Z = \sqrt{R^2 + (wL)^2} \ ,$$

where R and L are the plasma-torus resistance and inductance, respectively. The radial force density acting on the plasma is:

$$f = \rho a = J \times B/c = IB/(c \, s^2) \ .$$

This is the point of deviation with the simpler theory given in Section II.D.3. We assume the plasma conserves magnetic flux: we are in the asymptotic limit of the excitation frequency. This means the plasma current is given by (B is the driving field):

$$I = - AB/Lc \ .$$

We solve these equation for the plasma acceleration as a function of radius:

$$a = \frac{-\pi r^2 B^2}{s^2 L c^2} = \frac{dv}{dt} = \frac{d^2 r}{dt^2} .$$

For modest changes in r we can assume L = rL_O/r_O, $\rho = \rho_O r_O/r$, s = constant, and B = constant. The resulting second order differential equation is non-linear and can be written as:

$$d^2r/dt^2 = -pr^2 ,$$

where,

$$p = B^2/(\rho s^2 Lc^2) .$$

This equation can readily be solved by forming a system of two simultaneous first order differential equations:

$$\frac{dr}{dt} = v$$

and

$$\frac{dv}{dt} = -pr2 .$$

The initial conditions are v(t=0) = 0, and r(t=0) = r_O. Rearranging we obtain:

$$\frac{dv}{dr} = \frac{-pr^2}{v}$$

(Note: a somewhat different derivation leading to identical results consists of multiplying the expression of Newton's first law by the velocity v and recognizing an exact differential.) In any event, the result is:

$$v^2/2 = p(r_0^3 - r^3)/3 \ .$$

This equation may then be solved for the time rate of change of the radius:

$$\frac{dr}{dt} = v = -\sqrt{\frac{2p(r_0^3 - r^3)}{3}}$$

Note that the negative value of the square root was taken. Physically this corresponds to a shrinking radius, (i.e. dr/dt < 0).

Separating exact differentials we get:

$$\frac{dr}{\sqrt{r_0^3 - r^3}} = \frac{-2p}{3}\,dt$$

After the substitution u = r/r_0 has been made, reference to the integral tables of Gradshteyn and Ryzhik [Gradshetyn and Ryzhik, 1965] yields the solution for the time required for the plasma current-ring to move under the magnetic force to the dimensionless radius u = r/r_0 we have:

$$t = \sqrt{\frac{3}{2pr_0}}\ \frac{F(\phi, \sin 75)}{\sqrt{3}}$$

where, F(ø\k) is the Elliptic Integral of the First Kind, and,

$$\phi = \arccos\{[\sqrt{3} - 1 + u]/[\sqrt{3} + 1 - u]\}.$$

Because of the awkwardness of the analytical solution, it is frequently more convenient to directly numerically integrate I(u), where I(u) is given by:

$$I(u) = \int_u^1 \frac{dx}{(1 - x^3)^{0.5}}.$$

When I(u) is defined as above, I(u) is identical with $F(\phi \backslash k=\sin 75)/\sqrt{3}$.

A short table of the values of $I(u) = F(\phi \backslash \sin 75)/\sqrt{3}$ is given in Figure V.C.2.

Figure V.C.2

VALUES OF RADIUS INTEGRAL

$u = r/r_O$	ϕ	$I(u) = F(\phi \backslash \sin 75)/\sqrt{3}$
0.9	27.	0.37
0.8	37.5	0.53
0.7	48.4	0.66
0.5	56.5	0.89
0.3	64.9	1.10
0.1	70.	1.30
0.0	74.5	1.40

V. Appendices: Appendix C Interruption Calculations

In order to illustrate application of the above formalism, we assume typical values for the relevant parameters, as given in Figure V.C.3. The resulting radius as a function of time is shown in Figure V.C.4.

Figure V.C.3

TYPICAL PARAMETERS VALUES FOR INTERRUPTION

$s = 1$ cm

$L_0 = 0.1$ uH $= 1.11 \times 10^{-19}$ s^2/cm

$r_0 = 6$ cm

$\rho_0 = 10^{-5}$ g/cm^3

Figure V.C.4

GRAPH OF SHRINKING PLASMA RADIUS AS A FUNCTION OF TIME

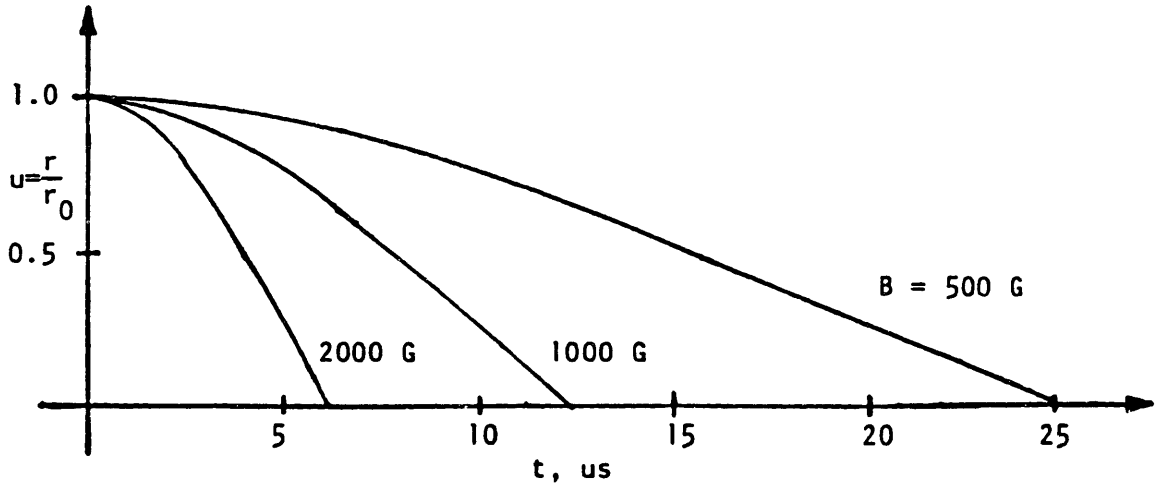

This graph shows that extinction times of order 10 microseconds are possible at applied fields of a few kiloGauss. These fields levels are readily produced in practice.

FOOTNOTES

1. Boxman, R. L. 1974. J. Appl. Phys.,45, p. 4835.

2. Braginski, S. I. 1965. Reviews of Plasma Physics Vol. 1 (New York: Consultants Bureau) p. 220.

3. Carlsaw, H. S. and Jaeger, J. C. 1980. Conduction of Heat in Solids, Second Edition, (Oxford, Britain: Oxford University Press) p. 75.

4. Cobine, J. D. and Burger, E. E. 1955. J. Appl. Phys., 26, p. 895.

5. Compton, K. T. 1931. Phys. Rev. 37 p. 1069.

6. D&M: Davis, W. D. and Miller, H. C. 1969. J. Appl. Phys. 40 p. 2212.

7. Ecker, G. 1980. Vacuum Arcs: Theory and Applications, ed. Lafferty (New York: Wiley) p. 228.

8. Erven, C. C. et al 1970. Proc. of the Fourth Intern'l Sym. on Discharges and Electrical Insulation in Vacuum, (Waterloo, Ont., Canada) Sept., 1970, p. 219.

9. Farrall, G. A. 1980. Vacuum Arcs: Theory and Applications, ed. Lafferty (New York: Wiley) p. 188.

10. Gilmour, S. [1980.] "The Present State and Projected Capabilities of Vacuum Arc Opening Switches", [SUNY, Buffalo].

11. Gradshetyn I. S. and Ryzhik, I. W. 1965. Table of Integrals, Series and Products (New York: Academic Press) p. 229, integral 3.139, #2.

12. Graneau, P. 1981. private communication.

13. Grissolm J. T. and Newton, J. C. 1974. J. Appl. Phys. 45 p. 2885.

14. Heberlein, J. V. R. and Gorman, J. G. 1980. IEEE Trans. on Plasma Science PS-8 p. 283.

15. Holmes, A. J. T. 1974. J. Phys. D: Appl. Phys. 7 p.1412.

16. Jenkins, J. E. et al 1975. J. Phys. D 8 p. L139.

17. Kamakshaiah S. and Rau, R. S. N. 1977. IEEE Trans. on Plasma Science PS-5 p. 1.

18. Kaneda, T. et al 1981. Physica, 104C, p. 124.

19. Kimblin, C. W. 1971. Proc. IEEE 59 p. 546.

20. Kimblin, C. W. 1973. J. Appl. Phys. 44 p. 3074.

21. Kittel, C. 1976. Introduction to Solid State Physics, (New York: Wiley) p. 32.

22. Lafferty, J. M. 1966. Proc. IEEE 54 p. 23.

23. Larmar, E. S. and Compton, K. T. 1931. Phys. Rev. 37 p. 1077.

24. Lee, T. H. 1959. J. Appl. Phys. 30 p. 166.

25. Lee, T. H. 1960. J. Appl. Phys. 31 p. 924.

26. Lifshitz E. M. and Pitaevskii, L. P. Physical Kinetics, (New York: Pergamon Press) p. 6.

27. McClure, G. W. 1974. J. Appl. Phys. 45 p. 2078.

28. McCoy, F. et al 1964. Proc. of the First Internat'l Sym. on Insulation Strength in Vaccum, Cambridge, MA, October 1964, p. 259.

29. Miller H. C. and Farrall, G. A. 1965. J. Appl. Phys. 36 p. 1338.

30. Miller, H. C. 1971. J. Appl.Phys. 43 p. 2175.

31. Miller, H. C. 1977. IEEE Trans. on Plasma Science PS-5 p. 181. 1977.

32. Mitchell, G. R. 1970. Proc. IEE 117 p.2315.

33. Mitchell, G. R. 1974. J. Appl. Phys. 45 p. 2078.

34. Mitchell, G. R. 19 . "The Influence of Vacuum Arcs on the design of Contacts for Vacuum Power Devices" p.117.

35. Mongeau, P. 1981. AIAA/JSASS/DGLR, Fifteenth International Electric Propulsion Conf. (New York: AIAA).

36. O'Hanlon, J. F. 1980. A User's Guide to Vacuum Technology (New York: Wiley) p. 251.

37. PR&K: Plyutto, A. A., Ryzhkov, V. N. and Kapin, A. T. 1965. Sov. Phys. JETP 20 p. 328.

38. Poeffel, K. 1980. IEEE Trans. on Plasma Sci. PS-8 p. 443.

39. Reece, M. P. 1963. Proc. IEE 110 p. 793.

40. Rich J. A. and Farrall, G. A. 1964. Proc. IEEE 52 p. 1293.

41. Rich, J. A. 1971. Proc. IEEE 59 p. 539.

42. Robson, A. E. 1978. J. Phys. D: Appl. Phys. 11 p. 1917.

43. Rozanova, N. B. and Granovskii, V. L. 1956. Sov. Phys. - Tech. Phys. 1 p. 471.

44. Schoenbach, K. et al 1981. Third IEEE International Pulsed Power Conf. (Albuquerque, N.M.) p. 74.

45. Tanberg, R. 1930. Phys. Rev. 35 p. 1080.

46. Tanberg R. and Berkey, W. E. 1931. Phys. Rev. 38 p. 296.

47. Touloukian, Y. S. 1981. Vade Mecum ed. Anderson (New York: American Institute of Physics) p. 319.

48. Tuma, D. T. et al 1978. J. Appl.Phys. 49 p. 3821.

49. Weast, R. C. ed. 1974. Handbook of Chemistry and Physics (Cleveland, Ohio: CRC Press, Cleveland) p. E-68.

50. Zel'dovich Ya. B. and Razier, Yu. P. 1966. Physics of Shock Waves and High Temperature Hydrodynamic Phenomena Vol. 1 (New York: Academic Press) p. 394.

51. Machine Design, 1983 Material Reference Issue, 14 April p. 65.

BIBLIOGRAPHY

Bettge, H. et al [1978.] "New Vacuum-Type Circuit Breaker for Medium Voltage Distribution Systems", (Siemens AG, Fed. Rep. of Germany) p. 24.

Boxman, R. L. 1974. J. Appl. Phys.,45, p. 4835.

Boxman, R. L. 1977. IEEE Trans. on Electron Devices ED-24 p. 122.

Bowman, C. D. Gilmour, A. S., and Dollinger, R. 1978. IEEE Pub. No. CH1371-4/78/0000-0213 p. 213.

Boxman, R. L. 1980. IEEE Trans. on Plasma Science PS-8 p. 308.

Boxman, R. L. et al 1982. Proc. Tenth International Symp. on Discharge and Electrical Insulation in Vacuum, Columbia, S. C. October 25-28, 1982 p. 161.

Boxman, R. L. 1983. J. Appl. Phys. 54 p. 592.

Braginski, S. I. 1965. Reviews of Plasma Physics Vol. 1 (New York: Consultants Bureau) p. 220.

Carlsaw, H. S. and Jaeger, J. C. 1980. Conduction of Heat in Solids, Second Edition, (Oxford, Britain: Oxford University Press) p. 75.

Childs, S. E. et al 1982. Proc. Tenth International Symp. on Discharge and Electrical Insulation in Vacuum, Columbia, S. C. October 25-28, 1982 p. 230.

Cobine, J. D., and Burger, E. E. 1955. J. Appl. Phys. 26 p. 895.

Cobine, J. D. and Farrall, G. A. 1960. J. Appl. Phys. 31 p. 2296.

Compton, K. T. 1931. Phys. Rev. 37 p. 1069.

Courts, A. L., et al 1982. IEEE Trans. on Power App. and Sys. p. 4112.

D&M: Davis, W. D. and Miller, H. C. 1969. J. Appl. Phys. 40 p. 2212.

Dettman, D. et al 1981. Proc. Third IEEE Pulsed Power Conf. (Albuquerque, N. M.) p. 432.

Djakov, B. E., and Holmes, R. 1974. J. Phys. D: Appl. Phys. 4 p. 504.

Dollinger, R. et al IEEE Trans. on Plasma Science PS-8 p. 302.

Dushman, S. 1949. Scientific Foundations of Vacuum Technigue, Second Edition, ed. J. Lafferty (New York: Wiley) p. 691.

Ecker, G. 1976. IEEE Trans. on Plasma Science PS-4 p. 218.

Ecker, G. 1980. Vacuum Arcs: Theory and Applications, ed. Lafferty (New York: Wiley) p. 228.

Eckhardt, W. O. Hofman, G. A. [1976.] "Ohmic Heating DC Circuit Breakers with Liquid Metal Plasma Valves", (Hughes Research Labs, Malibu, Calif.) p. 717.

Eckhardt, G. 1980. IEEE Trans. on Plasma Science PS-8 p. 295.

Emtage, P. R. et al IEEE Trans. on Plasma Science PS-8 p. 314.

Erven, C. C. et al 1970. Proc. of the Fourth Intern'l Sym. on Discharges and Electrical Insulation in Vacuum, (Waterloo, Ont., Canada) Sept., 1970, p. 219.

Fang, D. Y. 1982. J. Phys. D: Appl. Phys. 15 p. 833.

Farrall, G. A. 1973. Proc. IEEE 61 p. 1113.

Farrall, G. A. [1976.] Voltage Effects of Low and High Current Arcing on Vacuum Interrupter Contacts", (Gen. Elec. Corp. R&D, Schenetady, New York) p. 111.

Farrall, G. A. 1980. Vacuum Arcs: Theory and Applications, ed. Lafferty (New York: Wiley) p. 228.

Frohlich, K. IEEE Trans. on Plasma Science PS-8 p. 319.

Gilmour, A. S., and Lockwood, D. L. 1975. IEEE Trans. on Electron Devices ED-22 p. 173.

Gilmour, A. S. et al 1978. IEEE Pub. No. CH1371-4/78/0000-0217 p. 217.

Gilmour, A. S. [1980.] The Present State and Projected Capabilities of Vacuum Arc Opening Switches", (State University of New York, Buffalo, New York) p. [101-1 or V-234].

Goldsmith, S. et al 1982. Proc. Tenth International Symp. on Discharge and Electrical Insulation in Vacuum, Columbia, S. C. October 25-28, 1982 p. 148.

Gradshetyn I. S. and Ryzhik, I. W. 1965. Table of Integrals, Series and Products (New York: Academic Press) p. 229, integral 3.139, #2.

Graneau, P. 1981. private communication.

Grissolm, J. T. and Newton, J. C. 1974. J. Appl. Phys. 45 p. 2885.

Hantzsche, E. 1982. Proc. Tenth International Symp. on Discharge and Electrical Insulation in Vacuum, Columbia, S. C. October 25-28, 1982 p. 131.

Harvey, R. J. and Lutz, M. A. [1976. IEEE Trans. on Plasma Science PS-4 Dec. p. 210.]

Heberlein, J. V. R. and Gorman, J. G. 1980. IEEE Trans. on Plasma Science PS-8 p. 283.

Heberlein, J. V. R. and Porto, D. R. 1982. Proc. Tenth International Symp. on Discharge and Electrical Insulation in Vacuum, Columbia, S. C. October 25-28, 1982 p. 181.

Holmes, A. J. T. 1974. J. Phys. D: Appl. Phys. 7 p.1412.

Hugel, H. IEEE Trans. on Plasma Science PS-8 p. 437.

Jolly, D. C. 1982. J. Appl. Phys. 53 p. 6121

Izraeli, I. et al 1982. Proc. Tenth International Symp. on Discharge and Electrical Insulation in Vacuum, Columbia, S. C. October 25-28, 1982 p. 193.

Jenkins, J. E. et al 1975. J. Phys. D 8 p. L139

Kamakshaiah, S. and Rau, R. S. N. 1977. IEEE Trans. on Plasma Science PS-5 p. 1.

Kaneda, T. et al 1981. Physica, 104C, p.124.

Kimblin, C. W. 1971. Proc. IEEE 59 p. 546.

Kimblin, C. W. 1973. J. Appl. Phys. 44 p. 3074.

Kittel, C. 1976. Introduction to Solid State Physics, (New York: Wiley) p. 32.

Krat'ko, S. A. 1981. Sov. Phys. Tech. Phys. 26 p. 1049.

Kristiansen, M., et al 1981. Proc. Third International Pulsed Power Conference (Albuquerque, N. M.) p. 67.

Kurose, Y. et al 1982. Proc. Tenth International Symp. on Discharge and Electrical Insulation in Vacuum, Columbia, S. C. October 25-28, 1982 p. 261.

Lafferty, J. M. 1966. Proc. IEEE 54 p. 23

Larmar, E. S. and Compton, K. T. 1931. Phys. Rev. 37 p. 1077.

Lee, T. H. 1959. J. Appl. Phys. 30 p. 166.

Lee, T. H. 1960. J. Appl. Phys. 31 p. 924.

Lee, T. H., and Greenwood, A. 1961. J. Appl. Phys. 32 p. 916.

Lifshitz, E. M. and Pitaevskii, L. P. Physical Kinetics, (New York: Pergamon Press) p. 6.

McClure, G. W. 1974. J. Appl. Phys. 45 p. 2078.

McCoy, F. et al 1964. Proc. of the First Internat'l Sym. on Insulation Strength in Vaccum, Cambridge, MA, October 1964, p. 259.

Miller H. C. and Farrall, G. A. 1965. J. Appl. Phys. 36 p. 1338.

Miller, H. C. 1972. J. Appl. Phys. 43 p. 2175.

Miller, H. C. 1977. IEEE Trans. on Plasma Science PS-5 p. 181. 1977.

Miller, H. C. 1982. Proc. Tenth International Symp. on Discharge and Electrical Insulation in Vacuum, Columbia, S. C. October 25-28, 1982 p. 142.

Miller, R. N., Dollinger, R. Gilmour, A. S. 1978. IEEE Pub. No. CH1371-4/78/0000-0200 p. 200.

Miller, R. N. et al IEEE Pub. No. CH1371-4/78/0000-0204. p. 204.

Mitchell, G. R. 1970. Proc. IEE 117 p.2315.

Mitchell, G. R. 1974. J. Appl. Phys. 45 p. 2078.

Mitchell, G. R. 19 . "The Influence of Vacuum Arcs on the design of Contacts for Vacuum Power Devices" p.117.

Mongeau, P. 1981. AIAA/JSASS/DGLR, Fifteenth International Electric Propulsion Conf. (New York: AIAA).

O'Hanlon, J. F. 1980. A User's Guide to Vacuum Technology (New York: Wiley) p. 251.

Okmura, H., et al [1978.] " Development of High Power Vacuum Circuit Breakers having Axial Magnetic Field Type Electrodes", (Toshiba Corp. Japan) p. 78.

PR&K: Plyutto, A. A., Ryzhkov, V. N. and Kapin, A. T. 1965. Sov. Phys. JETP 20 p. 328.

Poeffel, K. 1980. IEEE Trans. on Plasma Sci. PS-8 p. 443.

Porto, D. R., Kimblin, C. W., and Tuma, D. T. 1982. J. Appl. Phys. 53 p.4740.

Premerlani, W. J. 1982. IEEE Trans. on Power Apparatus and Systems, PAS-101 p. 2721.

Reece, M. P. 1963. Proc. IEE 110 p. 793.

Reece, M. P. 1963. Proc. IEE 110 p. 803.

Rich, J. A. and Farrall, G. A. 1964. Proc. IEEE 52 p. 1293.

Rich, J. A. et al 1971. Proc. IEEE 59 p. 539.

Robson, A. E. 1978. J. Phys. D: Appl. Phys. 11 p. 1917

Rondeel, W. G. J. 1973. J. Phys. D: Apply. Phys. 6, p.1705.

Rozanova, N. B. and Granovskii, V. L. 1956. Sov. Phys. - Tech. Phys. 1 p. 471.

Scheffler, C. P., et al 1981. Proc. Thrid International Pulsed Power Conference (Albuquerque, N. M.) p. 428.

Schellekens, H. 1983. J. Appl. Phys. 54 p. 144.

Schoenbach, K. et al 1981. Third IEEE International Pulsed Power Conf. (Albuquerque, N.M.) p. 74.

Schoenberg, K. H. , and Kristiansen, M. 1983. Proc. Fourth IEEE Pulsed Power Conf., (Albuquerque, N. M.) June 6-8, 1983.

Swen, Y., and Gilmour, A. S. 1978. IEEE Pub. No. CH1371-4/78/0000-0208.

Tanberg, R. 1930. Phys. Rev. 35 p. 1080.

Tanberg, R. and Berkey, W. E. 1931. Phys. Rev. 38 p. 296.

Touloukian, Y. S. 1981. Vade Mecum ed. Anderson (New York: American Institute of Physics) p. 319.

Tuma, D. T. et al 1978. J. Appl.Phys. 49 p. 3821.

Van Den Heuvel, W. M. C. 1980. IEEE Trans. on Plasma Science PS-8 p. 326.

Voshall, R. E. 1969. IEEE Trans. on Power Apparatus and Systems PAS-88 p. 120.

Ware, K. D. et al 1971. Rev. of Sci. Instruments 42 p. 512.

Warren, F. T. et al 1981. Proc. Third IEEE International Pulsed Power Conf. (Albuquerque, N. M.) p. 436.

Weast, R. C. ed. 1974. Handbook of Chemistry and Physics (Cleveland, Ohio: CRC Press, Cleveland) p. E-68.

Zel'dovich, Ya. B. and Razier, Yu. P. 1966. Physics of Shock Waves and High Temperature Hydrodynamic Phenomena Vol. 1 (New York: Academic Press) p. 394.

VIII. Afterword

A doctoral thesis has a multitude of goals: some of which are achieved and some of which are not. The work represented by this thesis has accomplished many of the goals set by the author, as well as the goals established by external agencies. From an academic point of view, the author feels several important theoretical issues have been clarified and/or explained in this work, which previously have not received attention.

From a practical point of view, a device has been constructed which not only provides an excellent learning experience, but, additionally, performs quite well. Interruption of 5 kA in 160 us is the present figure of merit. It must be remembered that no external parallel capacitors or series saturable inductors have been used to achieve this performance level.

The author has thoroughly enjoyed the camaraderie associated with his study; the other graduate students and the excellent staff of professionals have made the entire experience especially rewarding.

IX. Biographical Note

The author was born and raised in Canton, Ohio. In 1975 he graduated from Glenwood High School. During high school, a self-paced mathematical program and courses at a local institution, Malone College, were important in providing some of the necesaary preparation for M.I.T. In addition, the author particpated in a variety of extracurricular activites including sports and church-related events. His extended family had (and still has) an influential effect on his development.

What is not widely recognized, concerning M.I.T. as an institution, is the people behind the scenes who keep MIT great. When the author experienced a very serious back injury due to a fall from a aubstantial height, the people at MIT made it possible for him to continue his academic program, even if it was an abbreviated schedule.

Prior to joining the staff at Electromagnetic Launch Research, (EML) Inc. of Cambridge, Mass. the author worked for AVCO's Systems Division and a development group at I.B.M. At EML, Inc. the author will continue research concerning the application of magnetic fields to acceleration of matter, including further research involving vacuum arcs and acceleration of metal with applications to national security.

The author currently lives in Medfield, Mass. with his wife and Collie, Ginger. Elizabeth Anne Bernhard Cope has assisted with the artwork for the combined Master's/Bachelor's Thesis and this work.